Computational geometry of soft matter

UMass Summer School on Soft Solids and Complex Fluids 2024
Lecture 3 (Wednesday June 5)

Chris H. Rycroft, University of Wisconsin–Madison
(chr@math.wisc.edu)

Outline

Monday

- A model of dense granular drainage
- Voronoi analysis of granular flow
- Neighbor relations

Tuesday

- Development of the Voro++ library
- Network analysis for CO_2 capture
- Alternative models and methods

Wednesday

- Topological Voronoi analysis
- Lloyd's algorithm and meshing
- Insect wing structure

Thursday

- Continuum representations of deformation
- The reference map technique
- Fluid–structure interaction

Computation of the "maximum free sphere"

- Combine Voronoi cells into a complete network of edges
- Each edge labeled with the minimum distance to an atom
- Use to compute the maximum-sized sphere that can move between the atoms

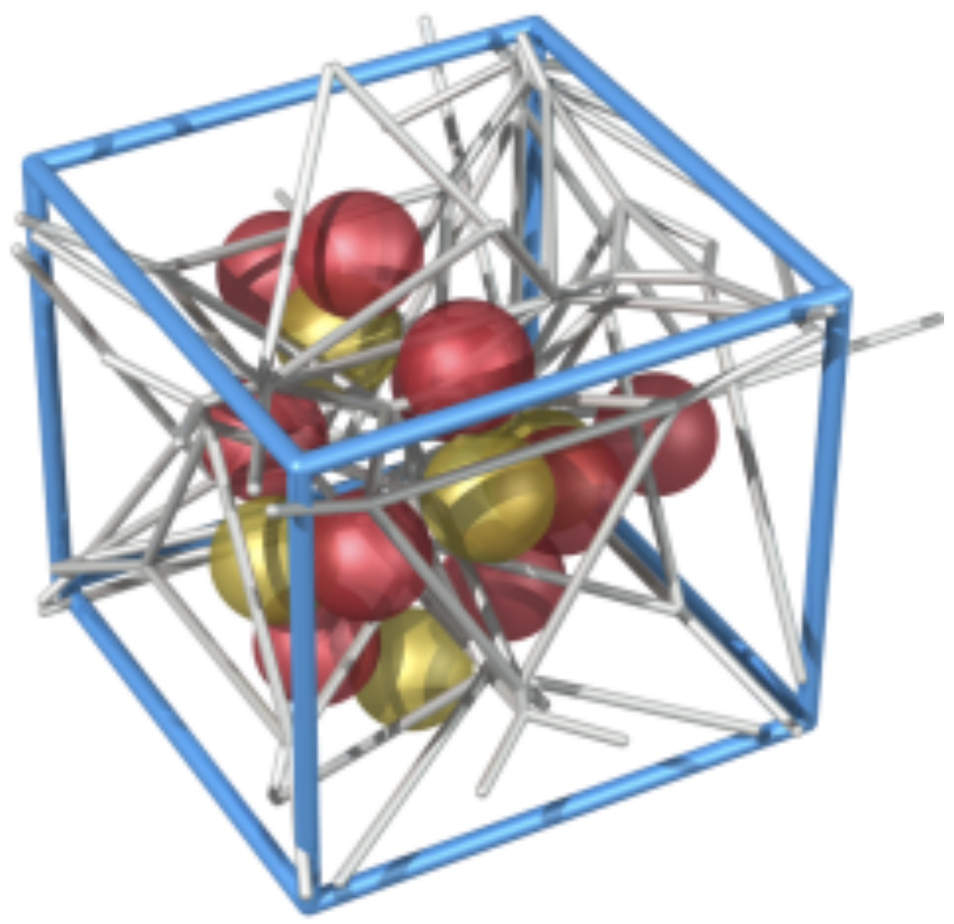

Voronoi network for EDI zeolite

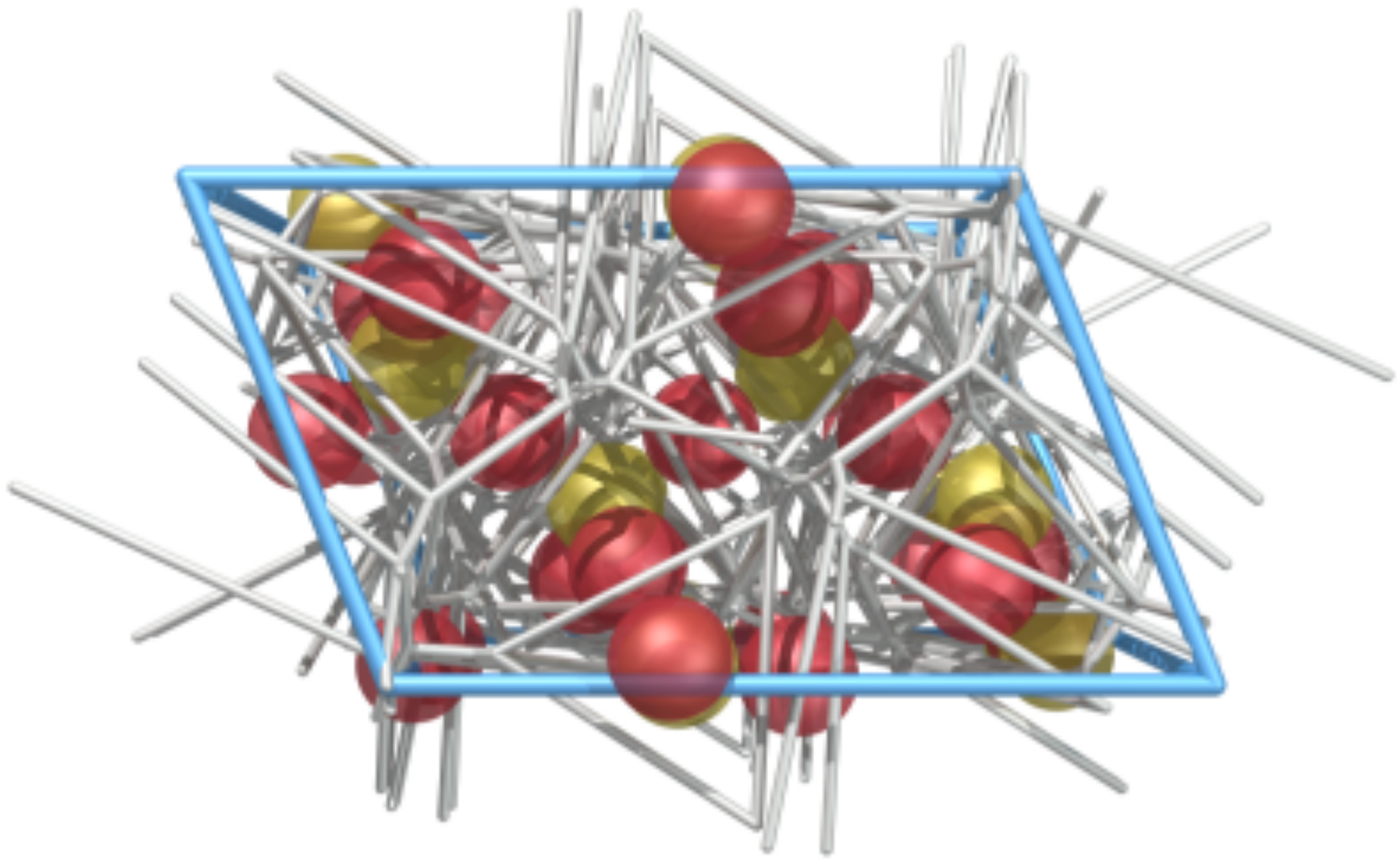

Voronoi network for YUG zeolite

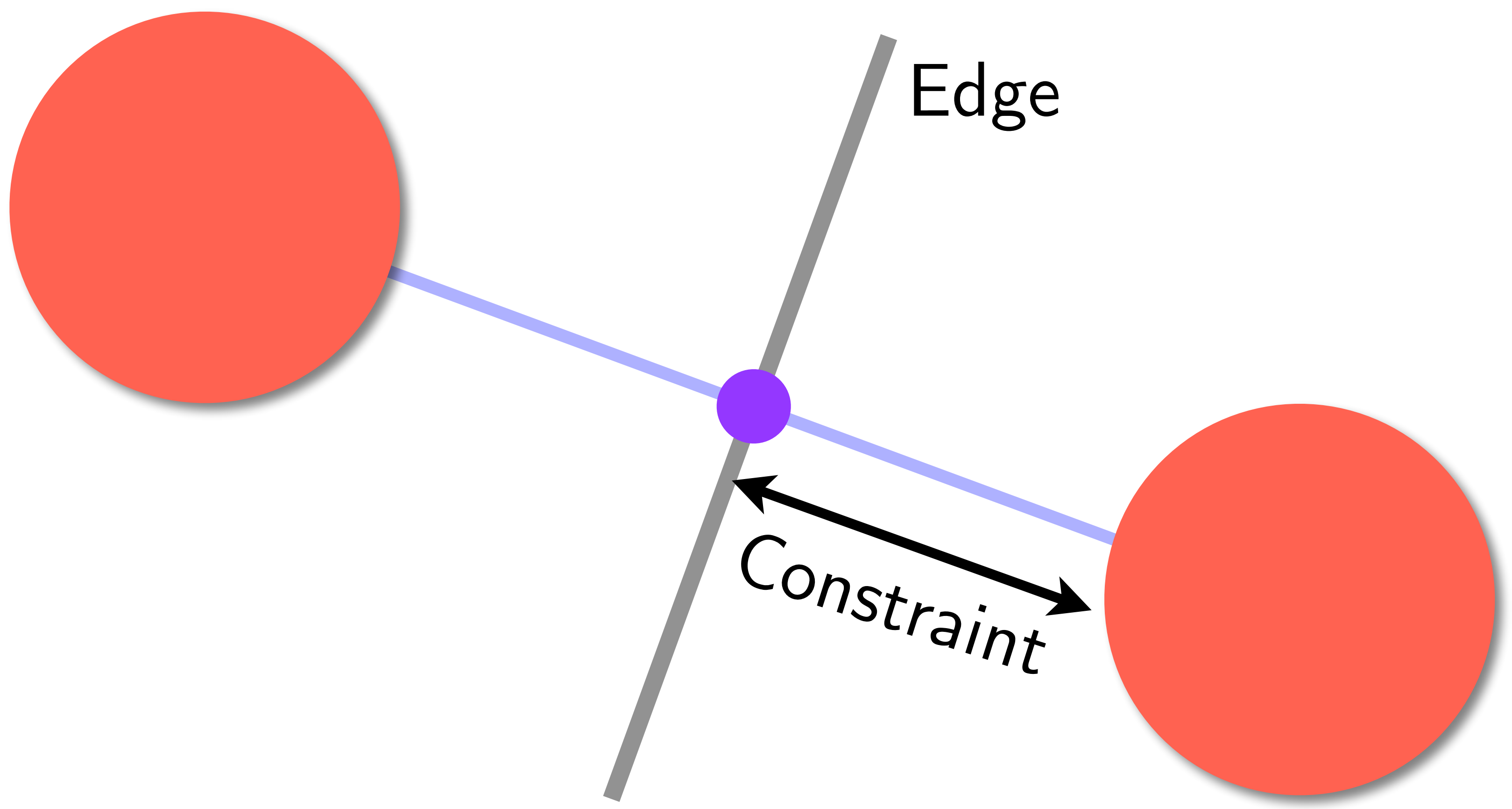

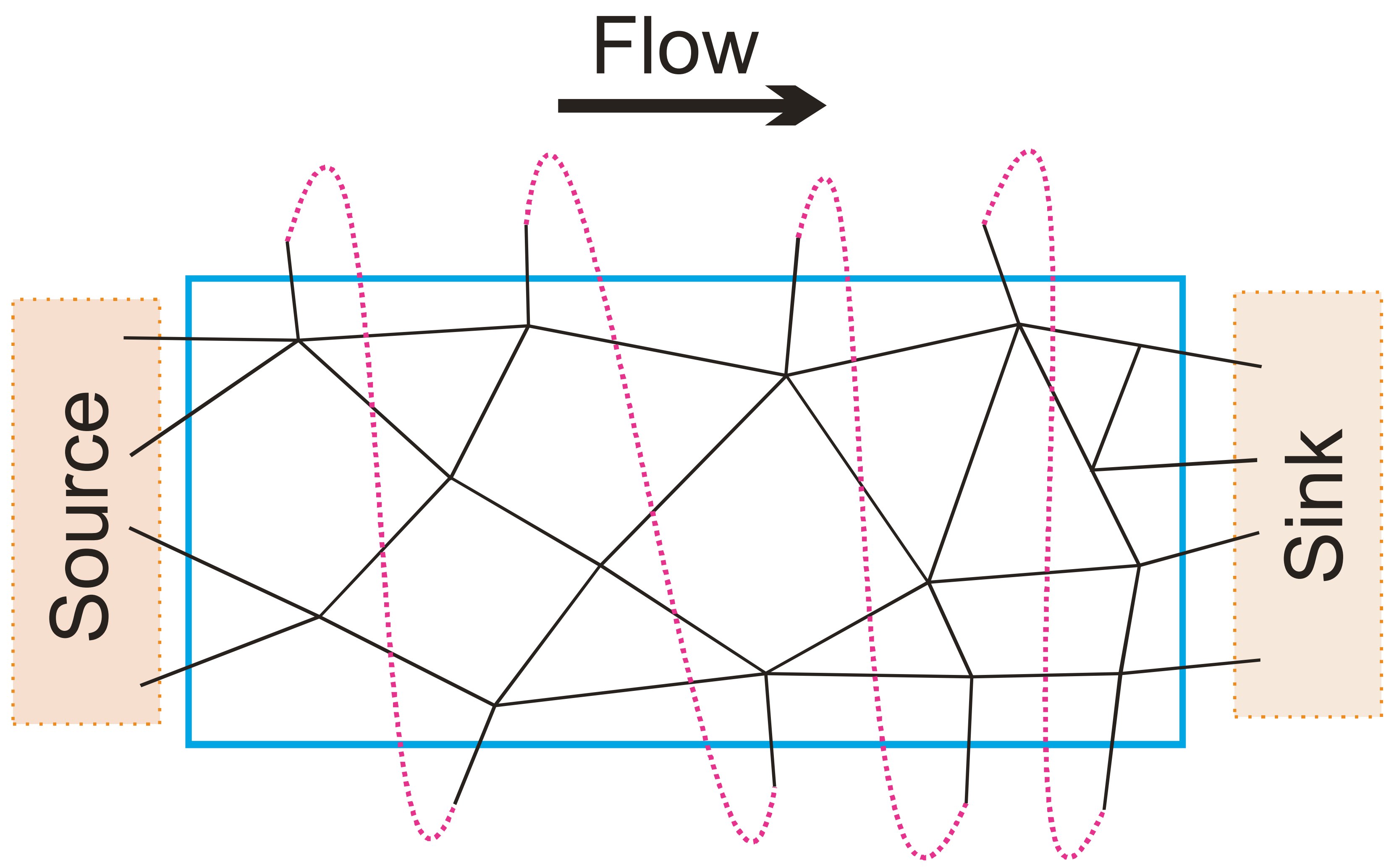

“Maximum free sphere” computation

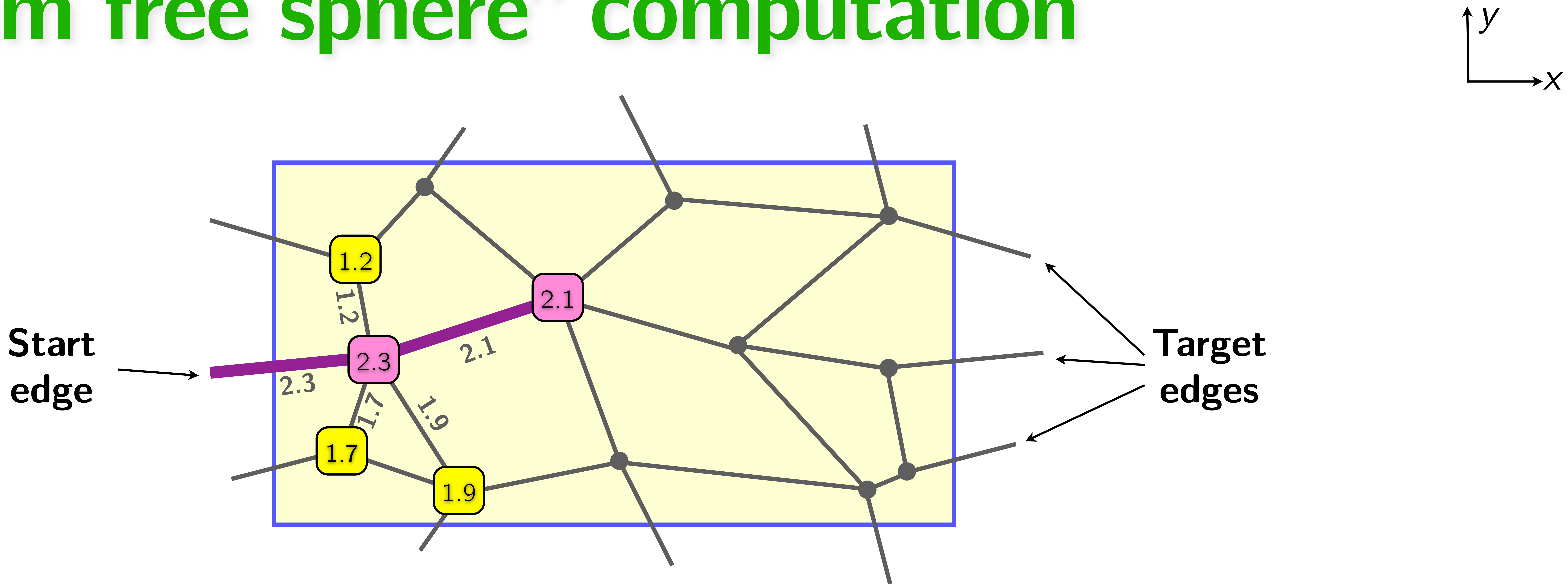

- Disable periodicity in x, and start from one edge going into the periodic image in $-x$ direction
- Create list of neighboring nodes and sort by constraint size
- Run modified Dijkstra algorithm:
  - Set node with largest constraint
  - Update list with new neighbors and repeat

“Maximum free sphere” computation

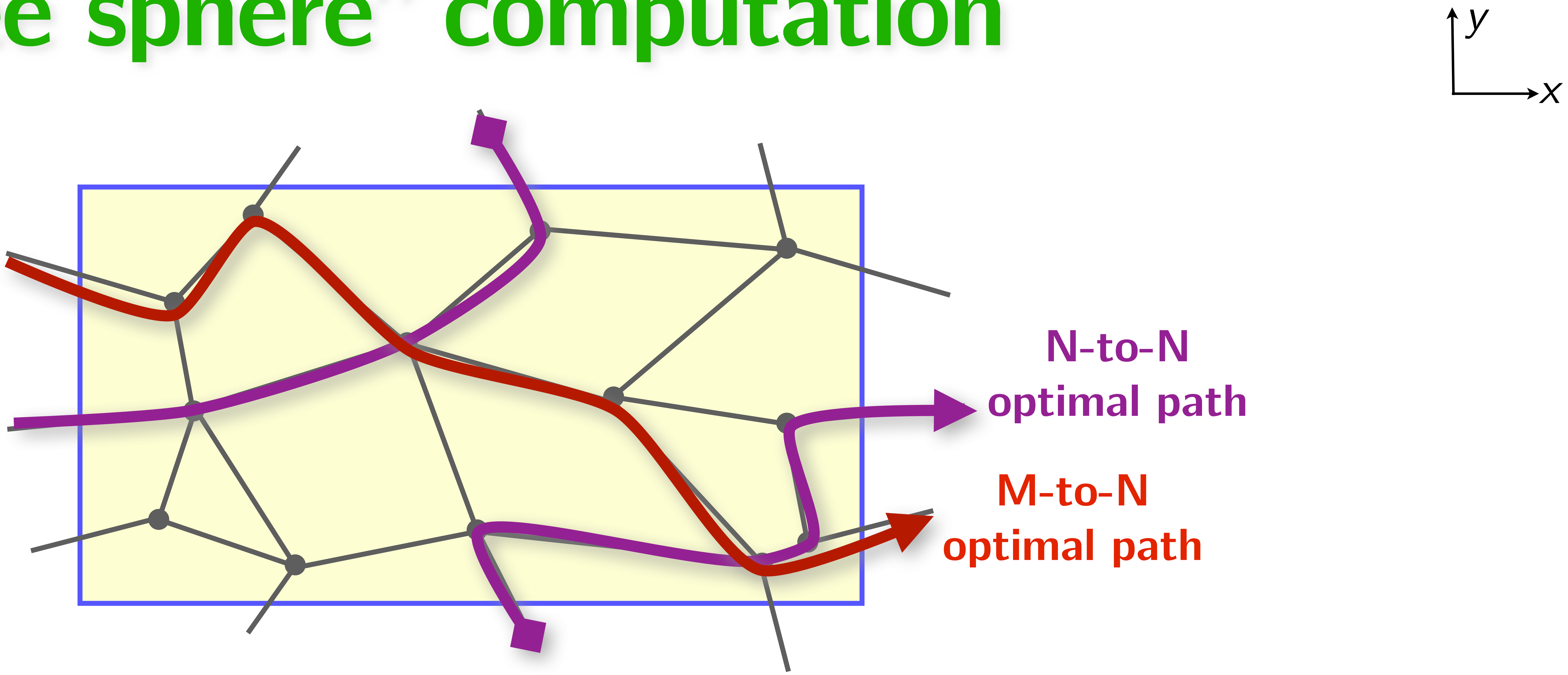

- Carry out algorithm for all edges from -x periodic image to find optimal path
- Two cases:
  - N-to-N: start and end edges are the same
  - M-to-N: start and end edges differ – consider supercell

“Maximum free sphere” computation

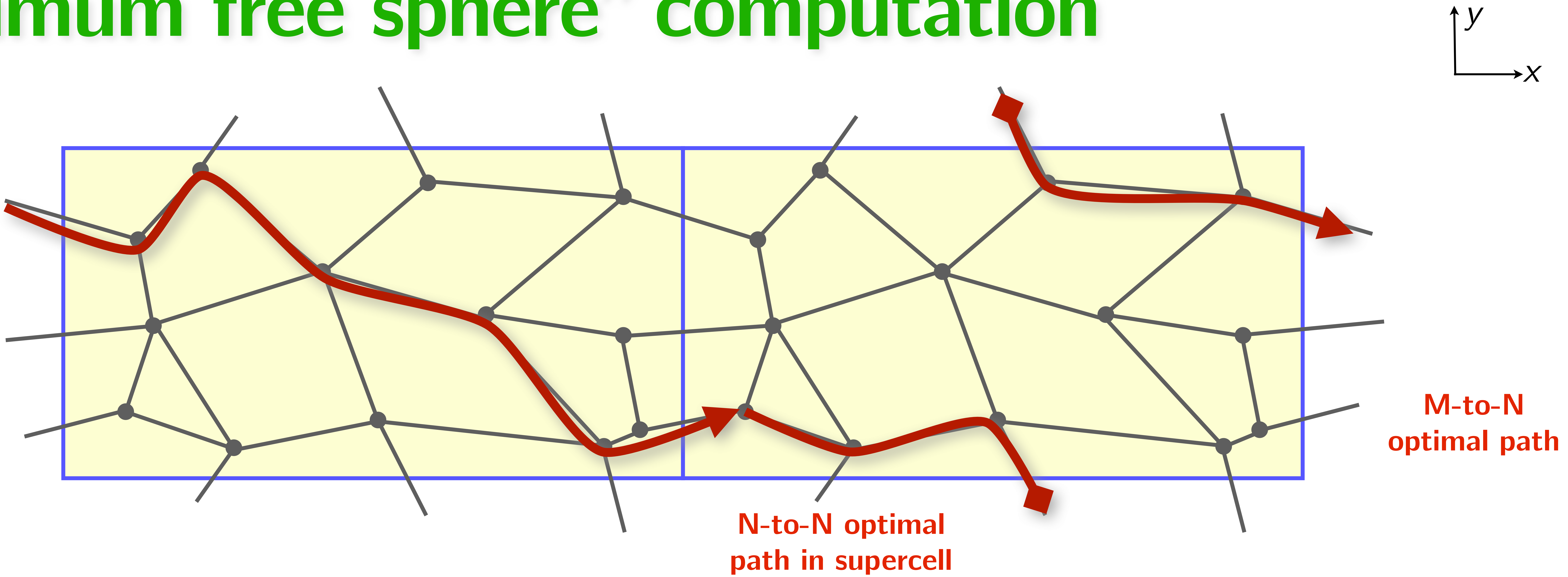

- Carry out algorithm for all edges from -x periodic image to find optimal path
- Two cases:
  - N-to-N: start and end edges are the same
  - M-to-N: start and end edges differ – consider supercell

Accessible surface area

- Previous work employs Monte Carlo sampling to estimate surface area accessible to probe
- Extend analysis by to detect inaccessible pockets by drawing rays from sample points to Voronoi vertices

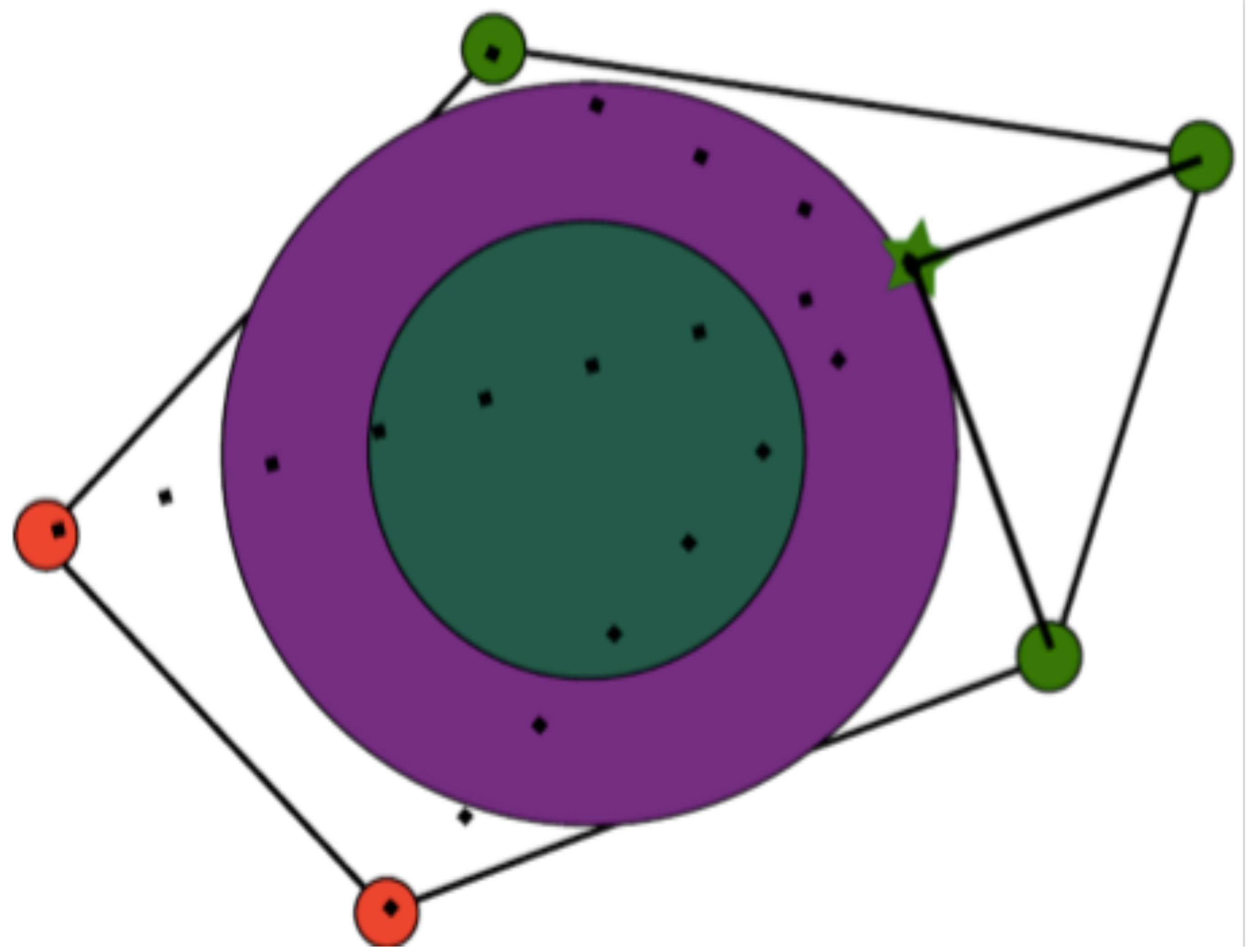

Rays exist from sampled point to accessible nodes

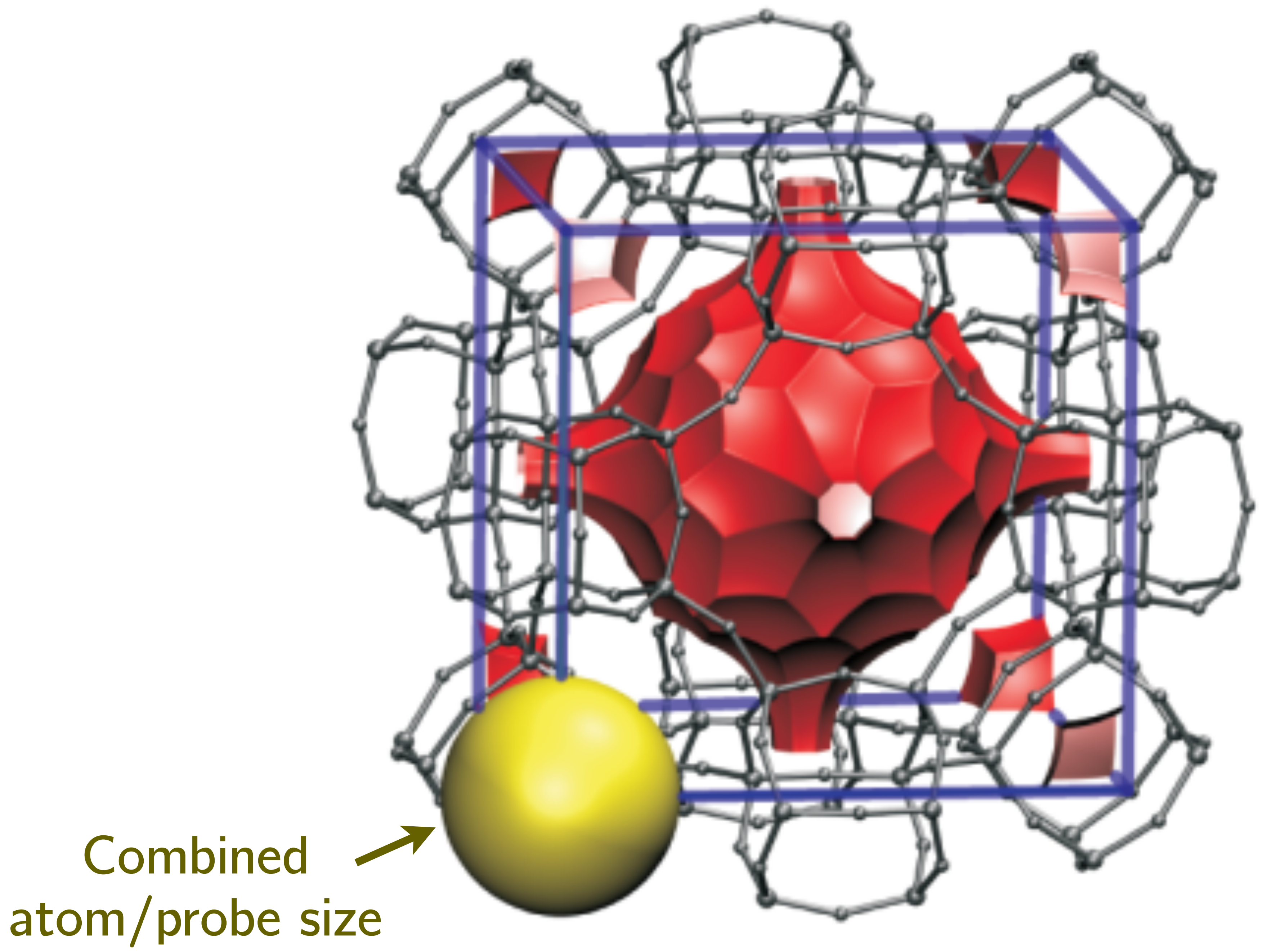

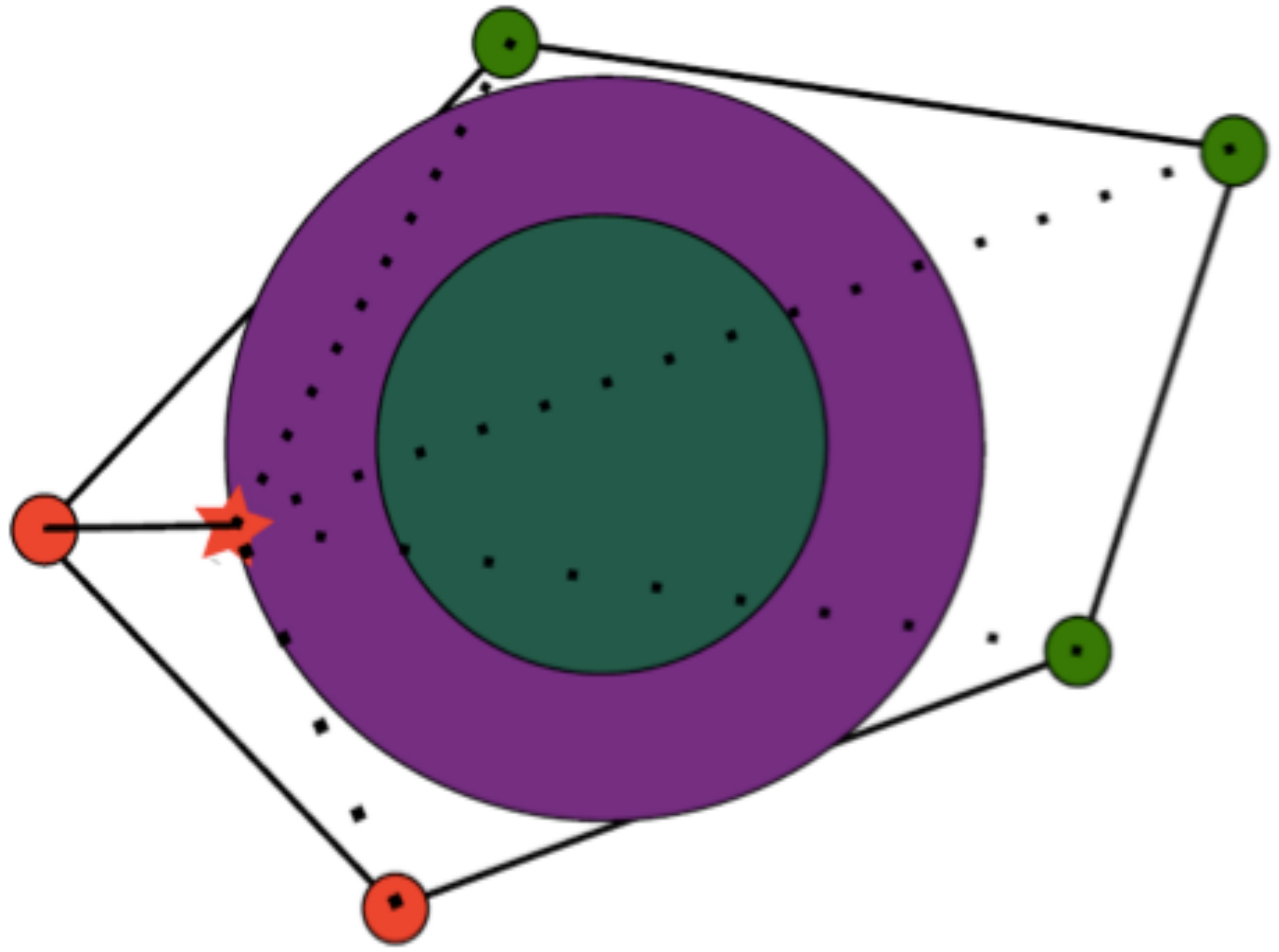

Ray exists from sampled point to inaccessible node

Inaccessible pocket detection

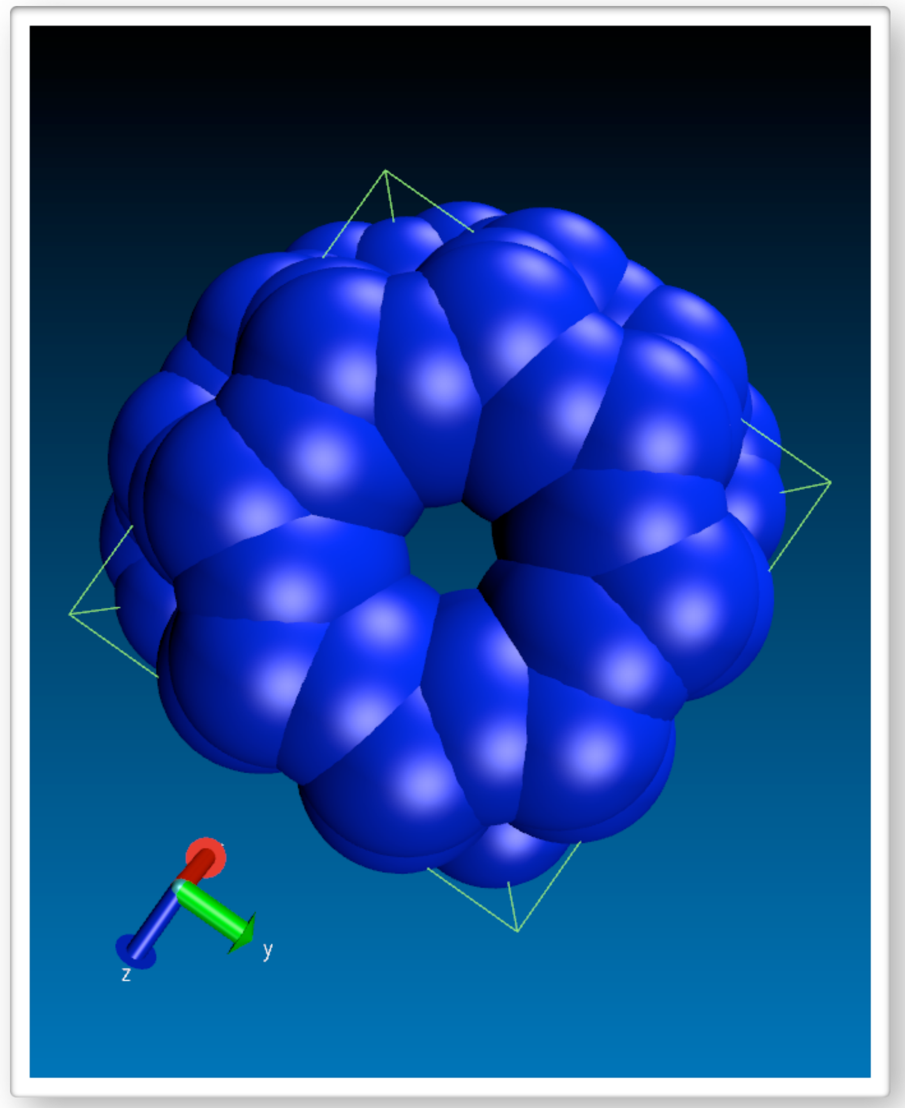

Consider the sampling surface
for an intermediate probe

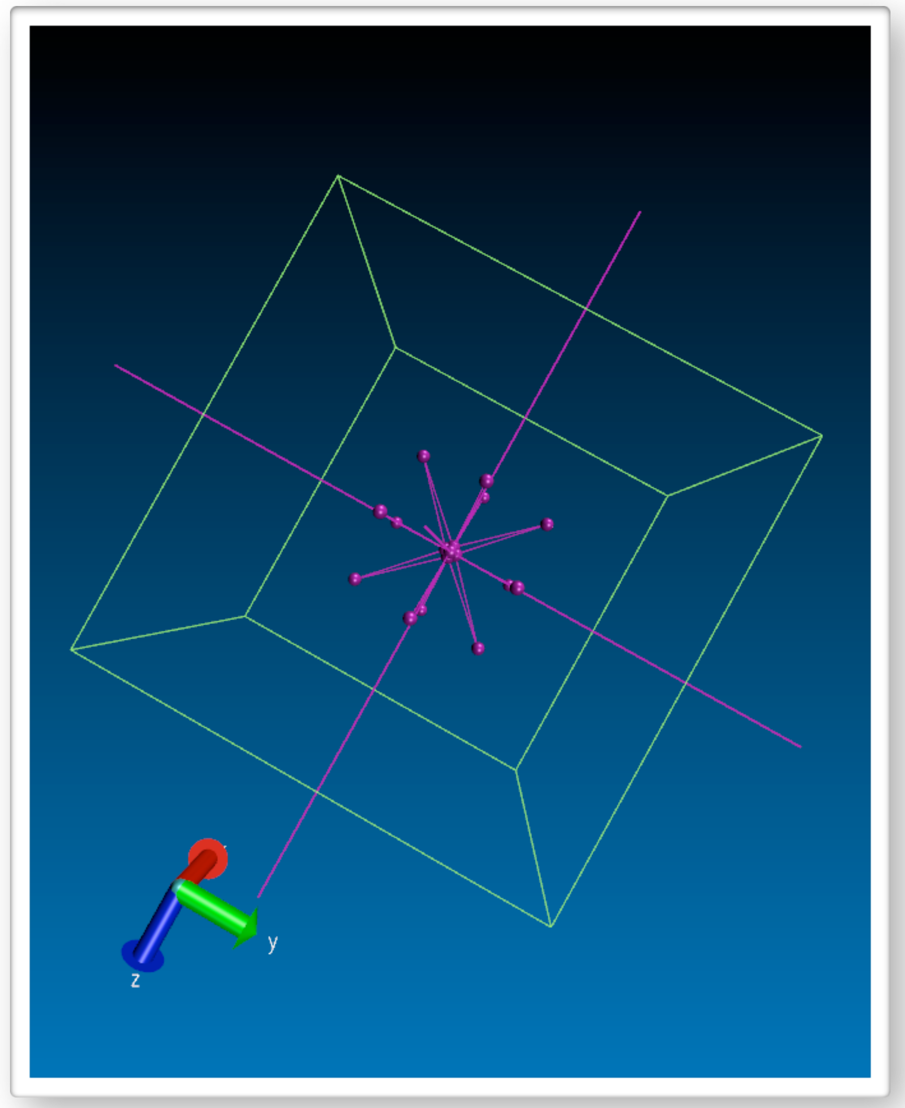

Calculate the channels in the
Voronoi network for the probe

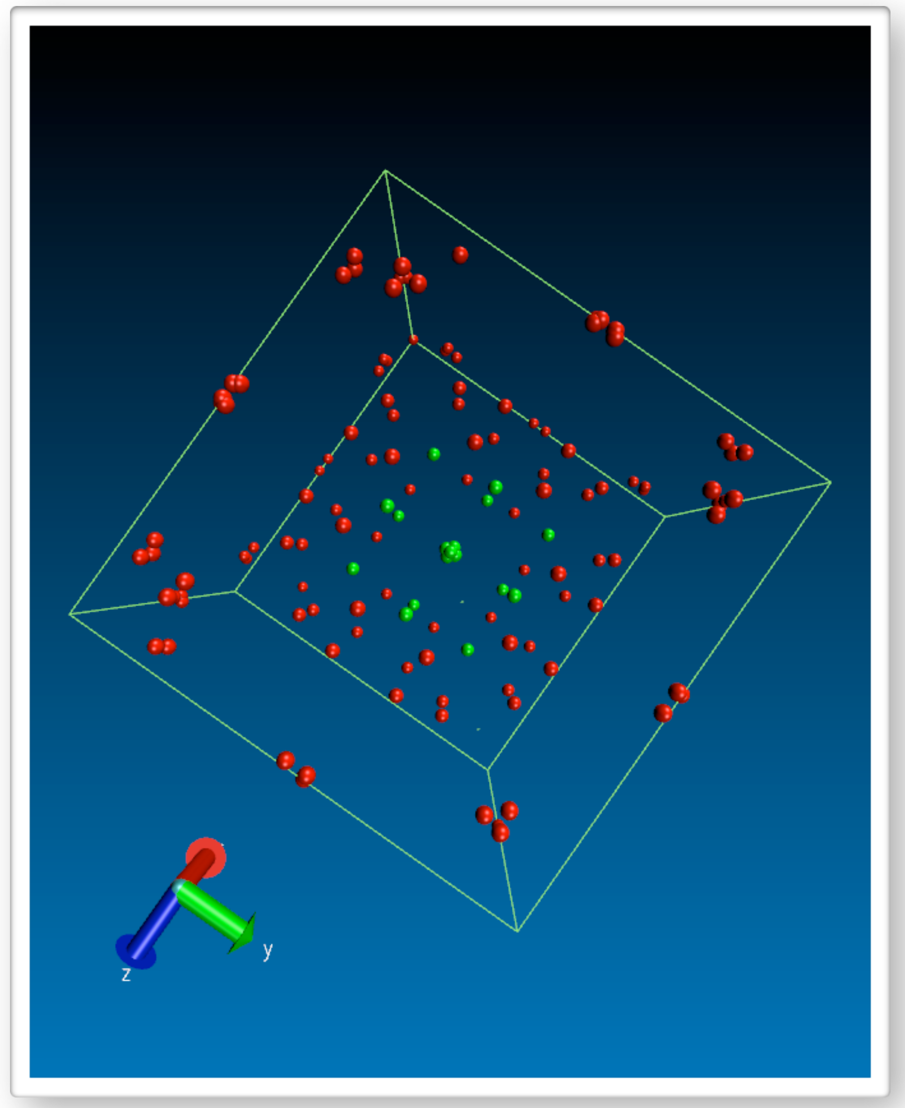

Only nodes within channels
are accessible (green)

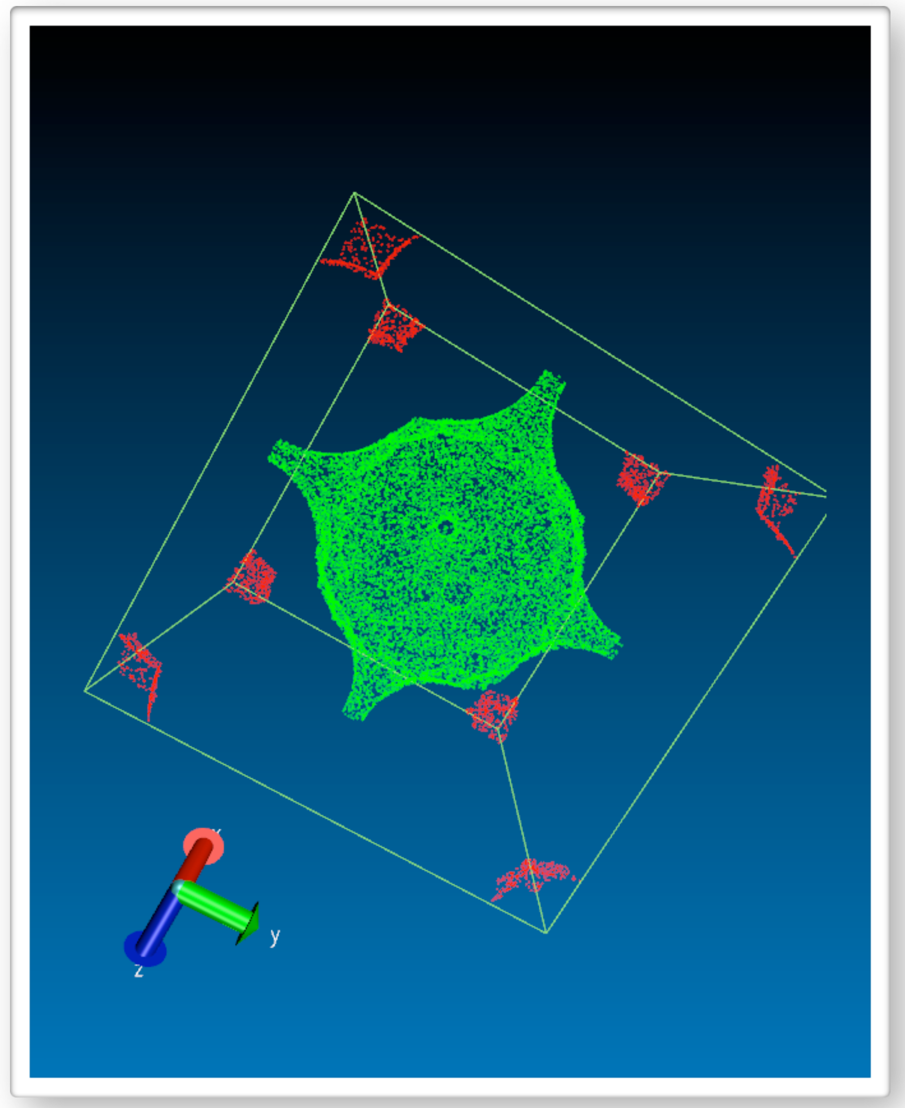

Sample surface area
using node information

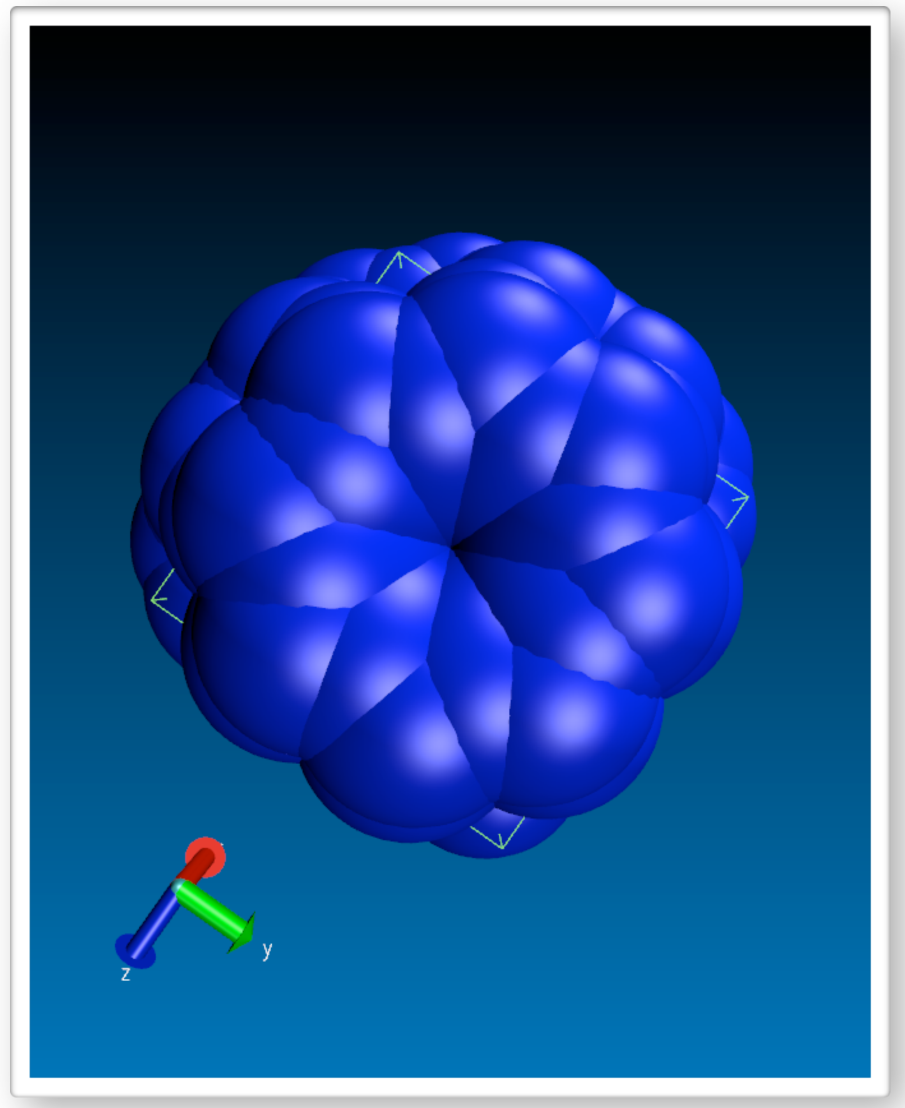

An increase in probe size closes
the passageway

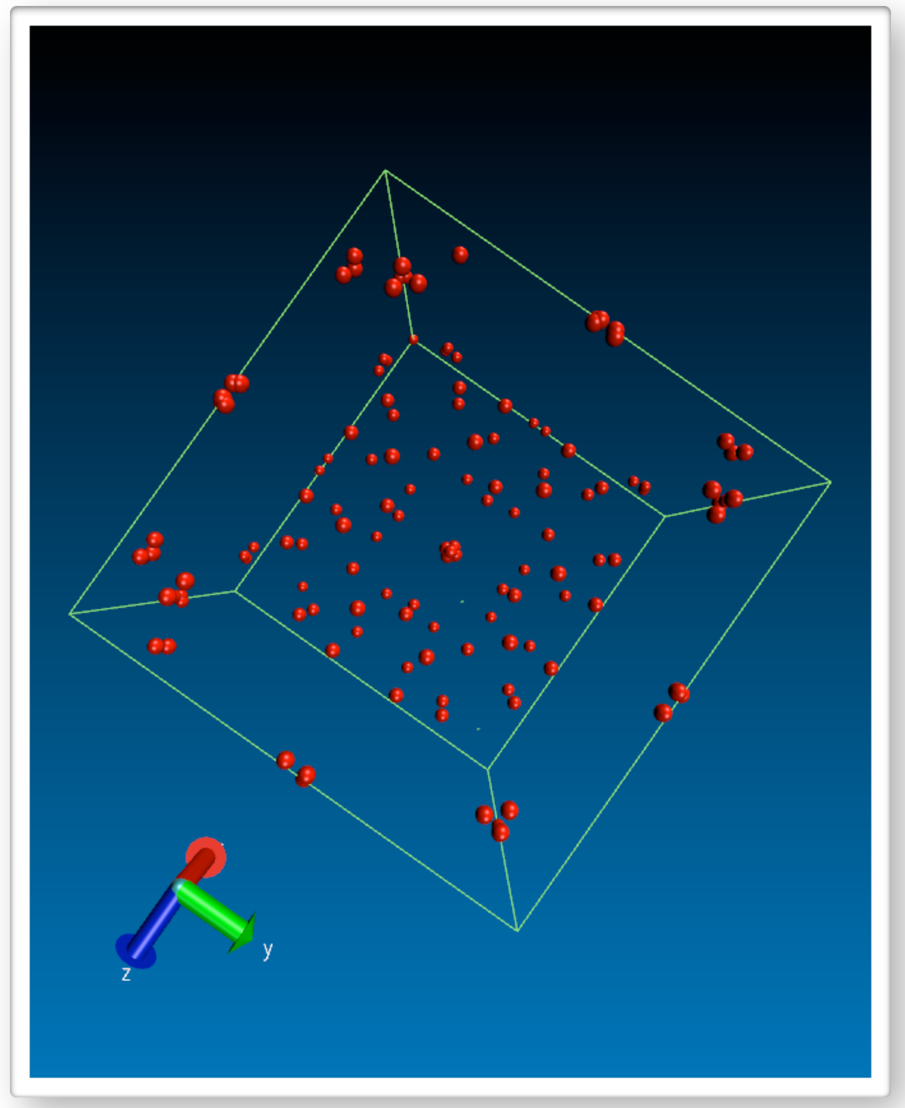

Without any channels, all nodes
are now inaccessible

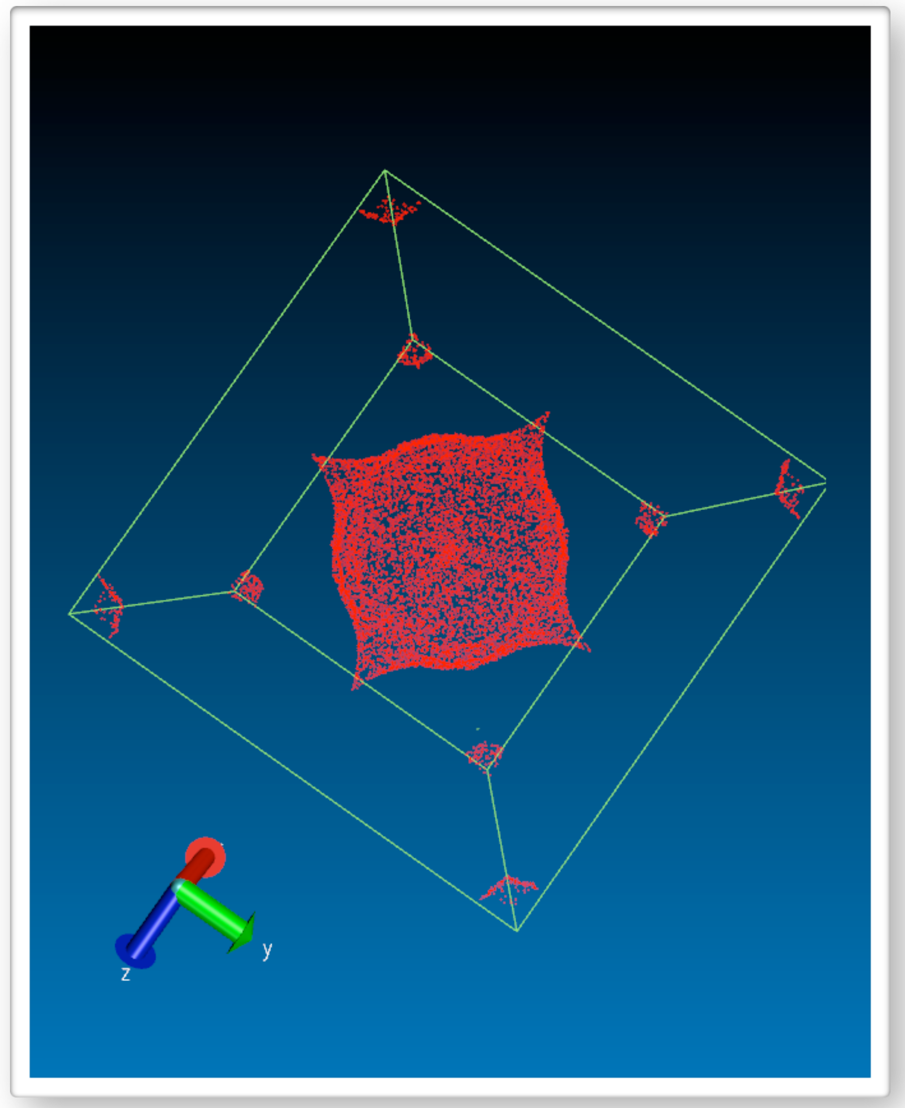

The interior cavity's surface thus
becomes inaccessible

Surface area computations

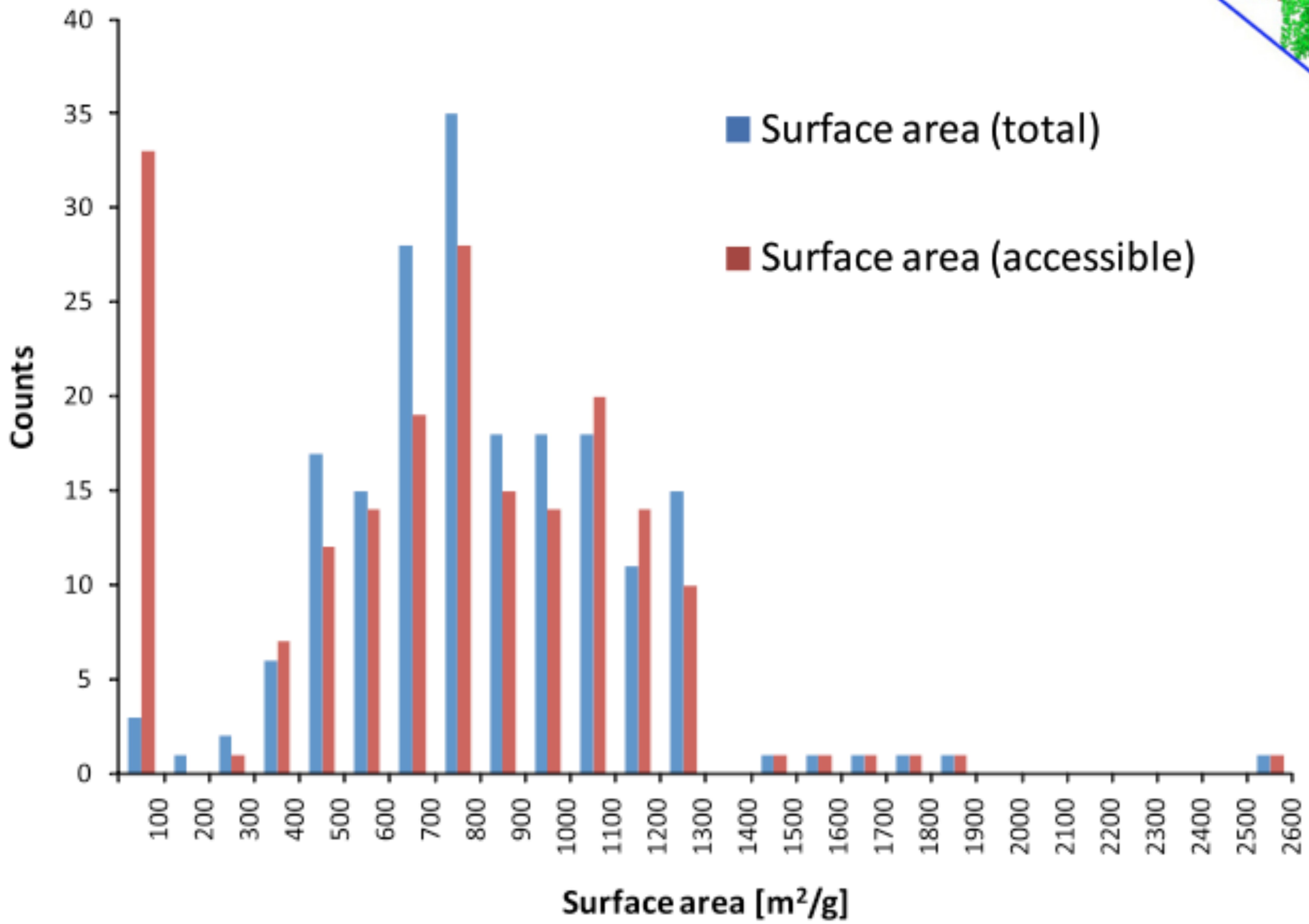

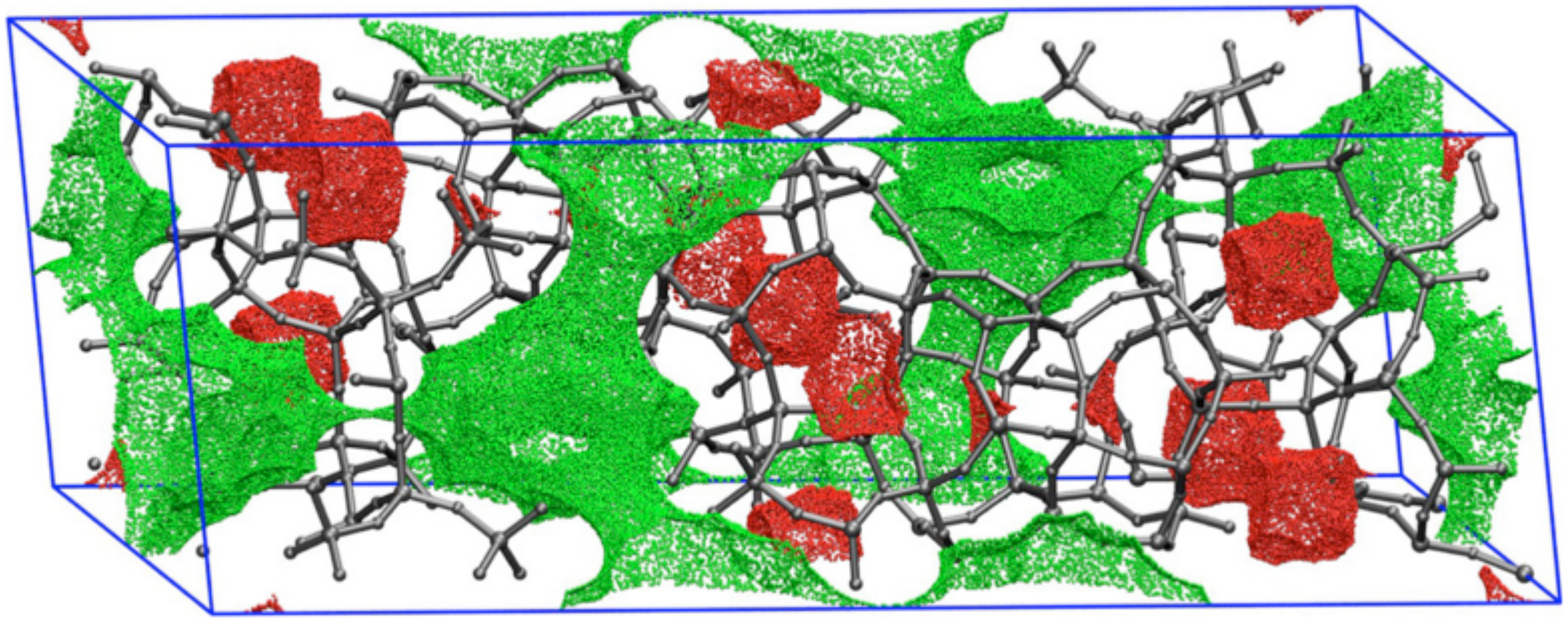

Accessible and inaccessible surface area for DDR zeolite

Accounting for inaccessible pockets significantly alters total surface area for zeolites in IZA database

T. F. Willems *et al.*, Microporous and Mesoporous Materials **149**, 134–141 (2012).

Screening for carbon capture materials

- Use porous materials as adsorbents:
  - Pump in flue gases from power plant to trap CO_2 while letting N_2 and other gases pass
  - Heat and purge CO_2 from adsorbent for sequestration
- Current technology has parasitic energy of 1060 kJ per kg CO_2

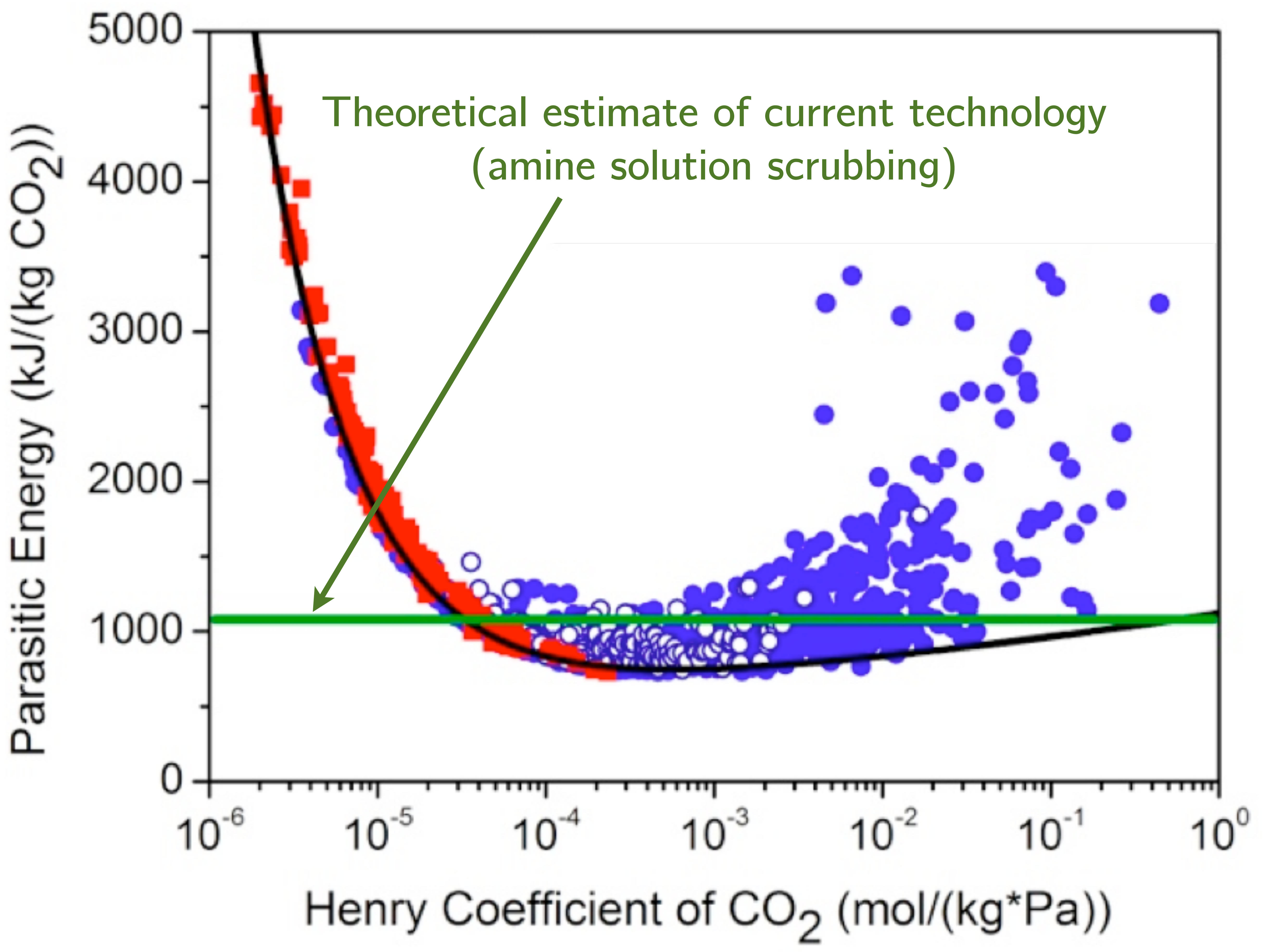

Use computational methods for:
- Pre-screening for large channels
- Surface area computations to determine absorbency
- Classification of optimal structures

L.-C. Lin *et al.*, *In Silico Screening of Carbon Capture Materials*, Nature Materials **11**, 633–641 (2012).

Examples of optimal structures

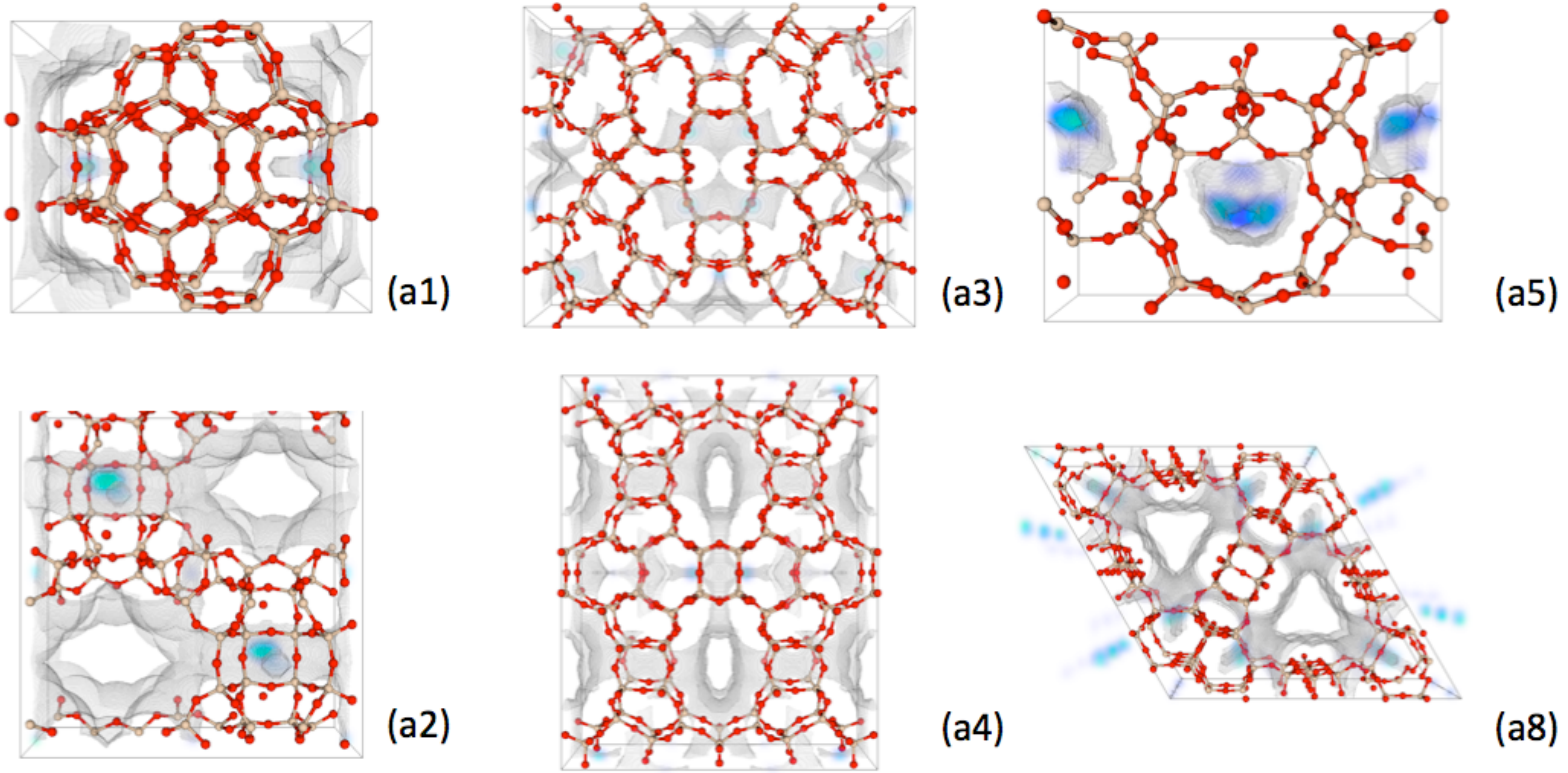

- Regions of blue represent those with high CO_2 adsorption
- Surprisingly different channel topologies among optimal materials

Zeo++: a software library for cheminformatics

(containing all of the algorithms described plus the following)

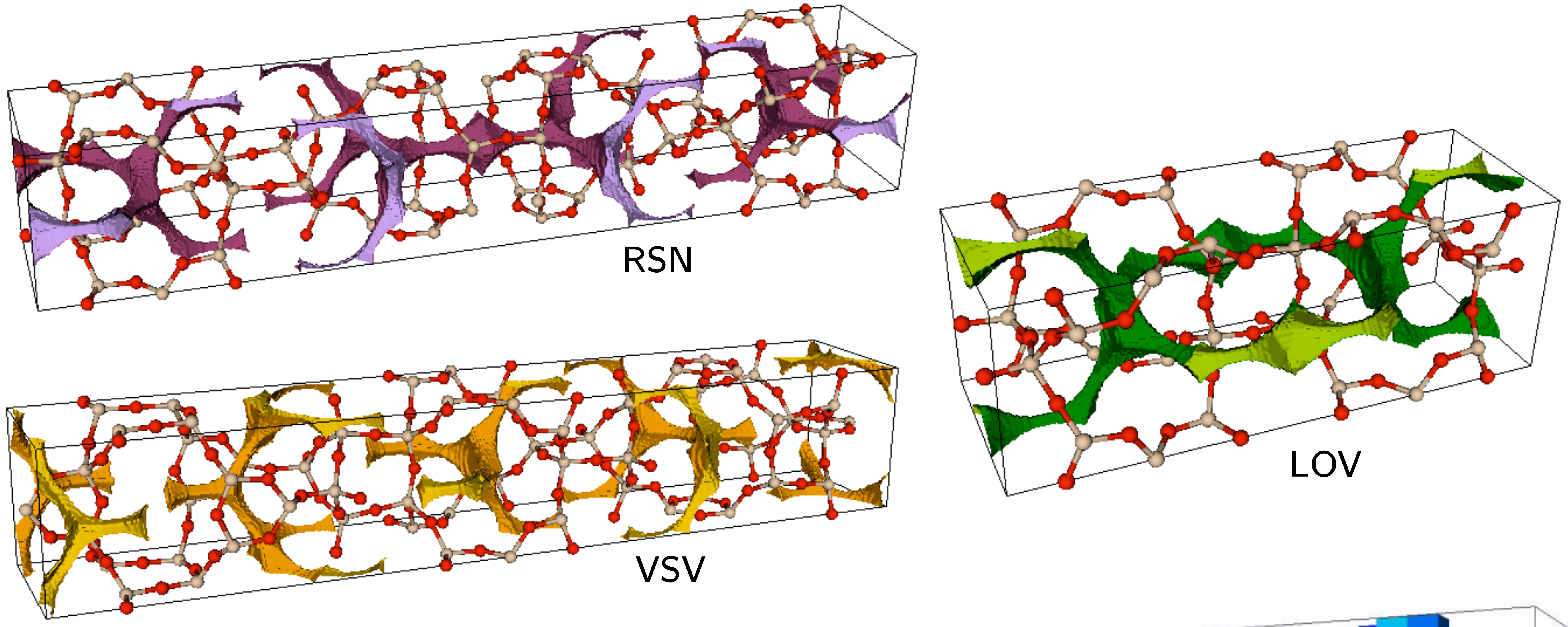

Identification of similar and dissimilar structures via Voronoi "hologram" comparison

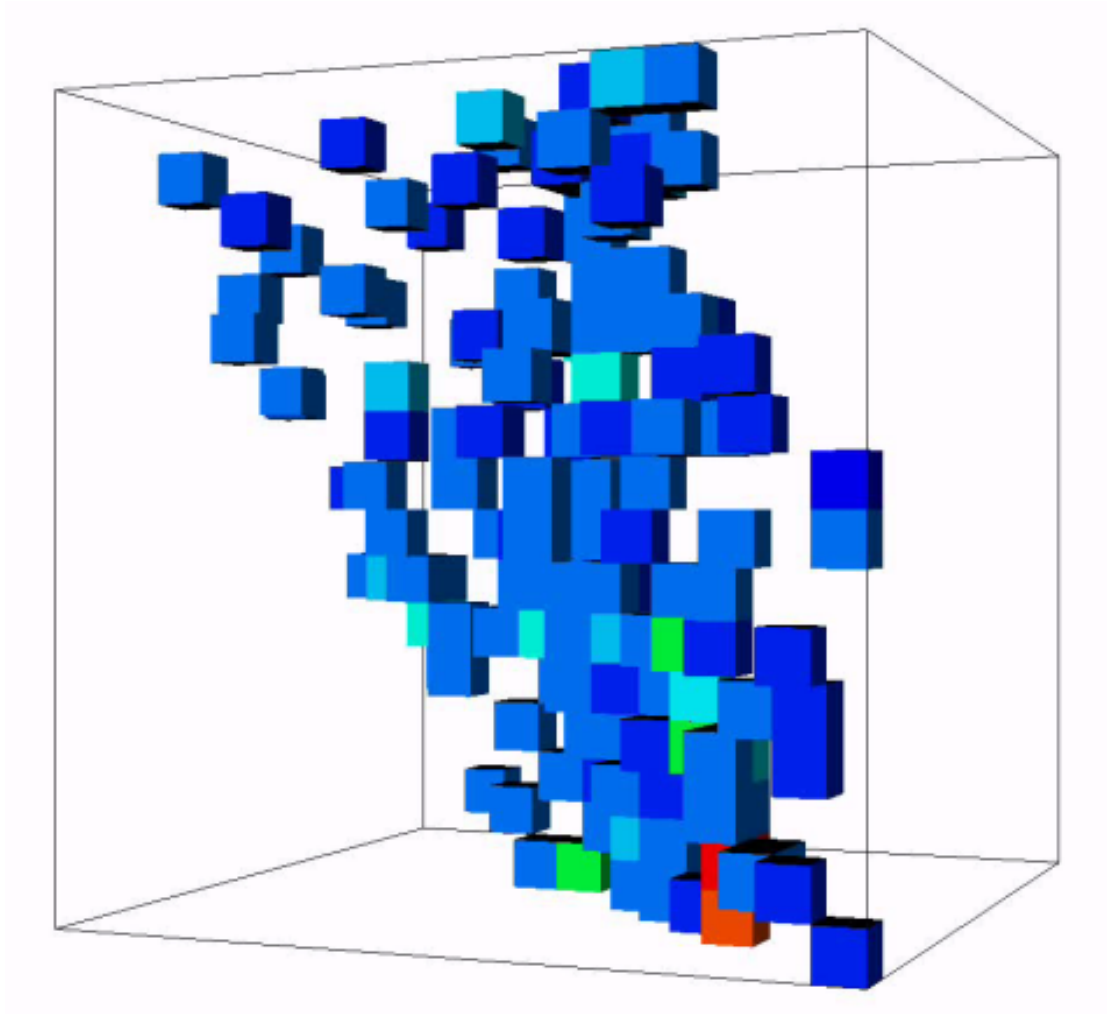

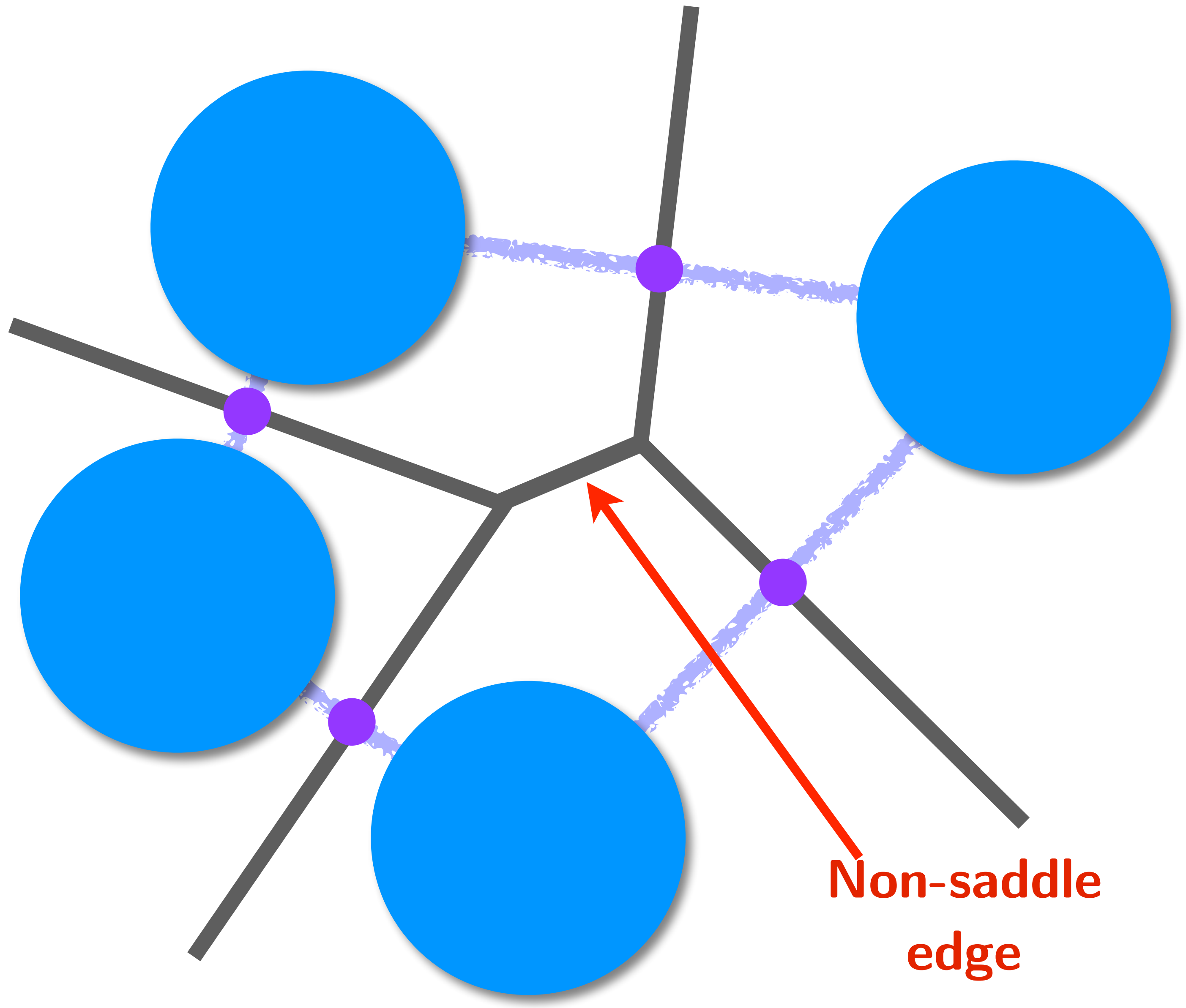

Network simplification via the removal of non-saddle edges

https://zeoplusplus.org

M. Pinheiro *et al.*, J. Mol. Graph. Model. **44**, 208–219 (2013).

Effect of atom radius

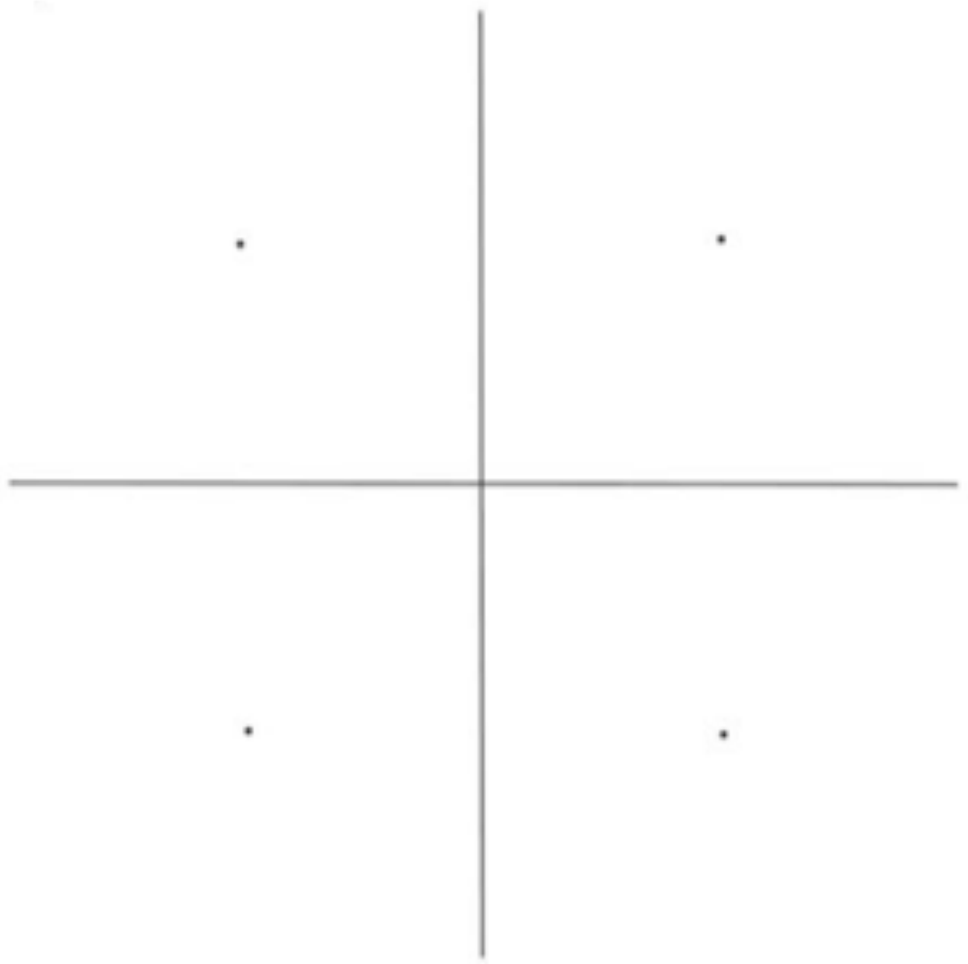

Voronoi tessellation
$d(\mathbf{x}, \mathbf{x}_i) < d(\mathbf{x}, \mathbf{x}_j)$

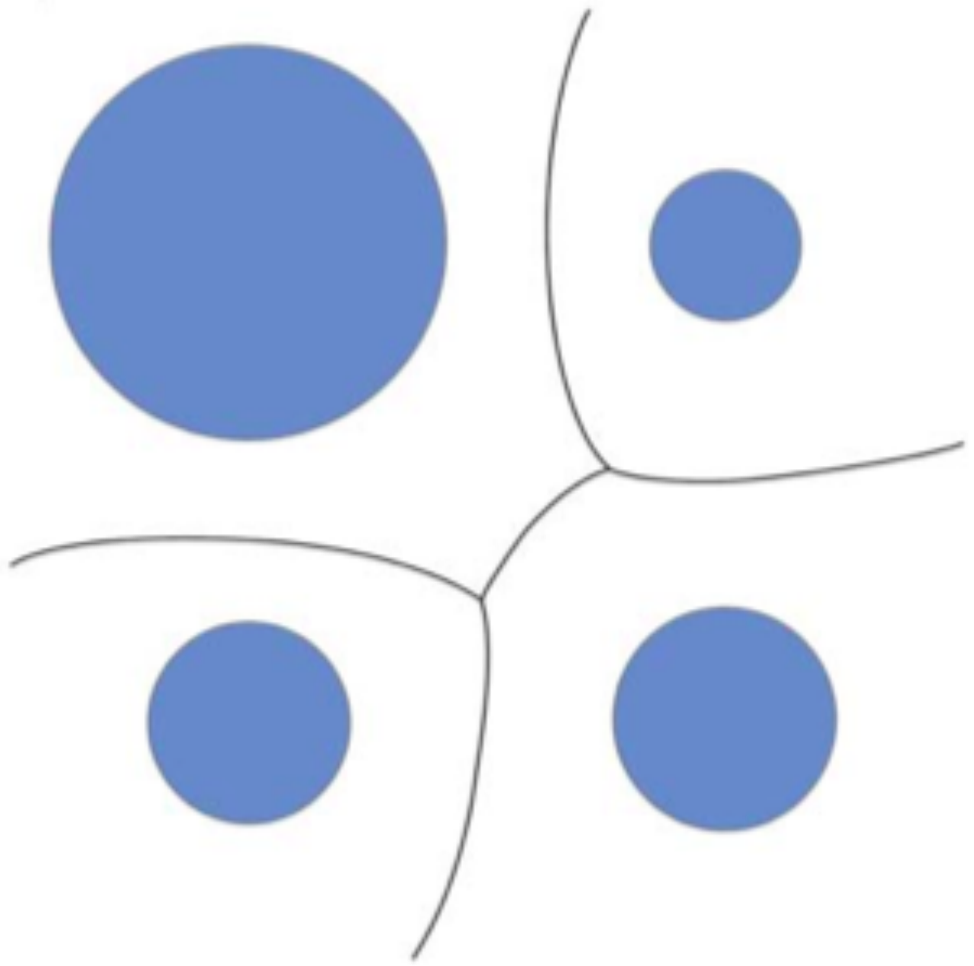

Voronoi S-cell
$d(\mathbf{x}, \mathbf{x}_i) - r_i < d(\mathbf{x}, \mathbf{x}_j) - r_j$

Radical tessellation
$d(\mathbf{x}, \mathbf{x}_i)^2 - r_i^2 < d(\mathbf{x}, \mathbf{x}_j)^2 - r_j^2$

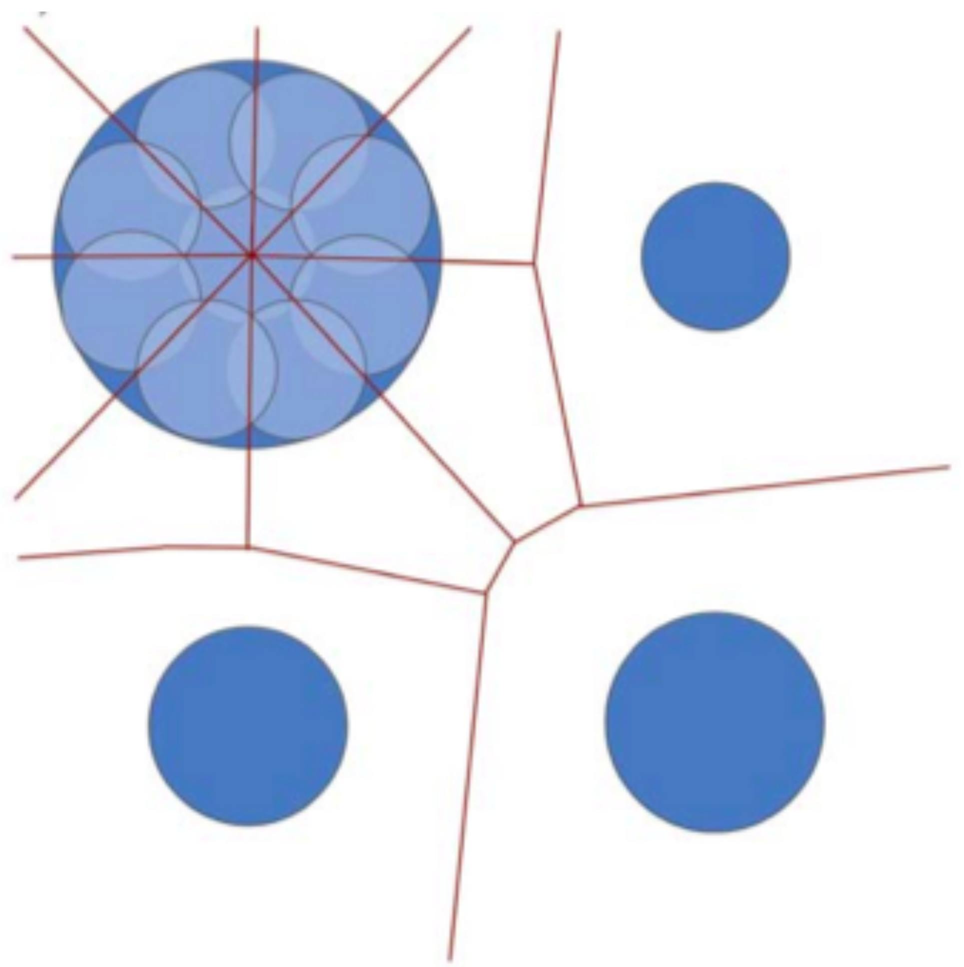

Sphere cluster approximation

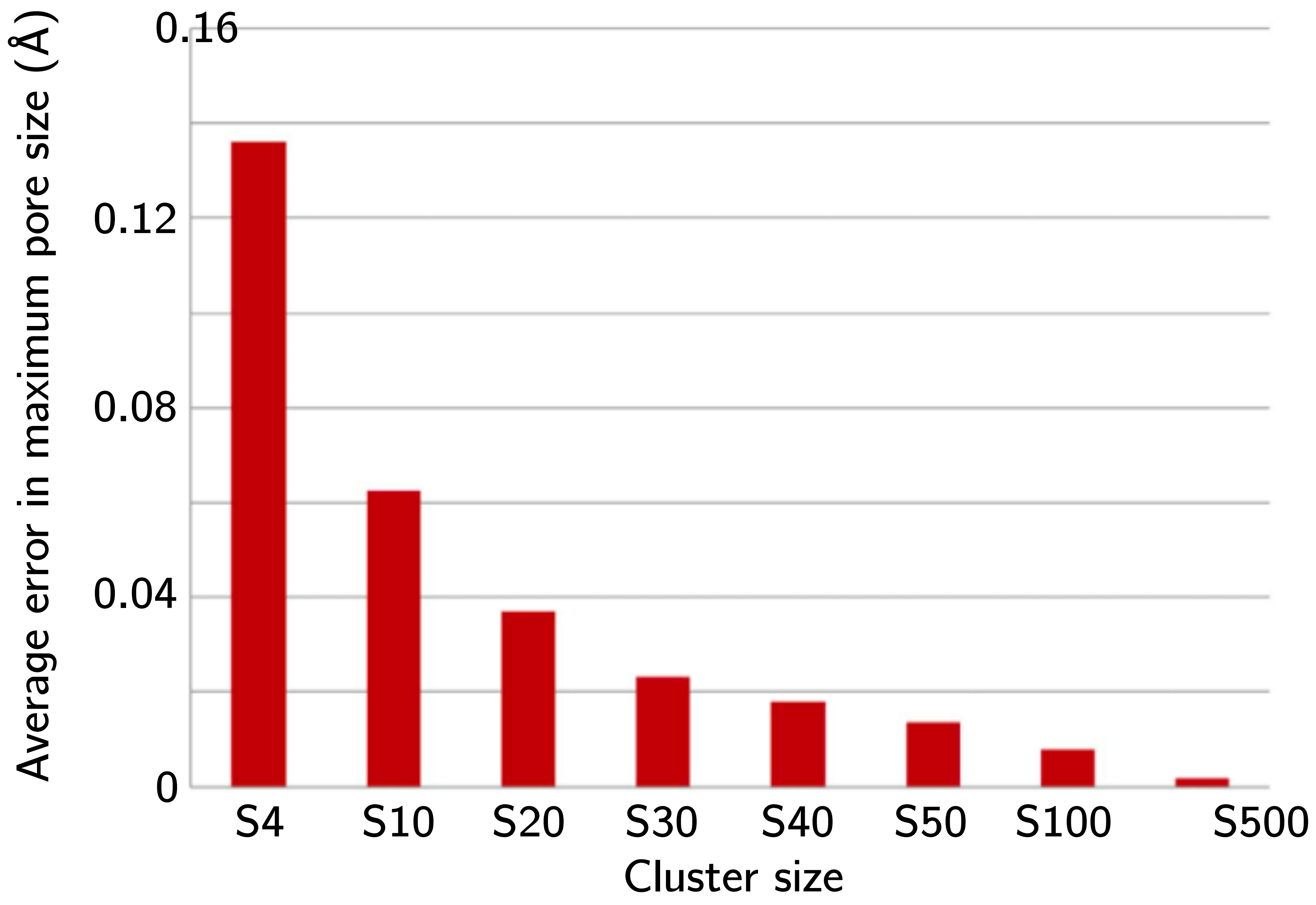

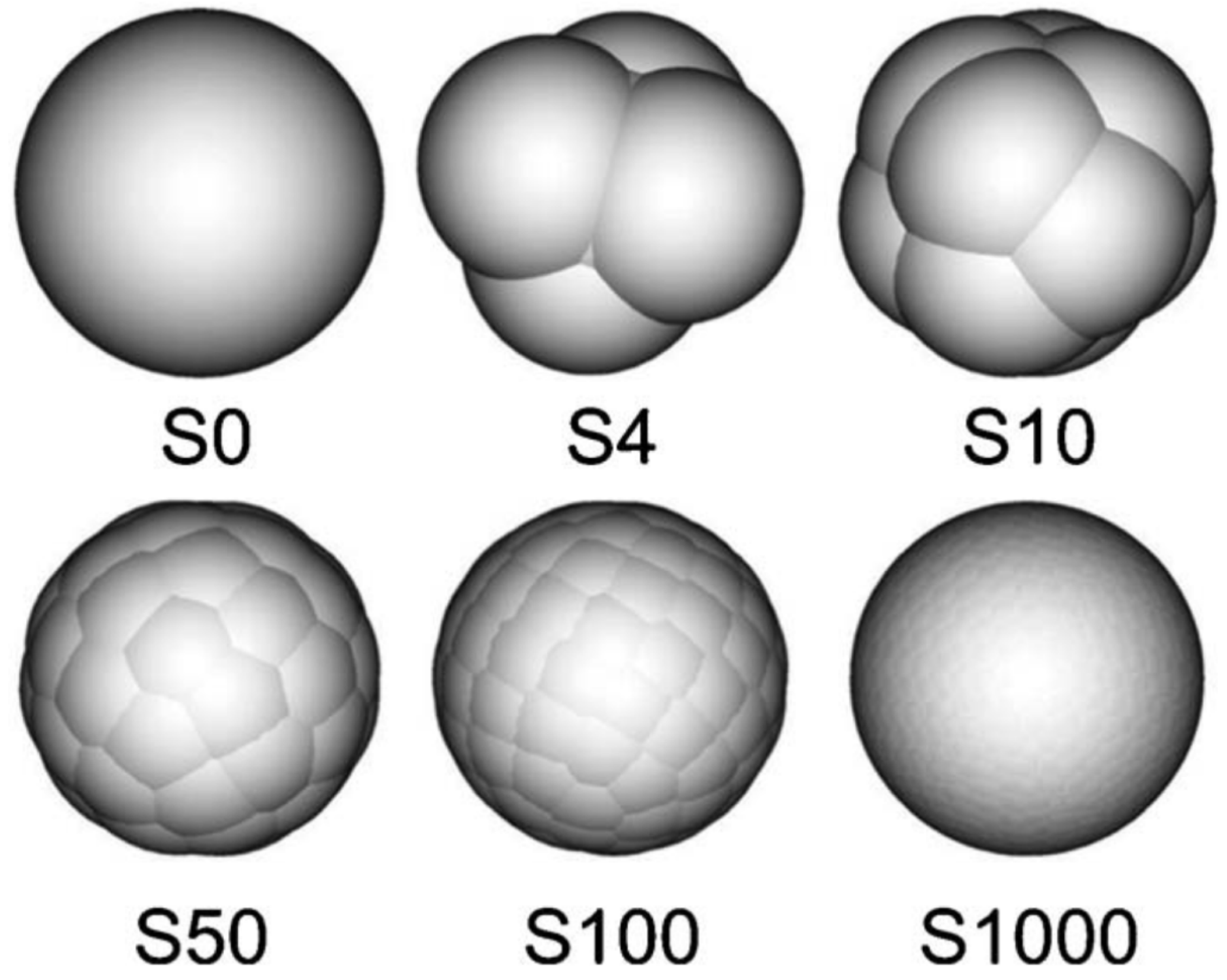

M. Pinheiro *et al.*, CrystEngComm **37**, 7531–7538 (2013).

Regularizing point arrangements

- Lloyd's algorithm: iteratively move points to the centroids of their Voronoi cells
- Mimics pattern formation PDEs and give direct description of region boundaries

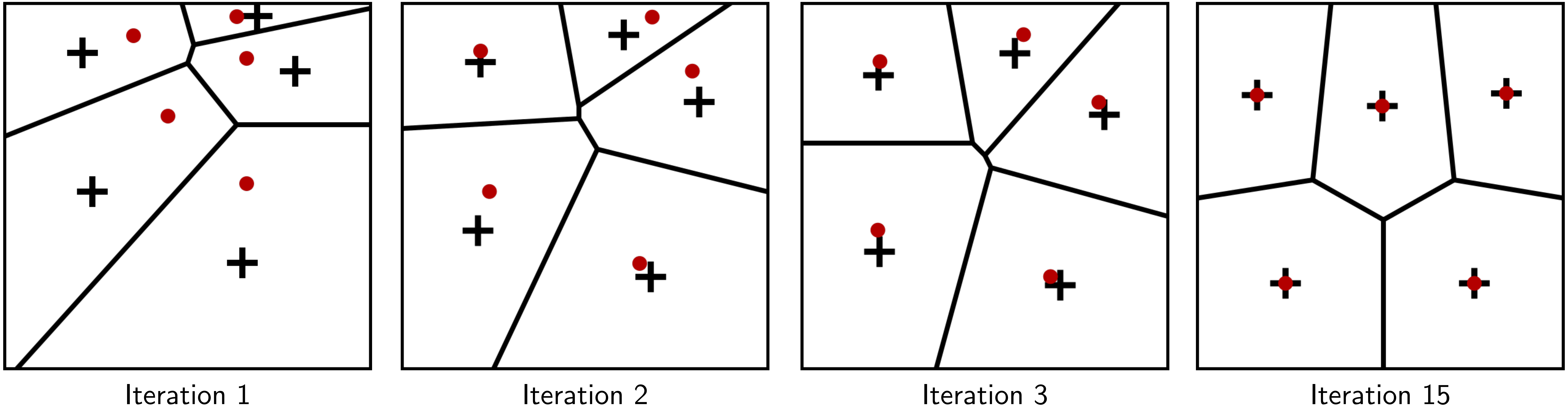

Converges to centroidal Voronoi tessellation (CVT)

Q. Du *et al.*, SIAM Review **41**, 637–676 (1999).

Lloyd's algorithm: example 2

- Start with 838 particles in a spiral and run 256 iterations of Lloyd's algorithm
- Particle positions even out
- Asymptotically in a large domain, the Voronoi cells become regular hexagons

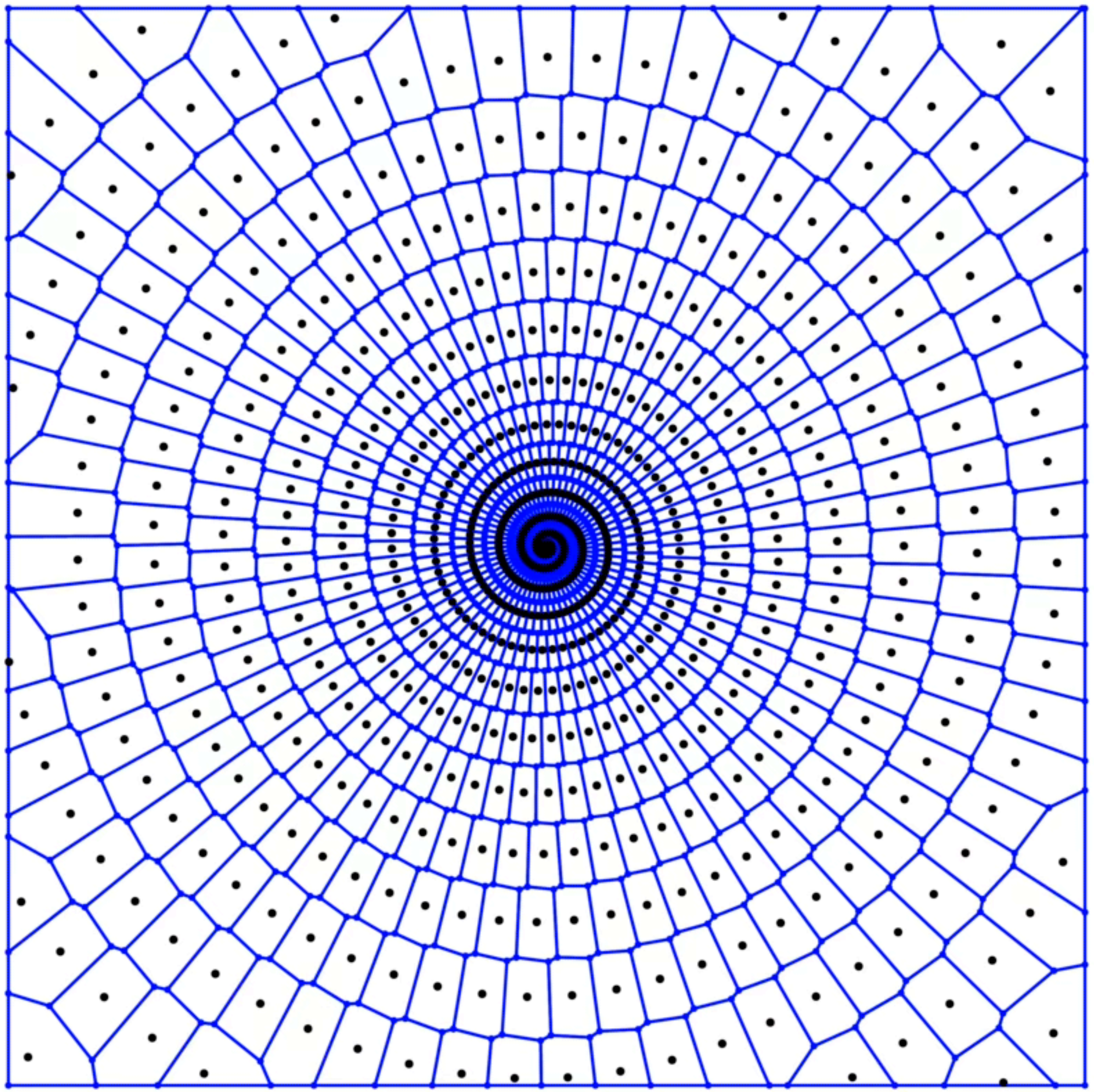

Lloyd's algorithm: example 2

- Start with 1000 particles in a domain covering a fifth of each side, and run 1024 Lloyd iterations
- Short-range density fluctuations are quickly damped out
- Long-range density fluctuations take longer to damp out

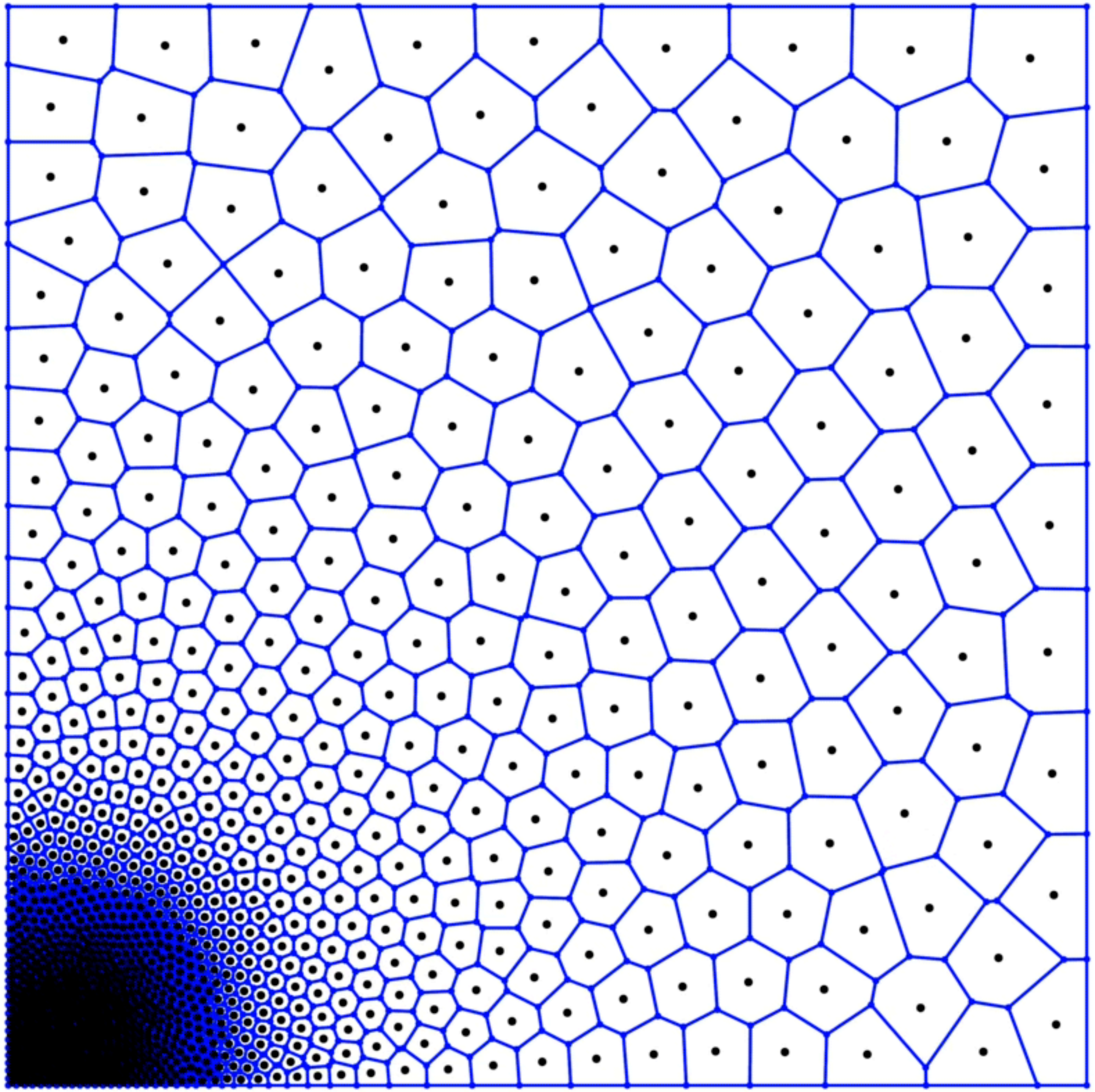

Mesh generation with Lloyd's algorithm

- The Delaunay triangulation of the particles after applying Lloyd iterations is a good computational mesh
- Tends to favor near-equilateral triangles, which are good for numerical methods like the finite-element method (FEM)

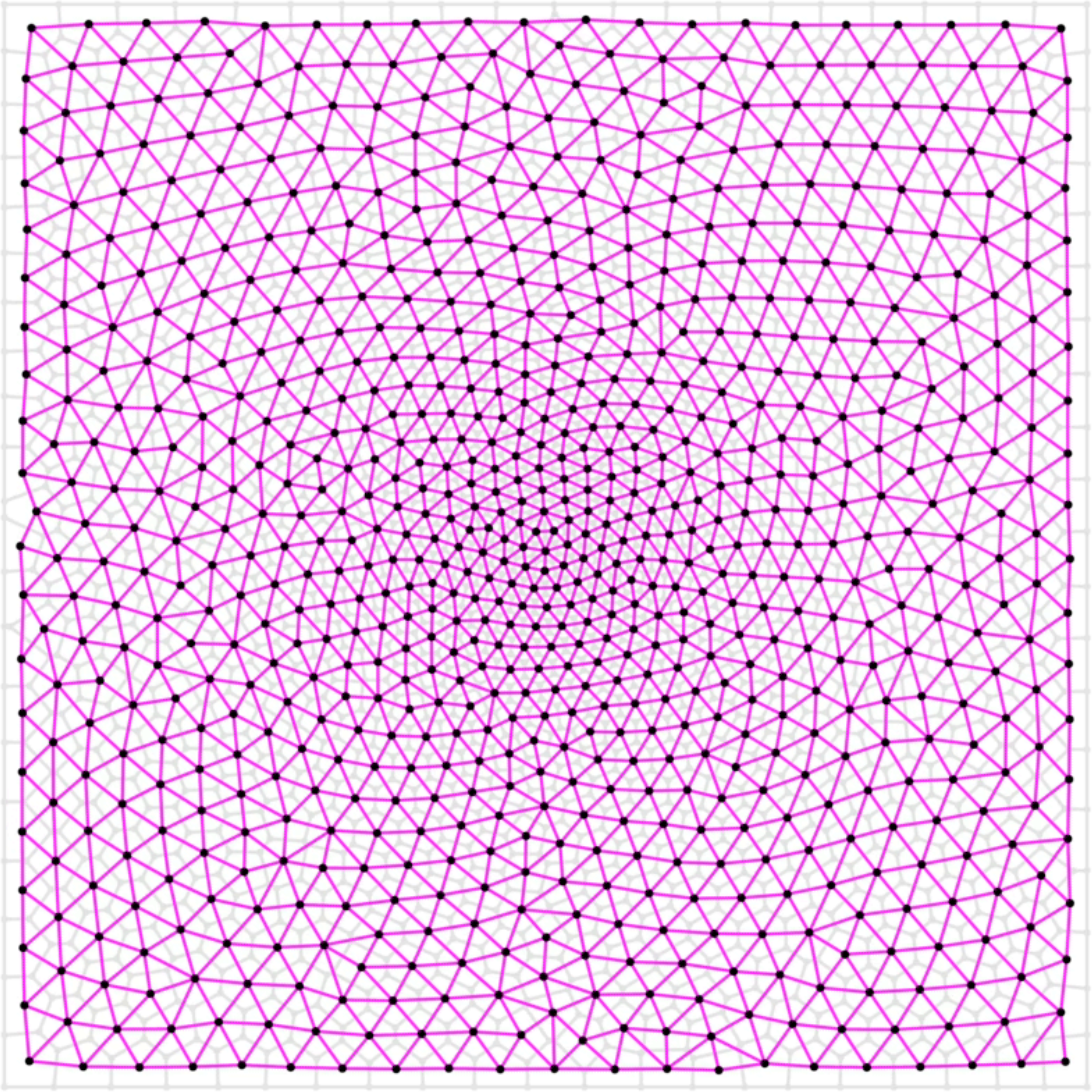

Meshing in complicated domains

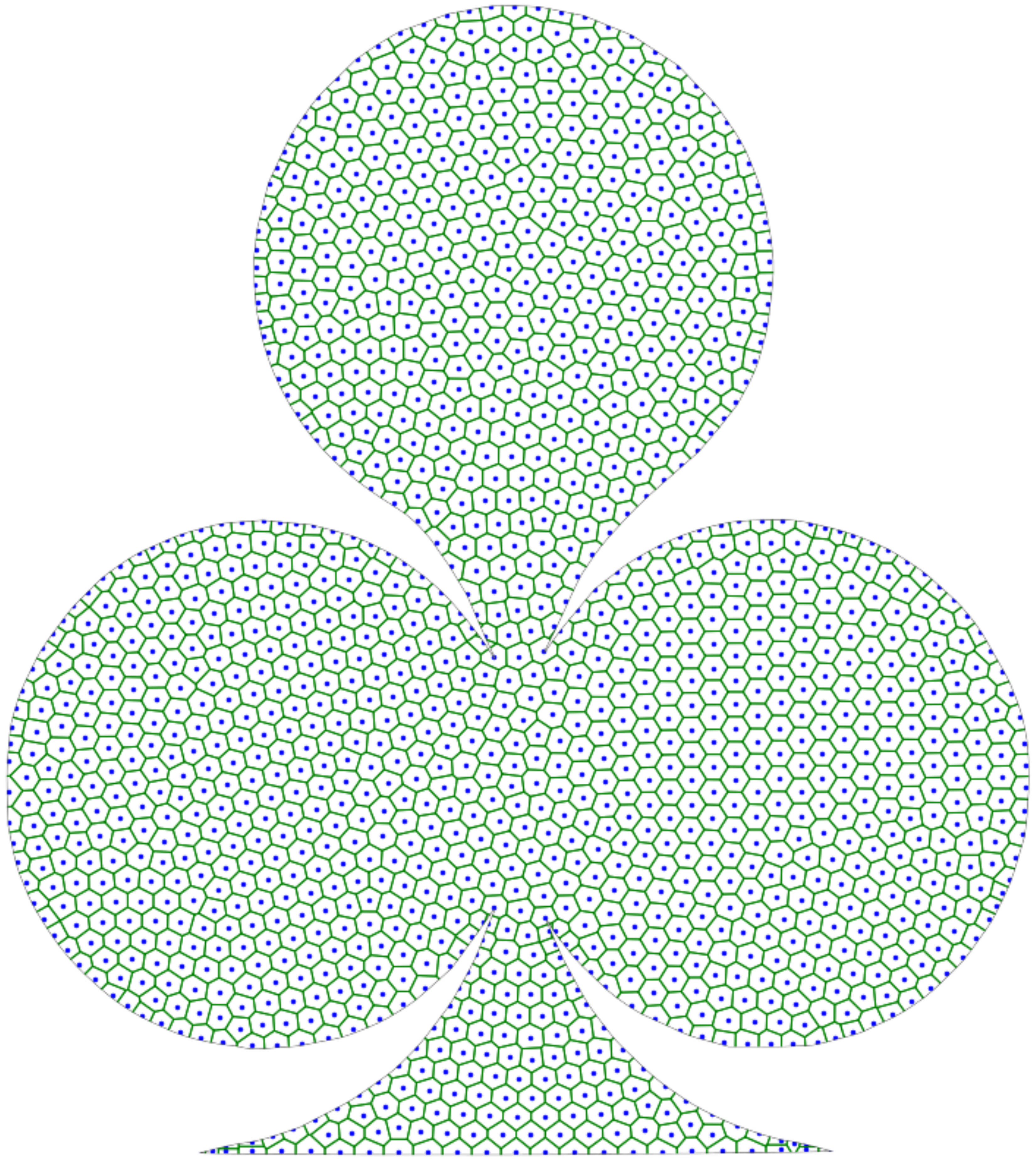

Voronoi cells in club shape after Lloyd's algorithm

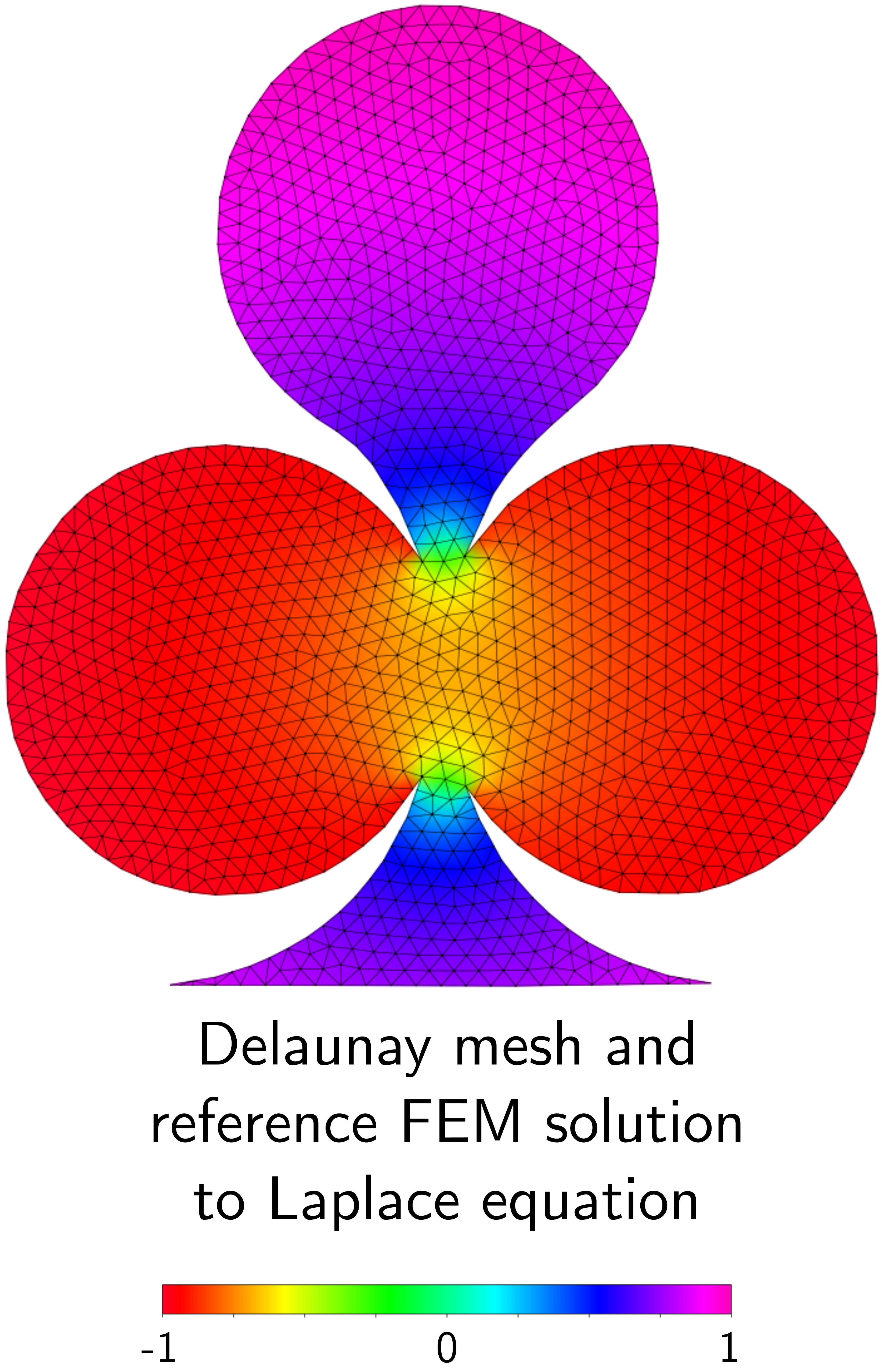

Delaunay mesh and reference FEM solution to Laplace equation

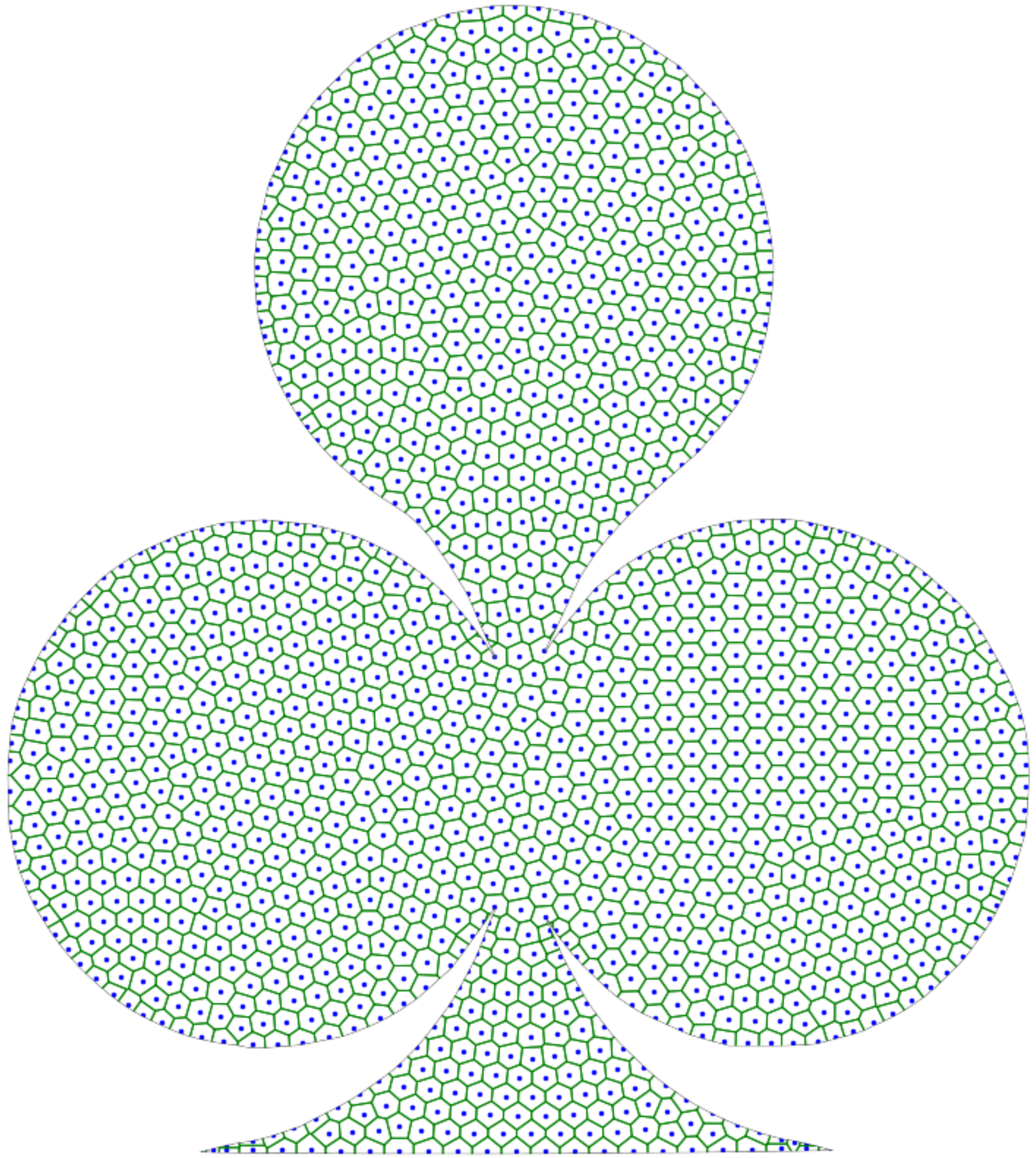

Voronoi cells in club shape after Lloyd's algorithm

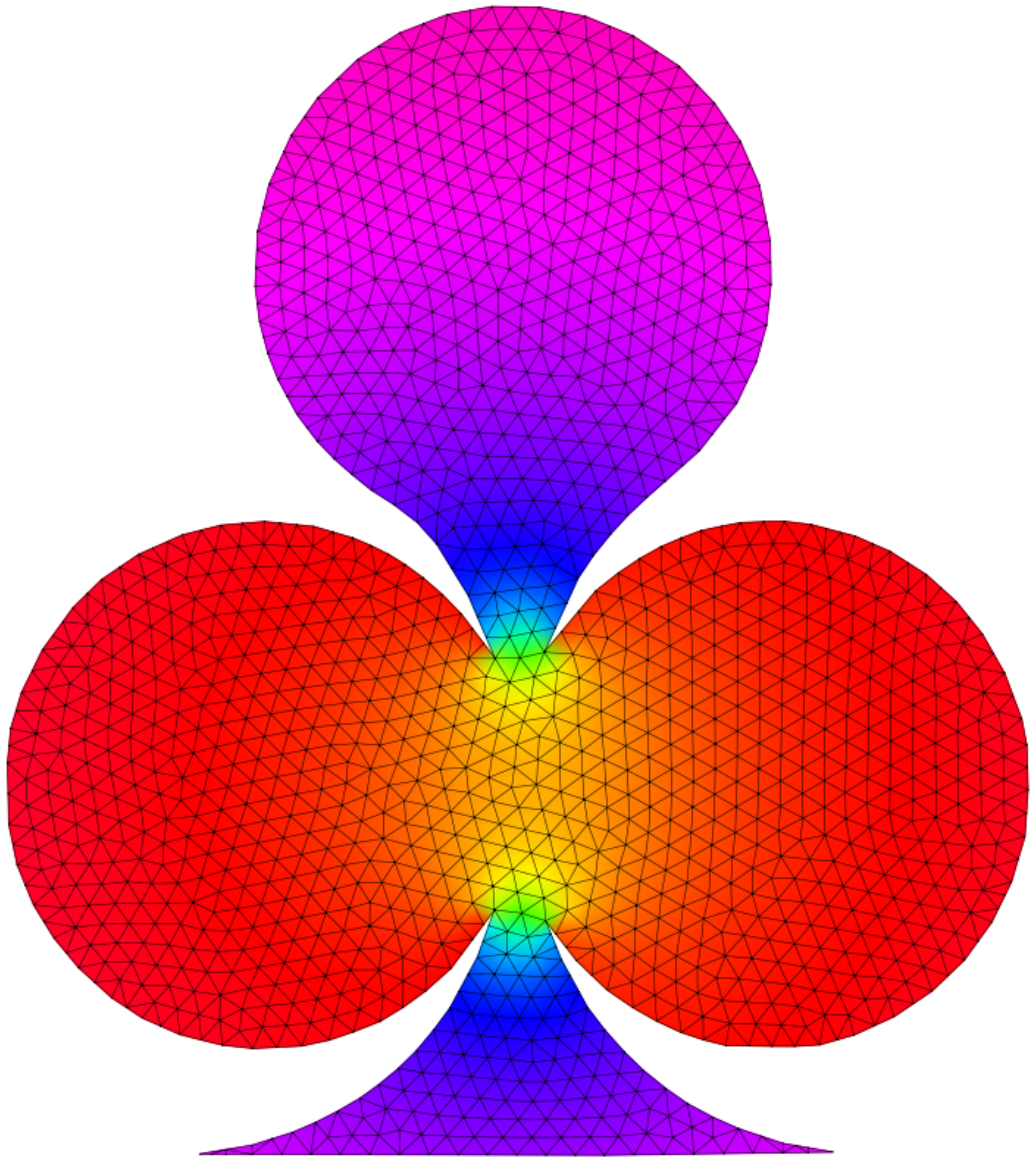

Delaunay mesh and reference FEM solution to Laplace equation

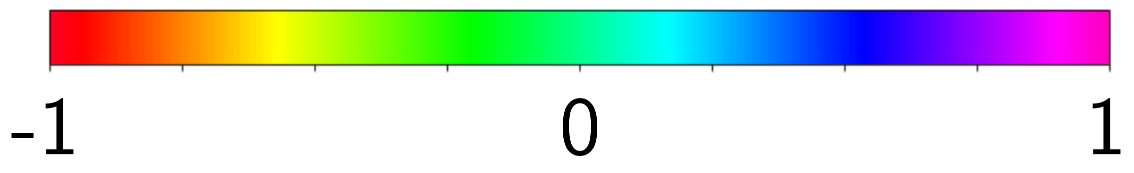

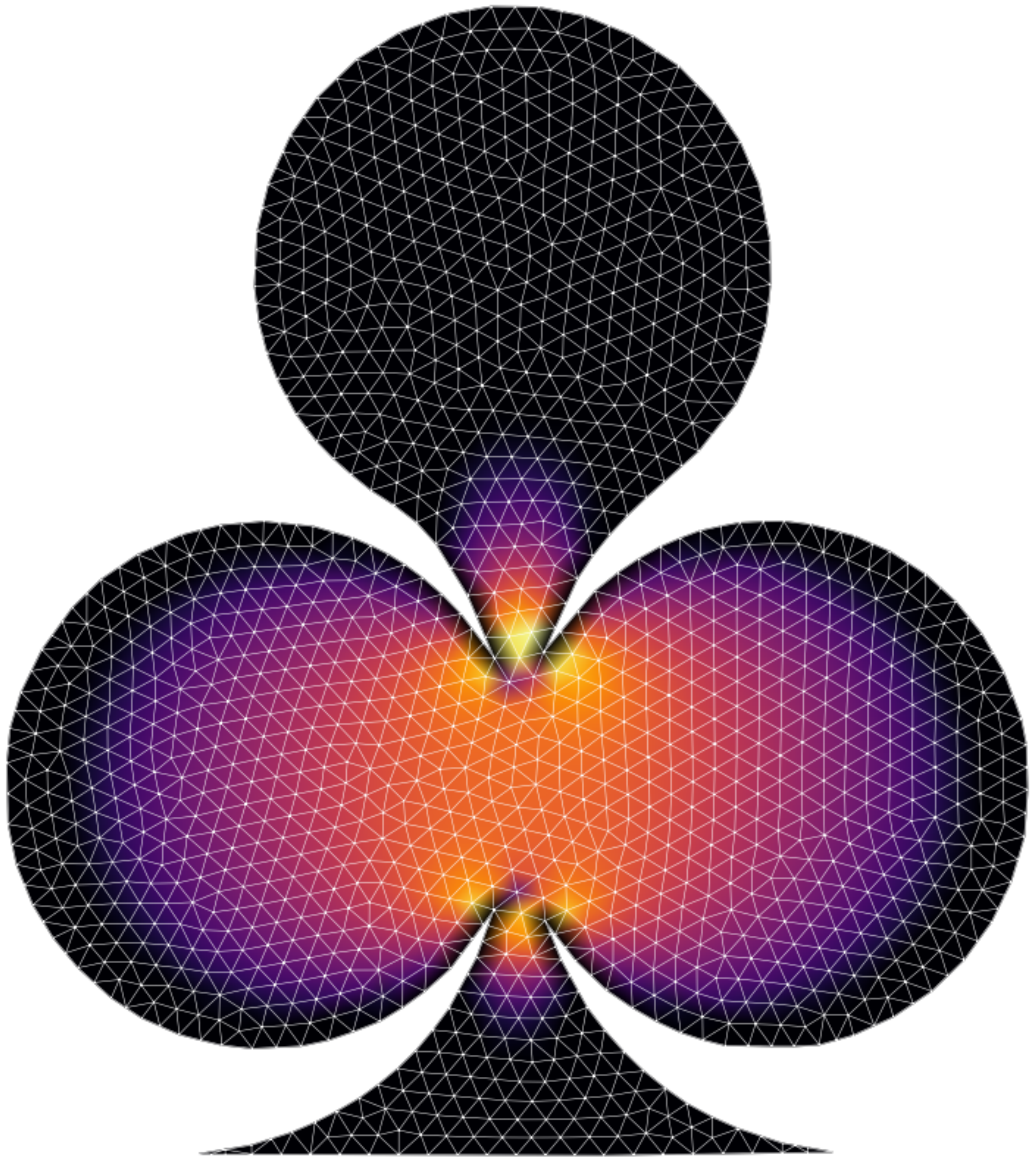

Error between FEM solution and exact solution

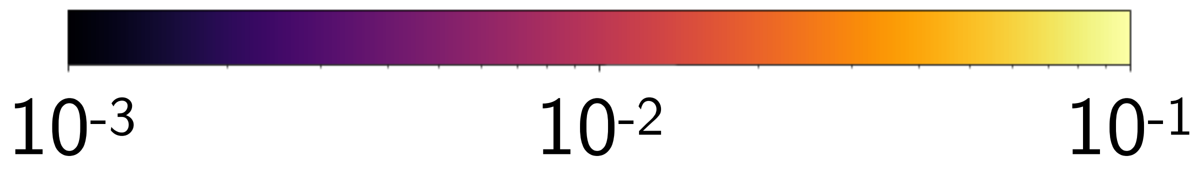

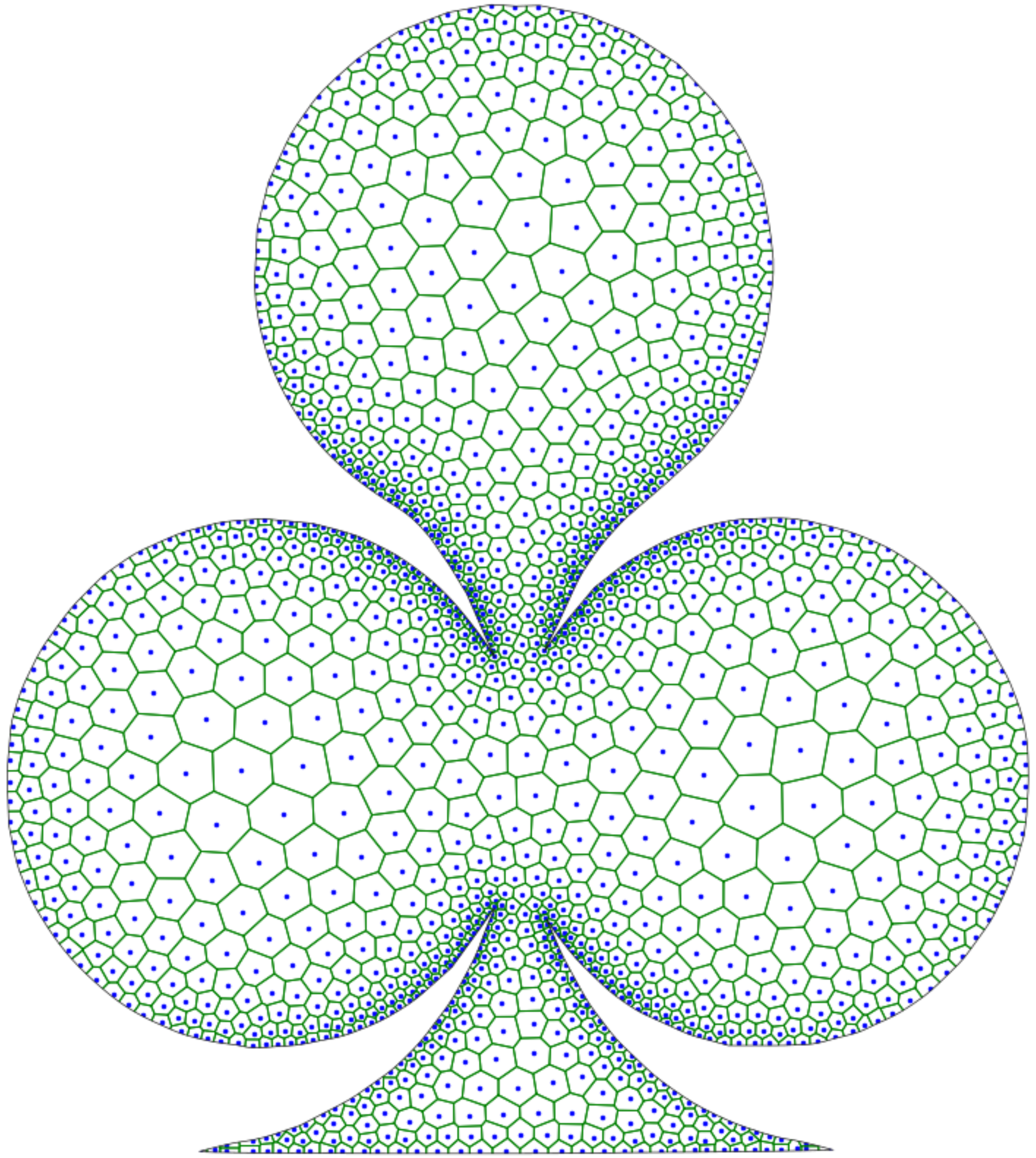

Voronoi cells in club shape after Lloyd's algorithm (with weighting)

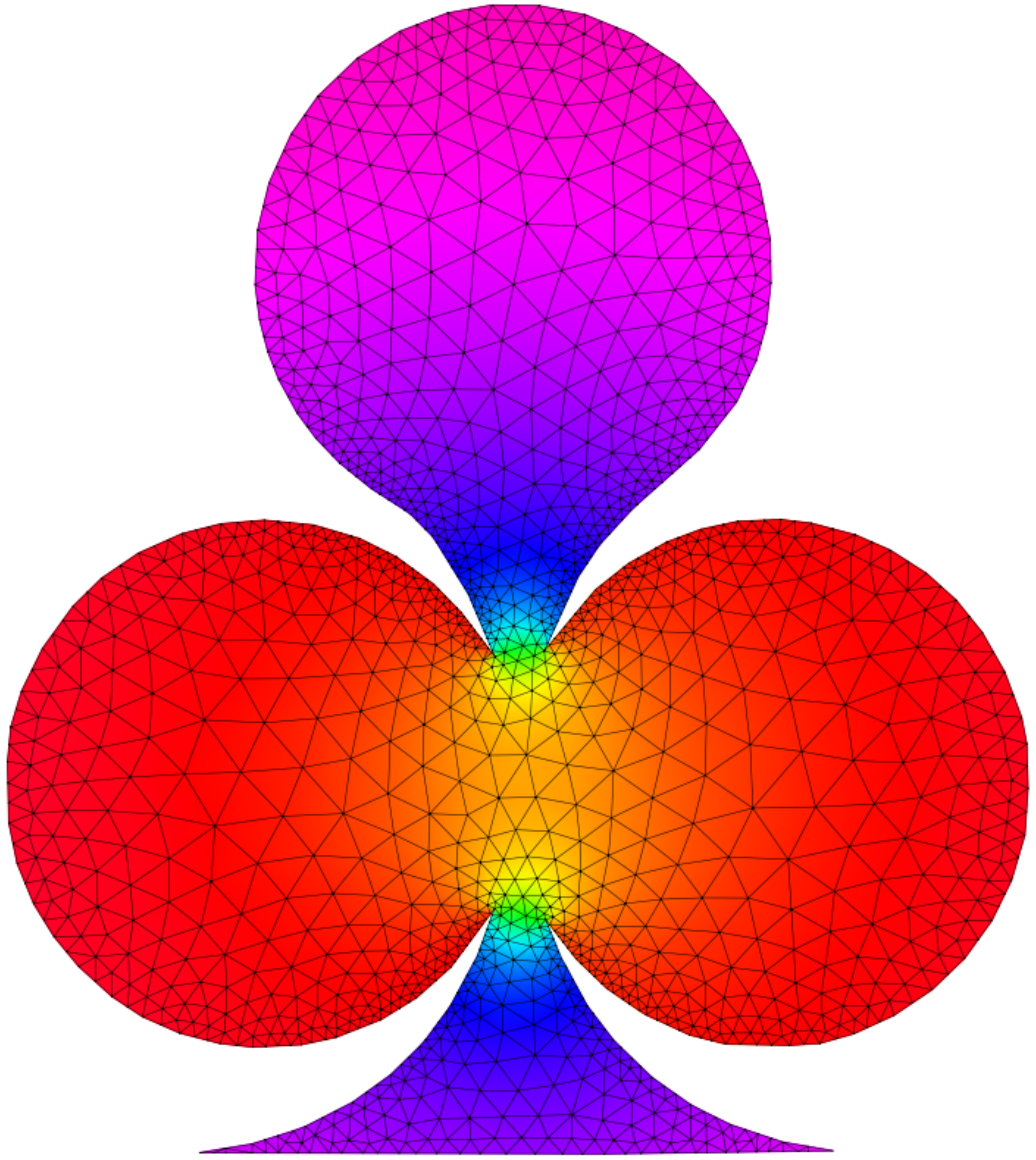

Delaunay mesh and reference FEM solution to Laplace equation

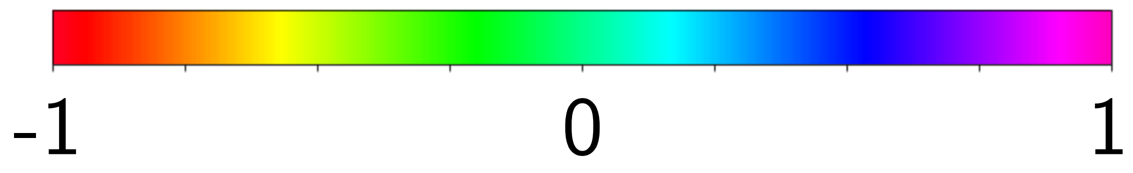

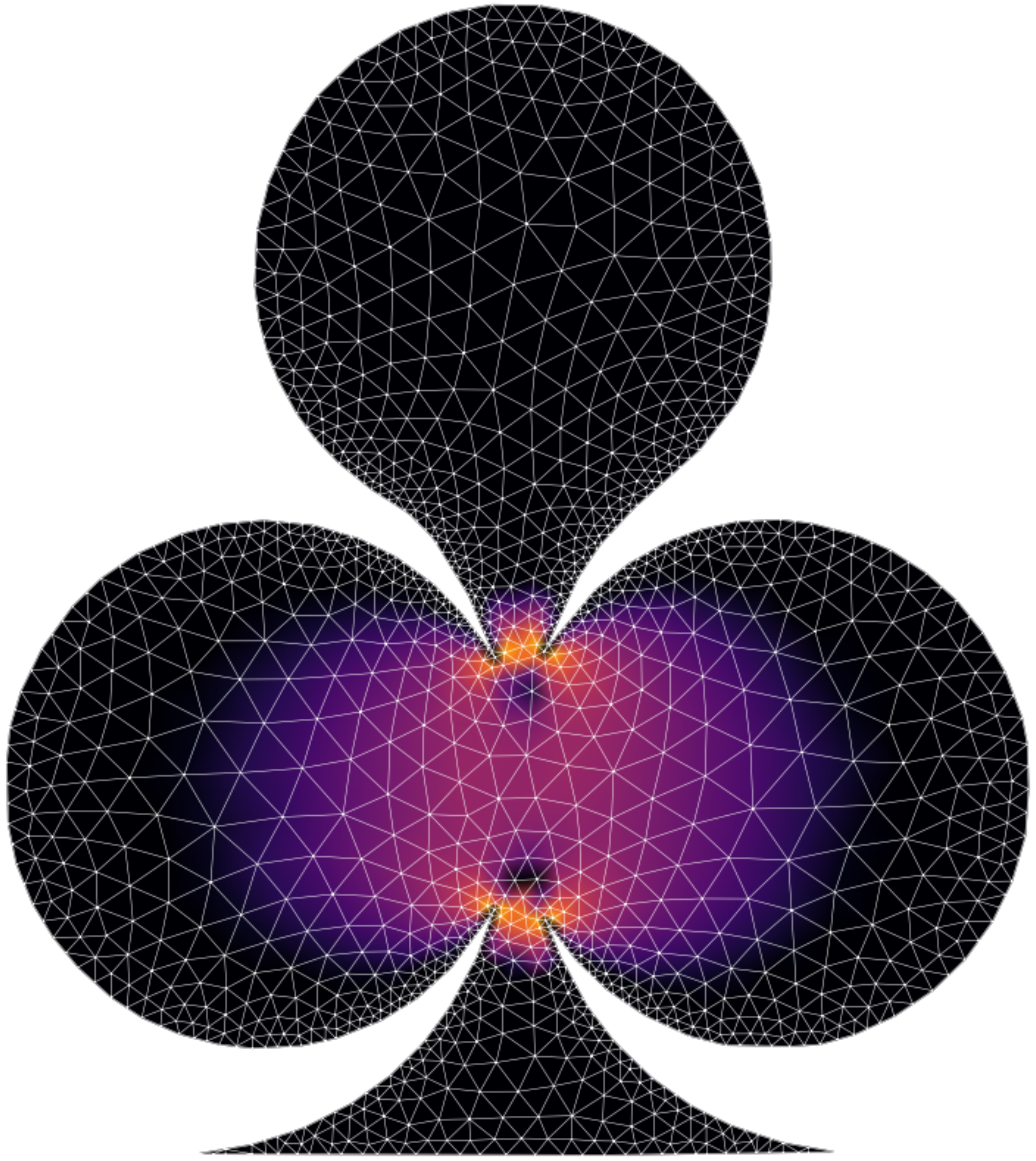

Error between FEM solution and exact solution

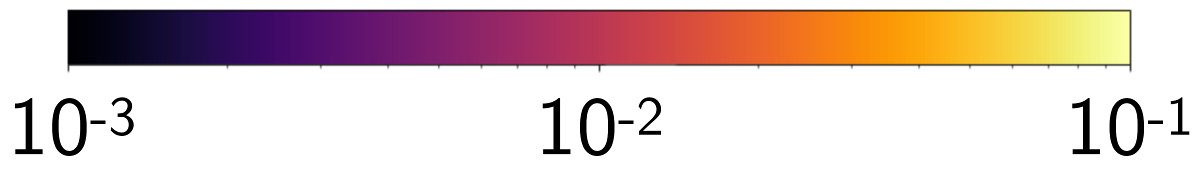

Three-dimensional domains

Using TriMe++ (TRIangular MEshing)

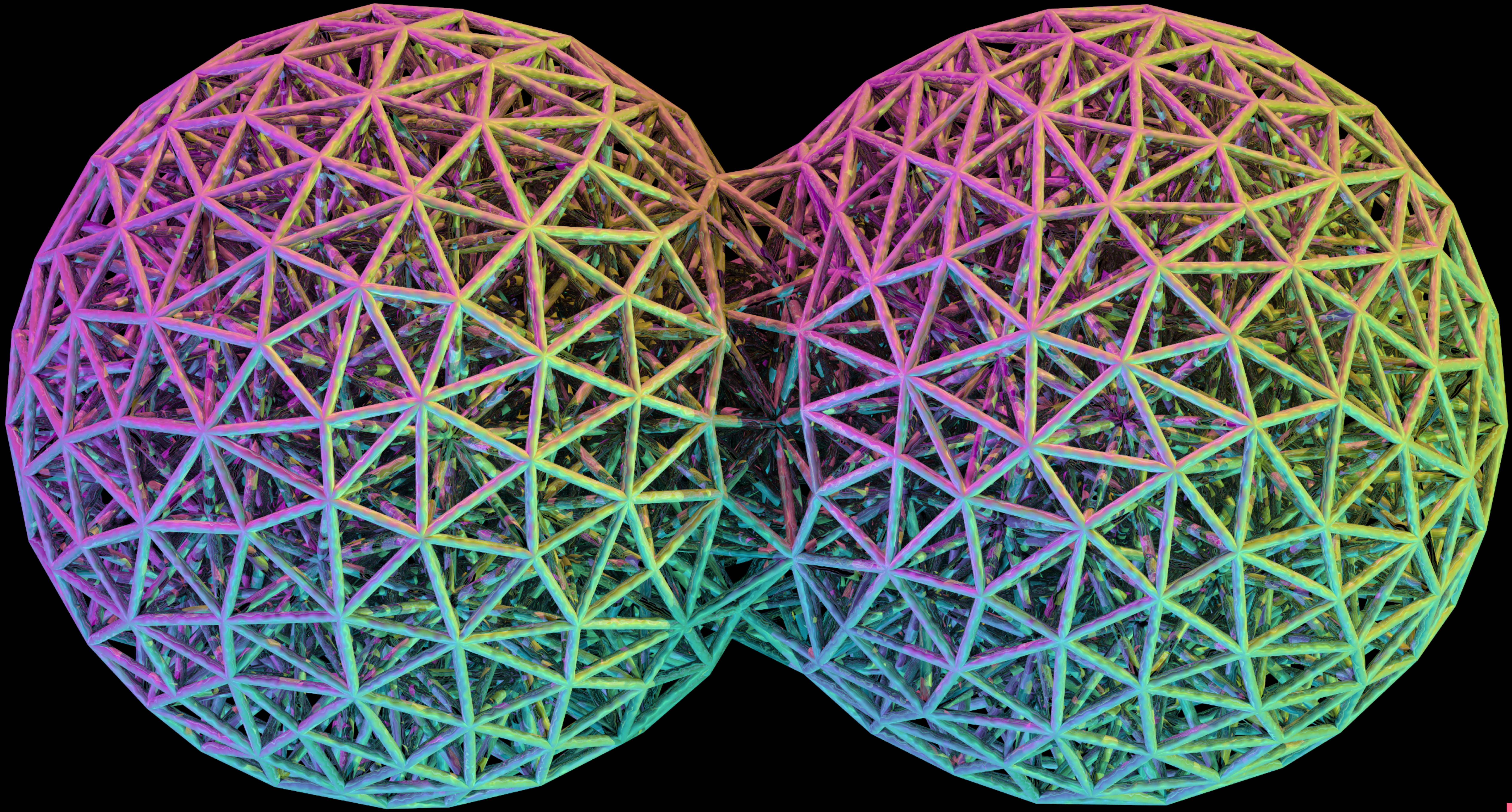

Jiayin Lu

(Using a combination of Lloyd's algorithm and the DistMesh algorithm)

J. Lu *et al.*, *An extension to Voro++ for multithreaded computation of Voronoi cells*, Comput. Phys. Commun. **291**, 108832 (2023).

J. Lu and C. H. Rycroft, *TriMe++: Multithreaded triangular meshing in two dimensions*, arXiv: 2309.13824 (2023).

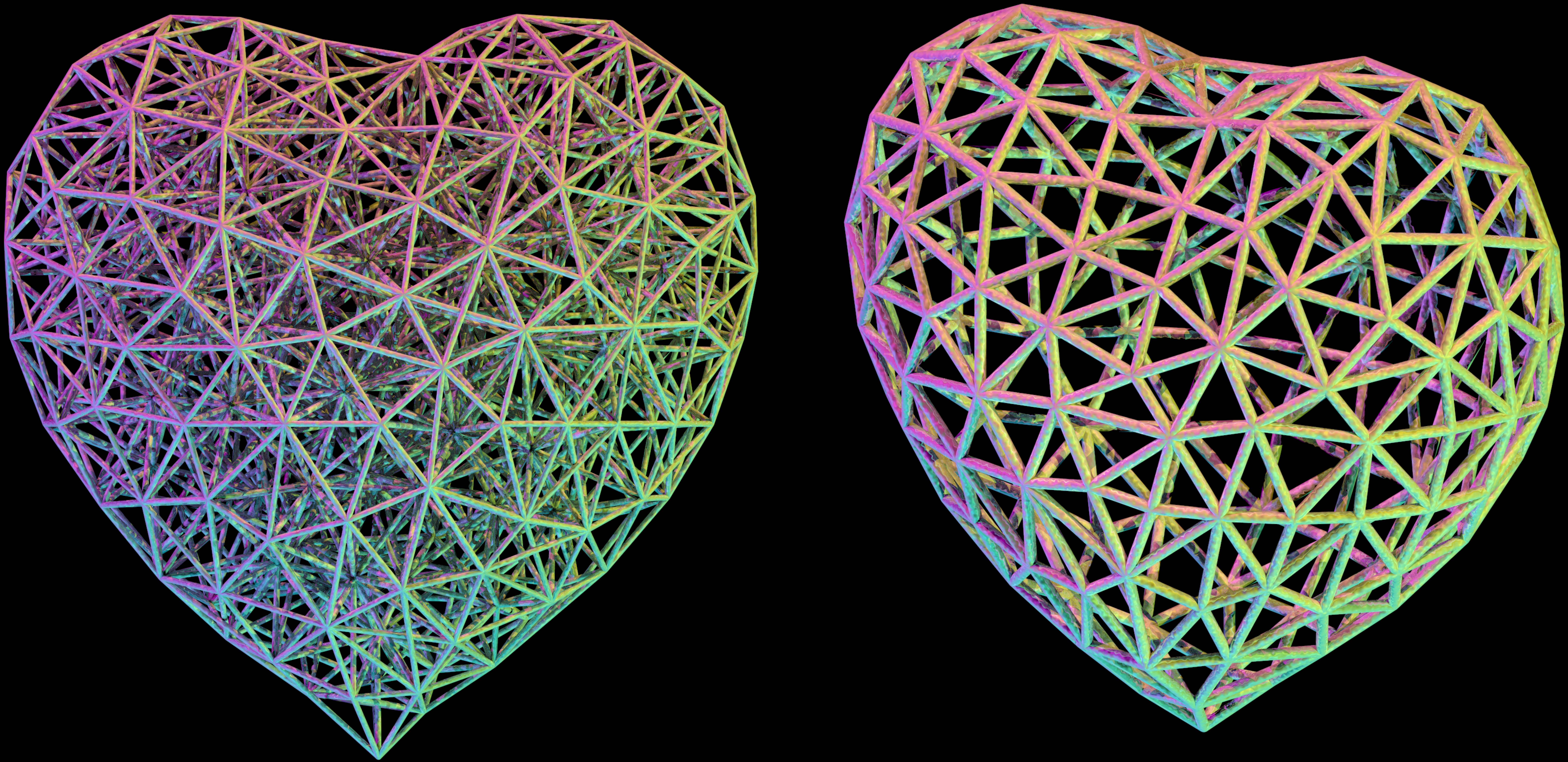

Topological considerations

- In 2D, three Voronoi cells will meet at a vertex
- Special arrangements (*e.g.* lattices) may lead to four or more Voronoi cells meeting at a vertex
- Floating point errors may lead to the creation of small extra faces
- The Voronoi topology of the cells may be not be consistent with each other

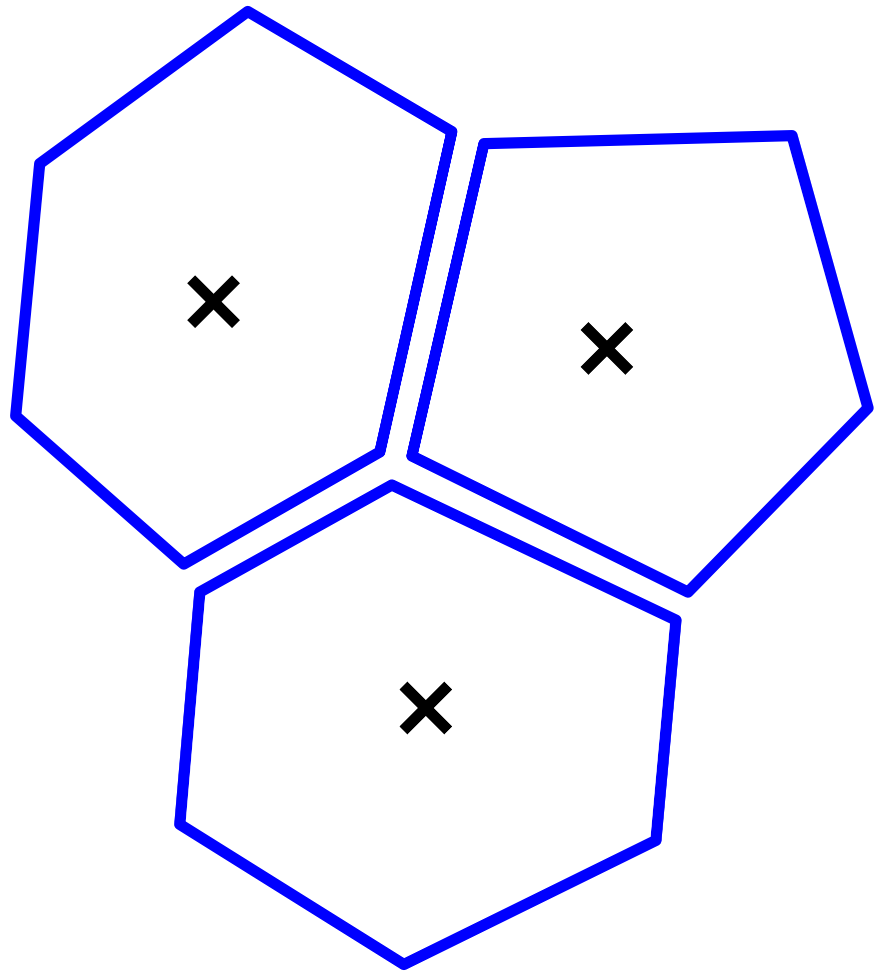

Typical case with three Voronoi cells meeting at a vertex

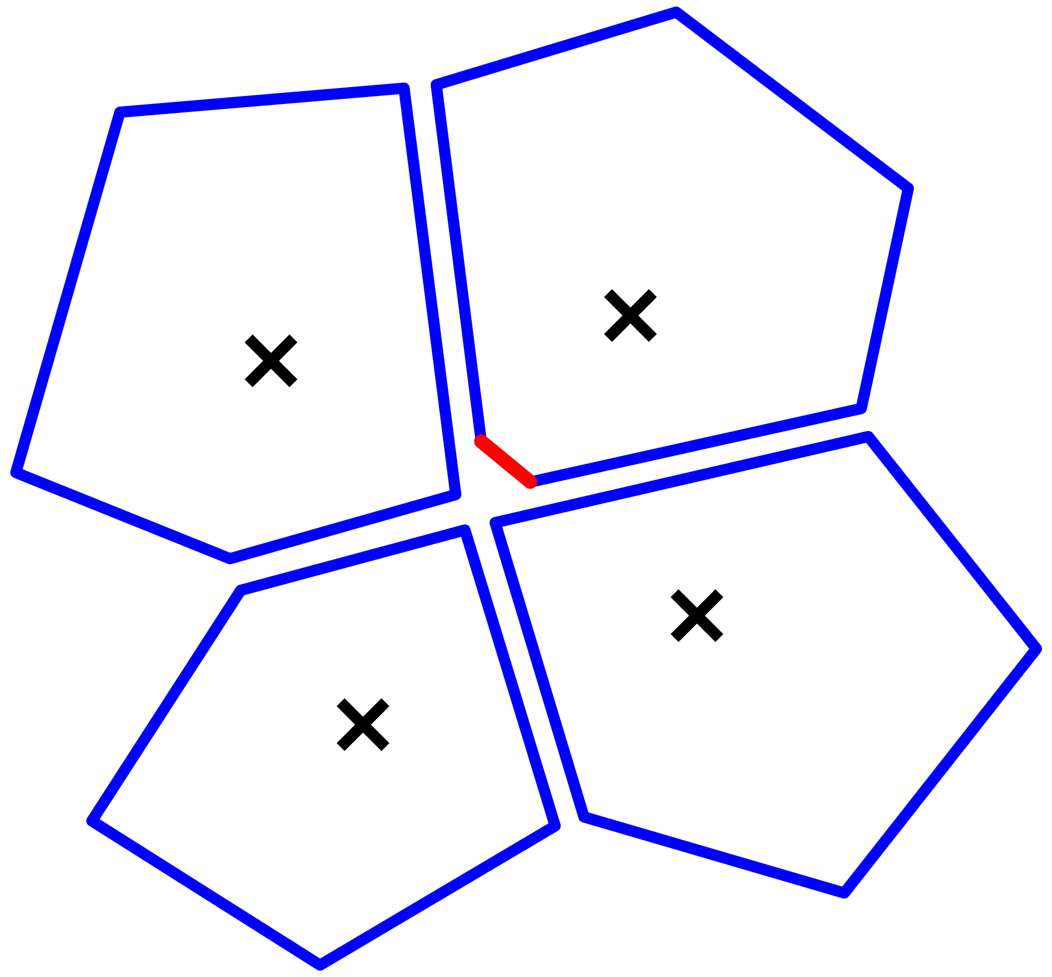

Special alignment of four Voronoi cells with extra face due to numerical rounding errors

Topological considerations

Even beyond numerical errors, this causes problems with analysis

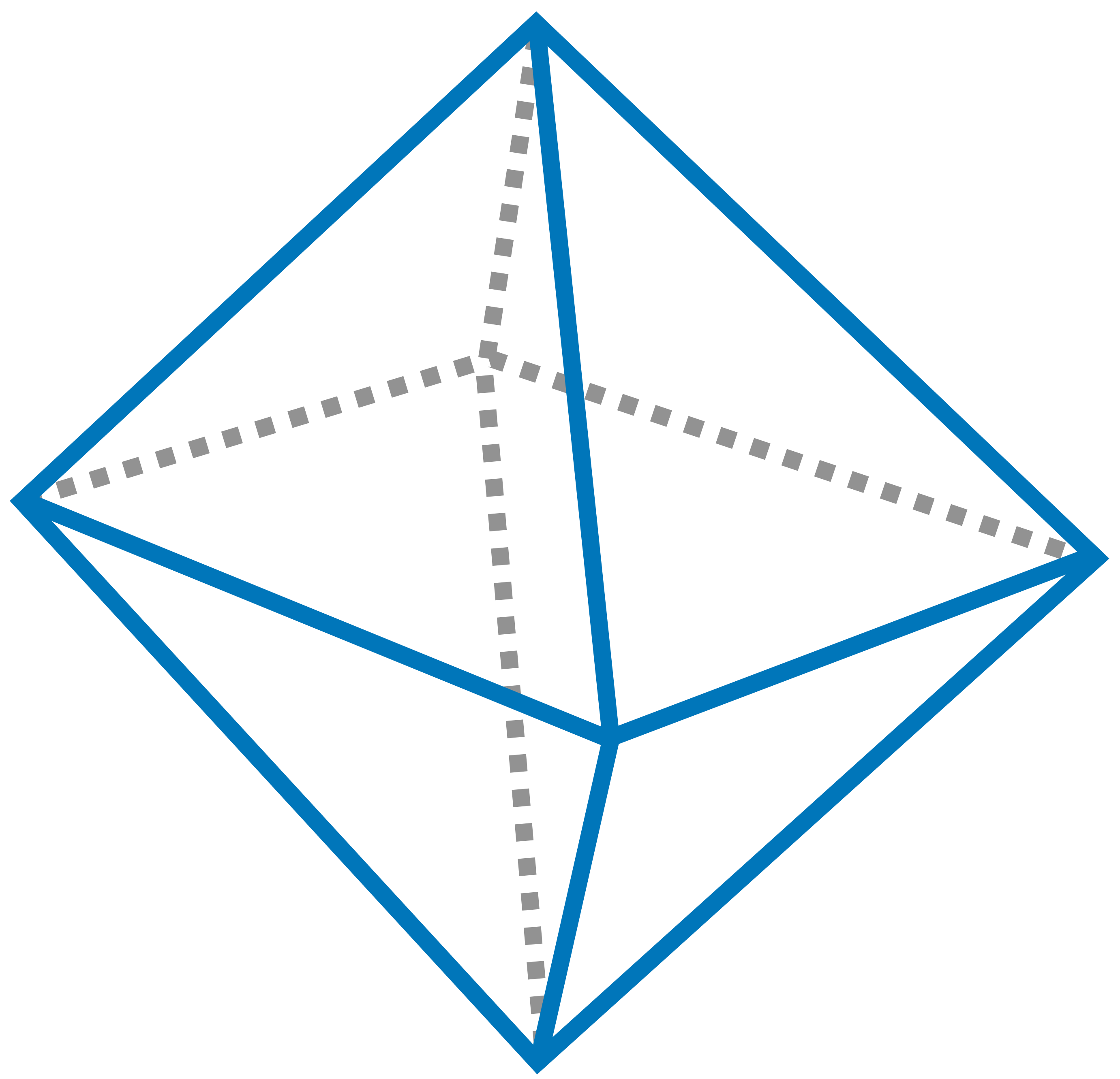

Perfect octahedron

8 triangular sides

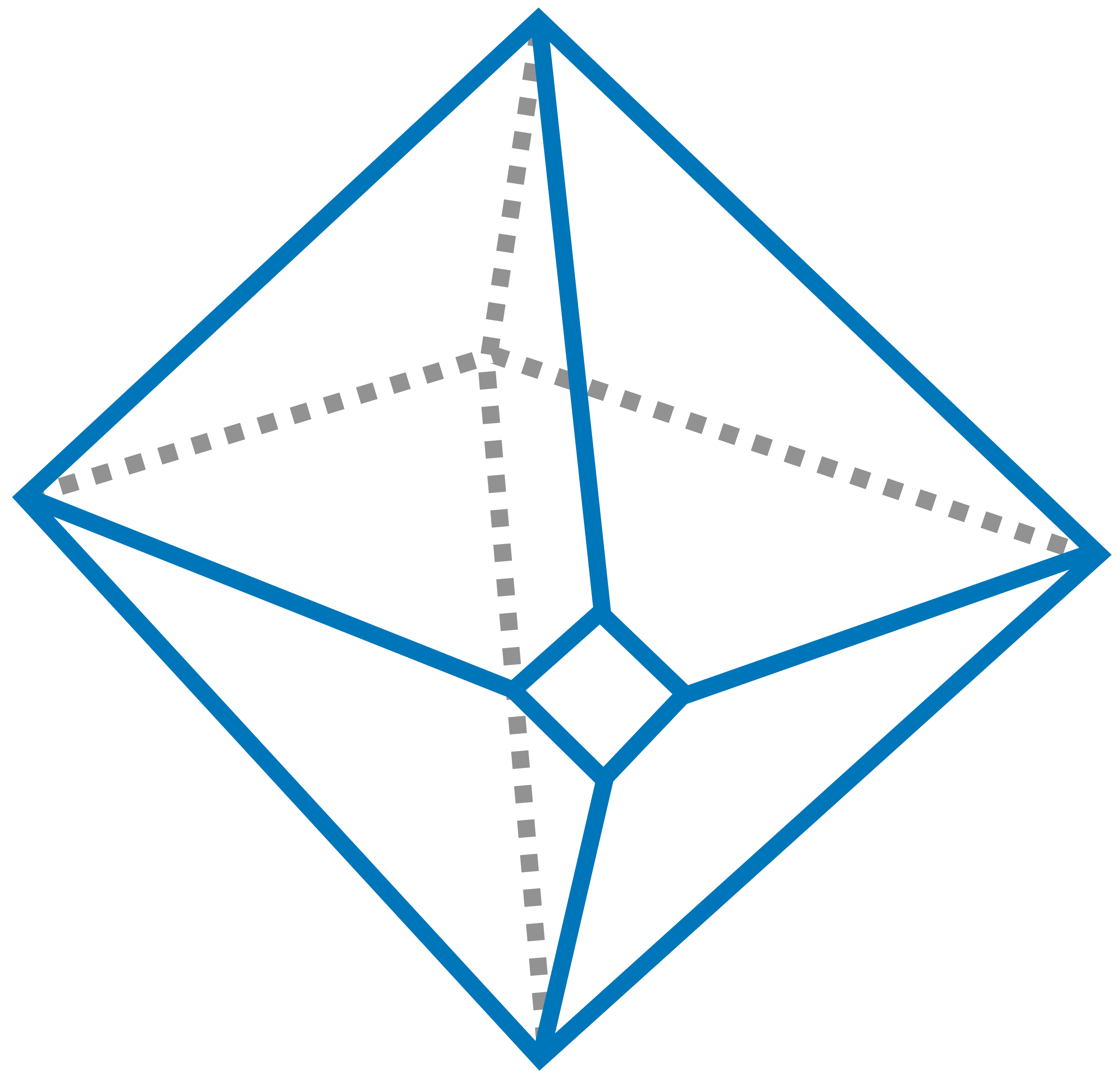

Small extra face

What to do? Apply threshold on area to remove it.

Back to octahedron—problem solved! 😎

But then four faces are still quadrilaterals 😱

VoroTop: a topological framework for local structure analysis

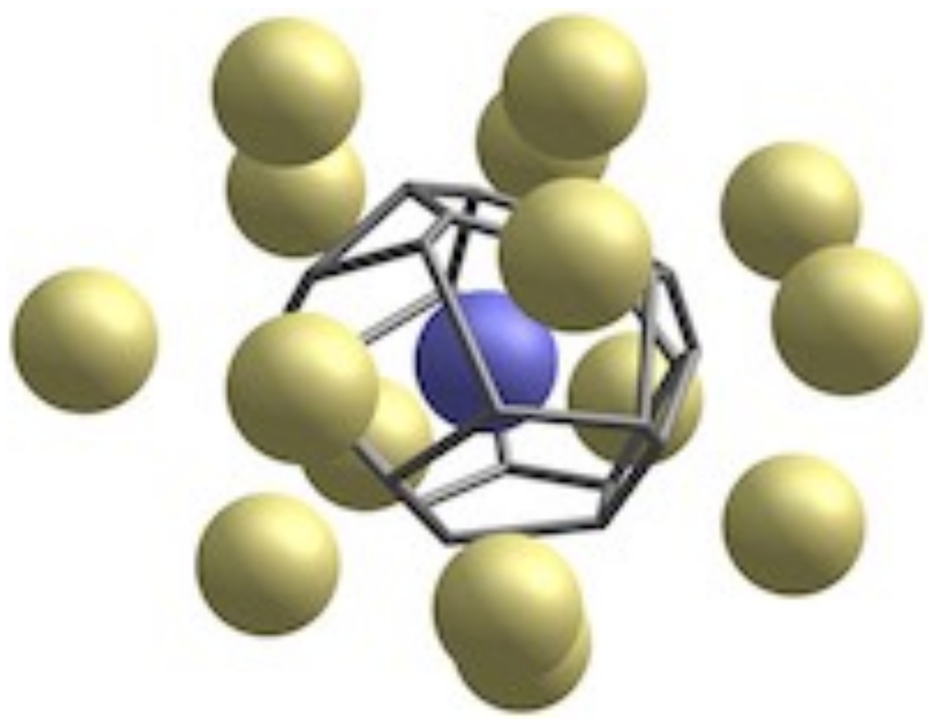

- A 3D Voronoi cell's topology (vertices, edges, faces) can be uniquely characterized by a Weinberg vector
- Think of Voronoi cells as living in an abstract topology space
- Voronoi cells for some lattices, like body-centered cubic (BCC) lie in the middle of a topological patch
- Small perturbations give the same topology

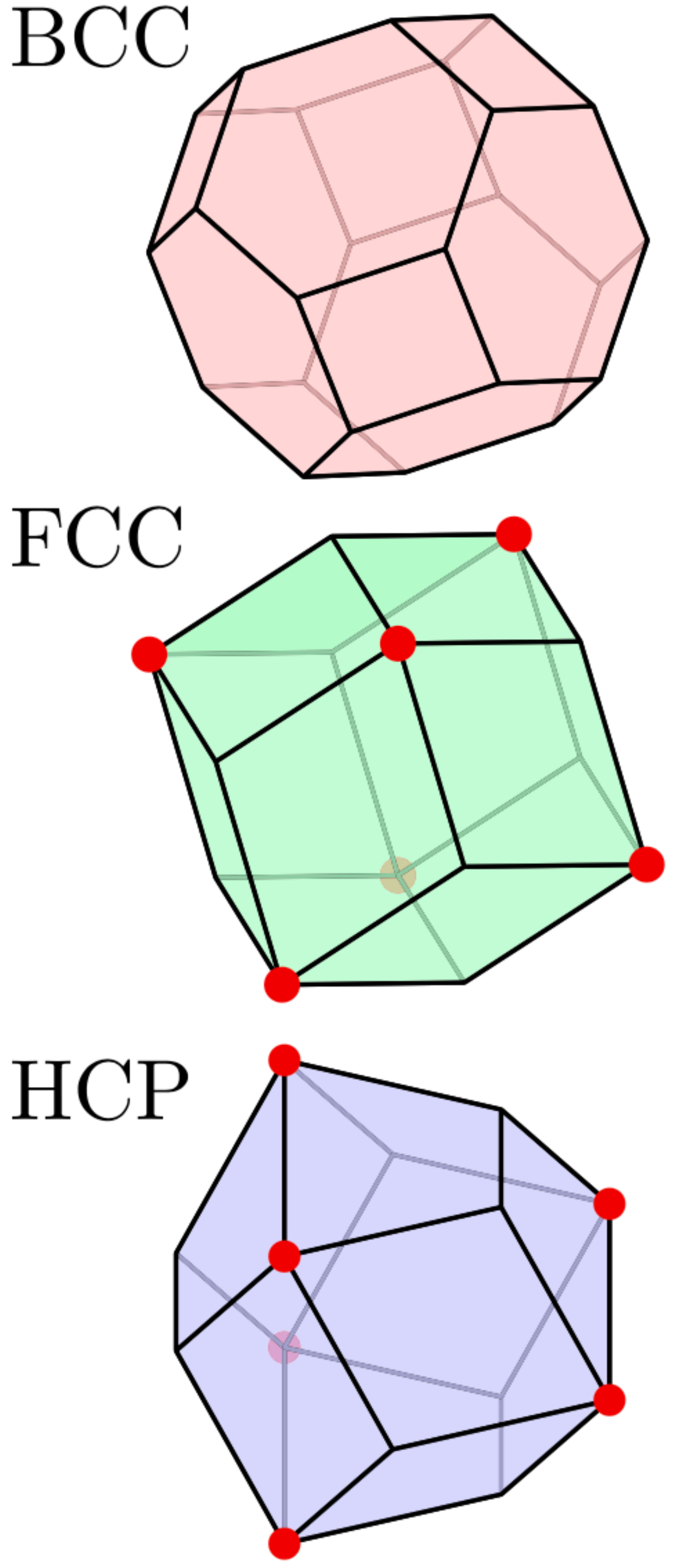

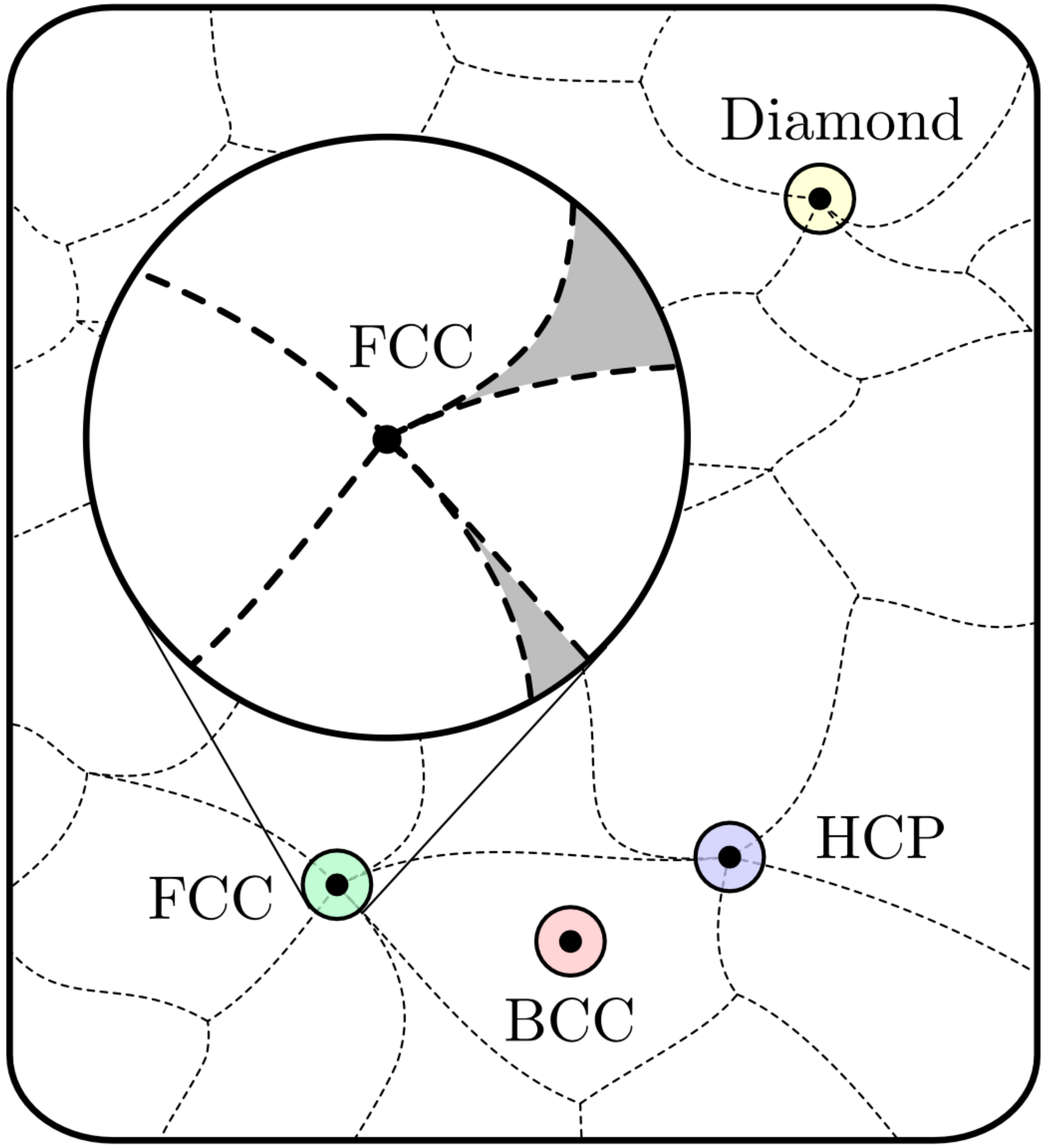

E. A. Lazar *et al.*, Proc. Natl. Acad. Sci. **112**, E5769–E5776 (2015).

VoroTop: a topological framework for local structure analysis

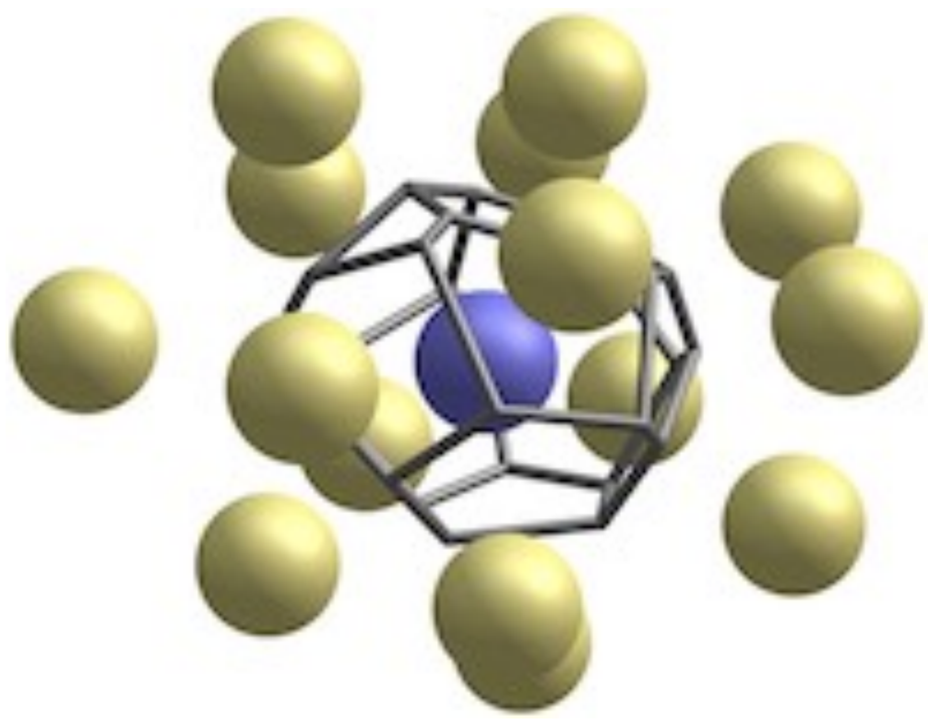

- But Voronoi cells for some lattices, like face-centered cubic (BCC) lie at the intersection of topologies
- Small perturbations give will give different topologies
- **But those topologies will appear in specific, reproducible proportions**

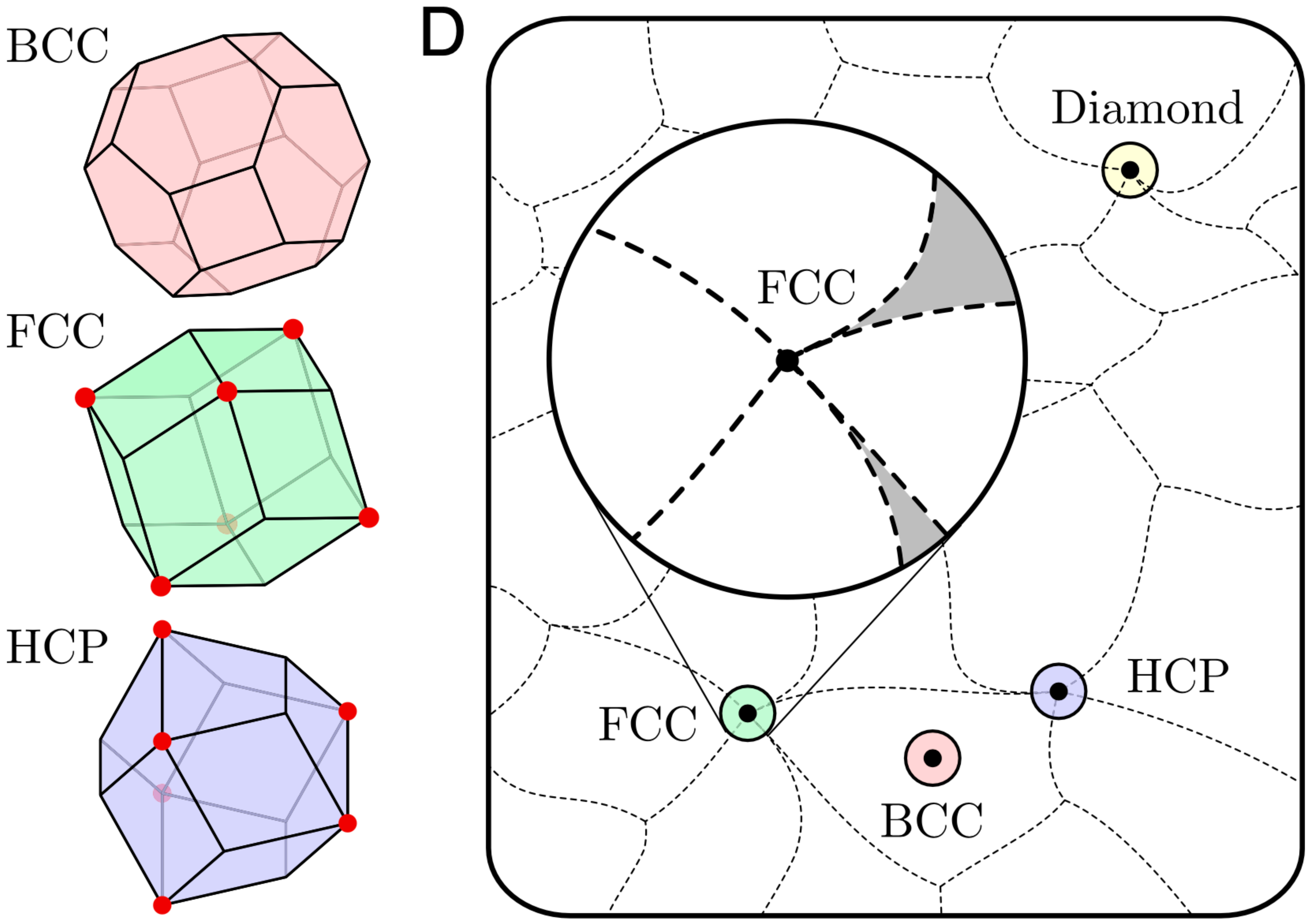

E. A. Lazar *et al.*, Proc. Natl. Acad. Sci. **112**, E5769–E5776 (2015).

Topological fractions for BCC and FCC

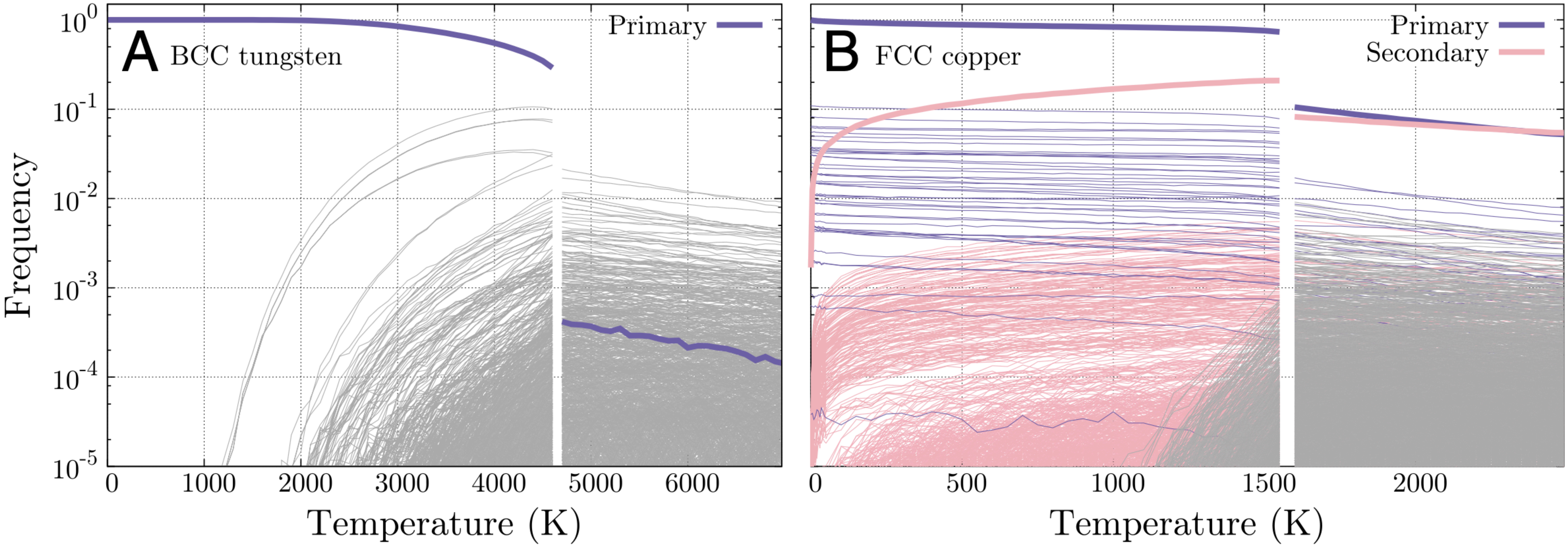

Primary types occur with a finite fraction under an infinitesimal perturbation

Thick lines indicate the sum of all fractions of each type

E. A. Lazar *et al.*, Proc. Natl. Acad. Sci. **112**, E5769–E5776 (2015).

Fig. 5. Polycrystalline aluminum at 938 K ($0.9T_m$); the width of each cross-section is 2 nm. Atoms that are FCC types are not shown for clarity. Of the ones remaining, those that are HCP types are shown in gold, and all other atoms are shown in dark blue. Grain boundaries are seen as a network of non-FCC types (dark blue and gold atoms). In cross-section *A*, defects are labeled as follows: vacancies, A; twin boundary, B; and stacking fault, C. Cross-sections *B* and *C* show magnified images of a dislocation and stacking fault. (*A*) Polycrystal cross-section. (*B*) Dislocation. (*C*) Stacking fault.

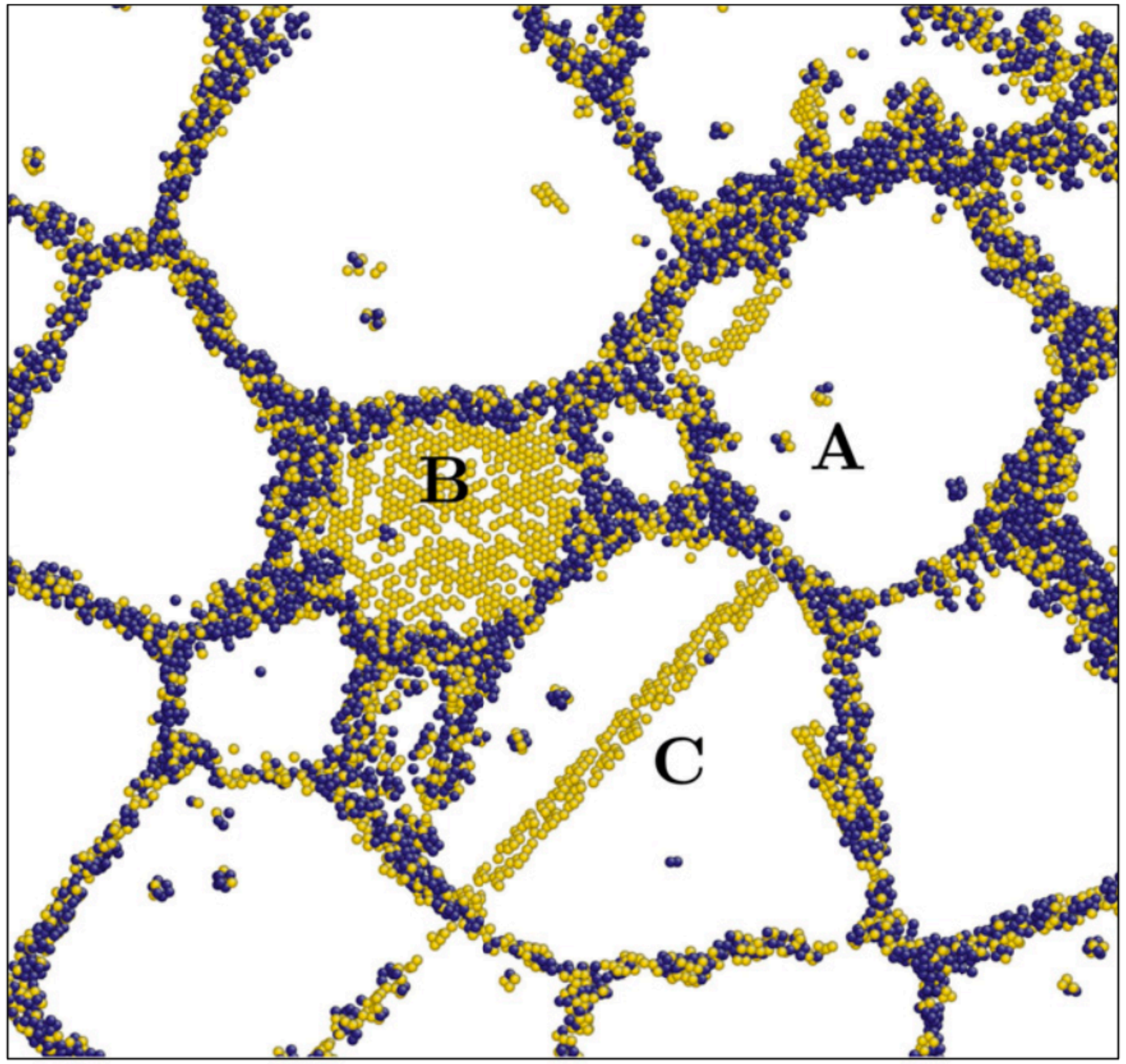

A Polycrystal cross-section

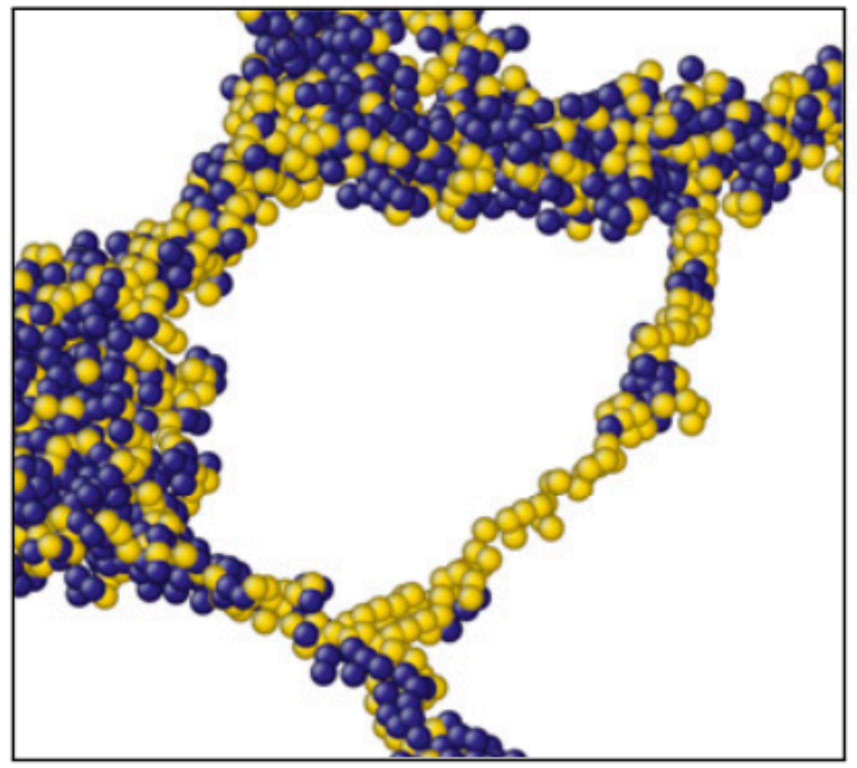

B Dislocation

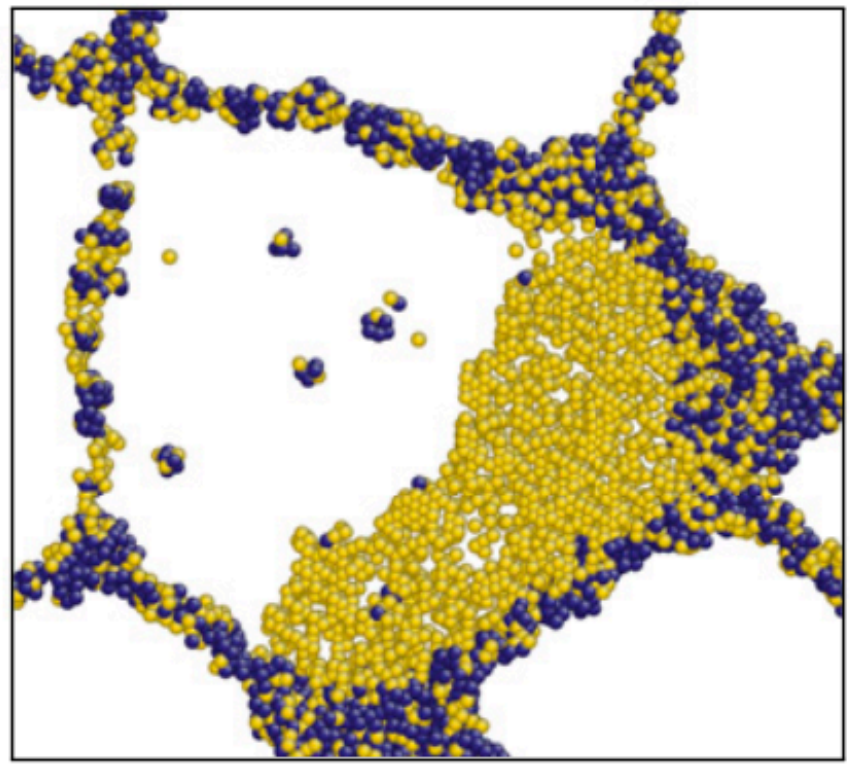

C Stacking fault

E. A. Lazar *et al.*, Proc. Natl. Acad. Sci. **112**, E5769–E5776 (2015).

VoroTop in 2D

Characterize topologies in terms of Voronoi cell neighbors, and number of neighbors of neighbors

https://vorotop.org
E. A. Lazar *et al.*, arXiv:2406.00553(2024).

Modeling the diverse geometry of insect wings

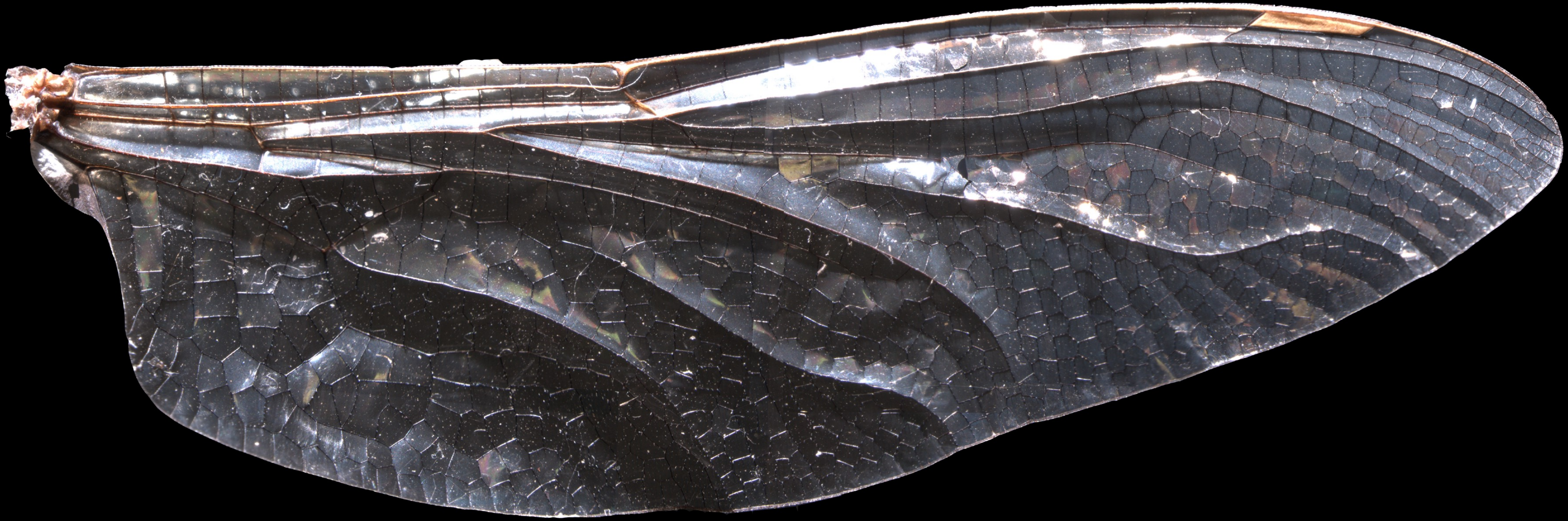

J. Hoffmann, S. Donoughe, *et al.*, *A simple developmental model recapitulates complex insect wing venation patterns*, Proc. Natl. Acad. Sci. **115**, 9905–9910 (2018)

Joint work with Jordan Hoffmann, Seth Donoughe, Kathy Li, and Mary Salcedo

Introduction

- Insect wings have been studied and illustrated for centuries, and exhibit a diverse range of morphologies
- Currently, wing veins have been studied in the most detail in *Drosophila Melanogoster*
- In this species, all wing veins are largely conserved—these are called **primary veins**

Illustration from Jan Swammerdam (1637–1680)

D. Melanogoster wing

Terminology

- Many insect wings also exhibit random variations in vein patterning
- We define veins that vary between individuals as **secondary veins**

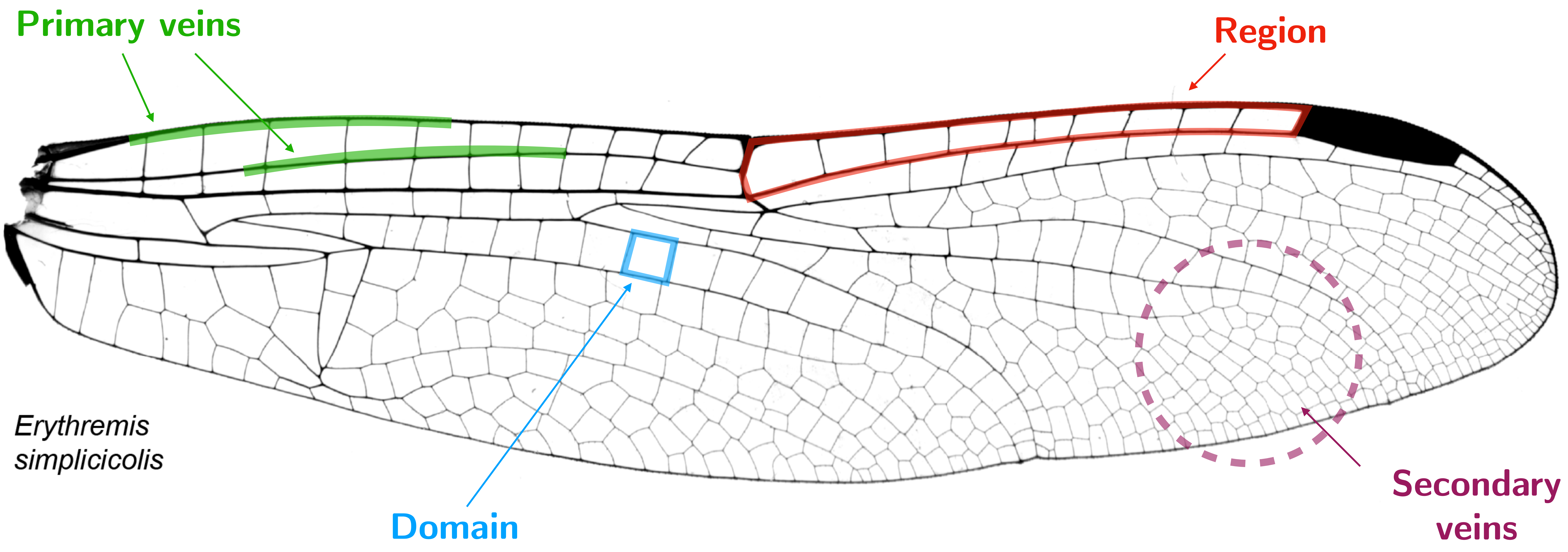

Distinction between primary and secondary veins

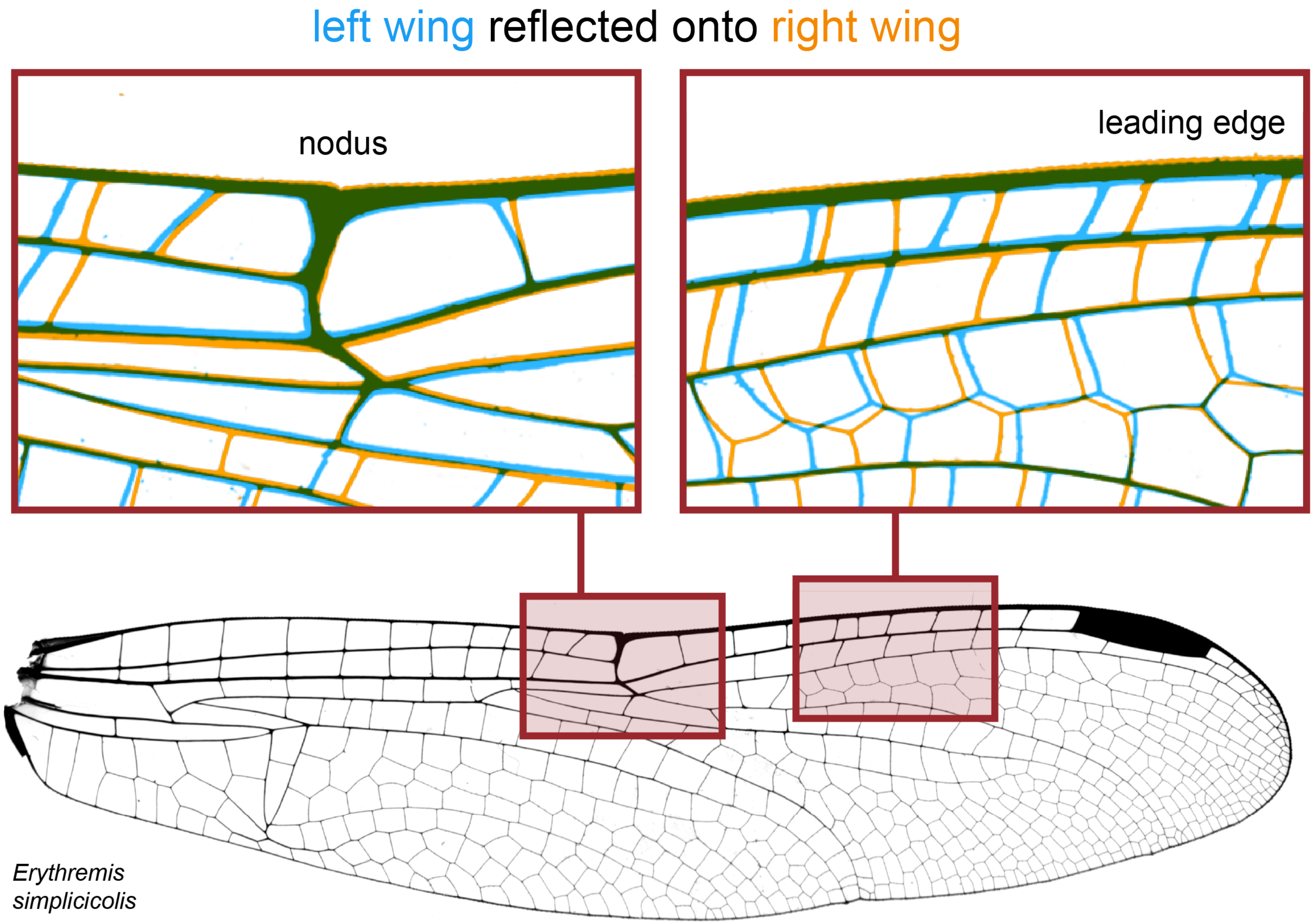

Distinction between primary and secondary veins

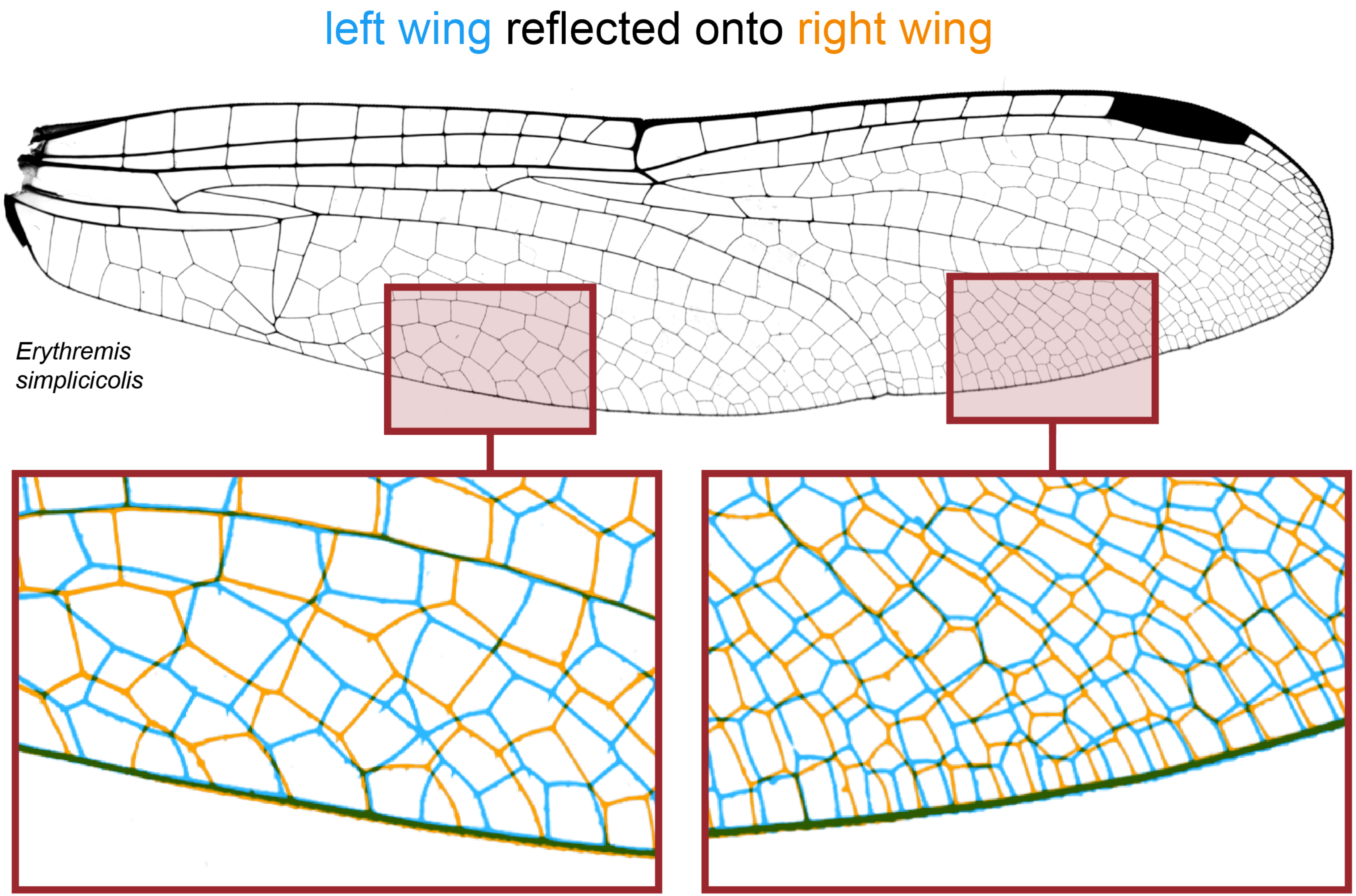

A computational study of secondary veins

- Secondary veins were not quantitatively characterized for any species
- It is not known whether a universal developmental process generates the diverse secondary vein arrangements seen in insects

Aims:

1. Perform a large-scale quantitative analysis of insect wing structure
2. Develop a mathematical model to explain secondary vein patterning

Data collection

- We collected data from multiple sources:
  - Original high-resolution micrographs
  - Published tracings from two books [1,2]
- Our database focused on the Odonata order, consisting of dragonflies and damselflies
- 468 wings taken from 232 species

[1] J. G. Needham, Minter J. Westfall, and Michael L. May, D*ragonflies of North America: the Odonata (Anisoptera) fauna of Canada, the continental United States, northern Mexico and the Greater Antilles*, Scientific Publishers. 2014.
[2] R.W. Garrison, N. von Ellenrieder, and Jerry A. Louton, *Dragonfly genera of the New World : an illustrated and annotated key to the Anisoptera*, JHU Press. 2006.

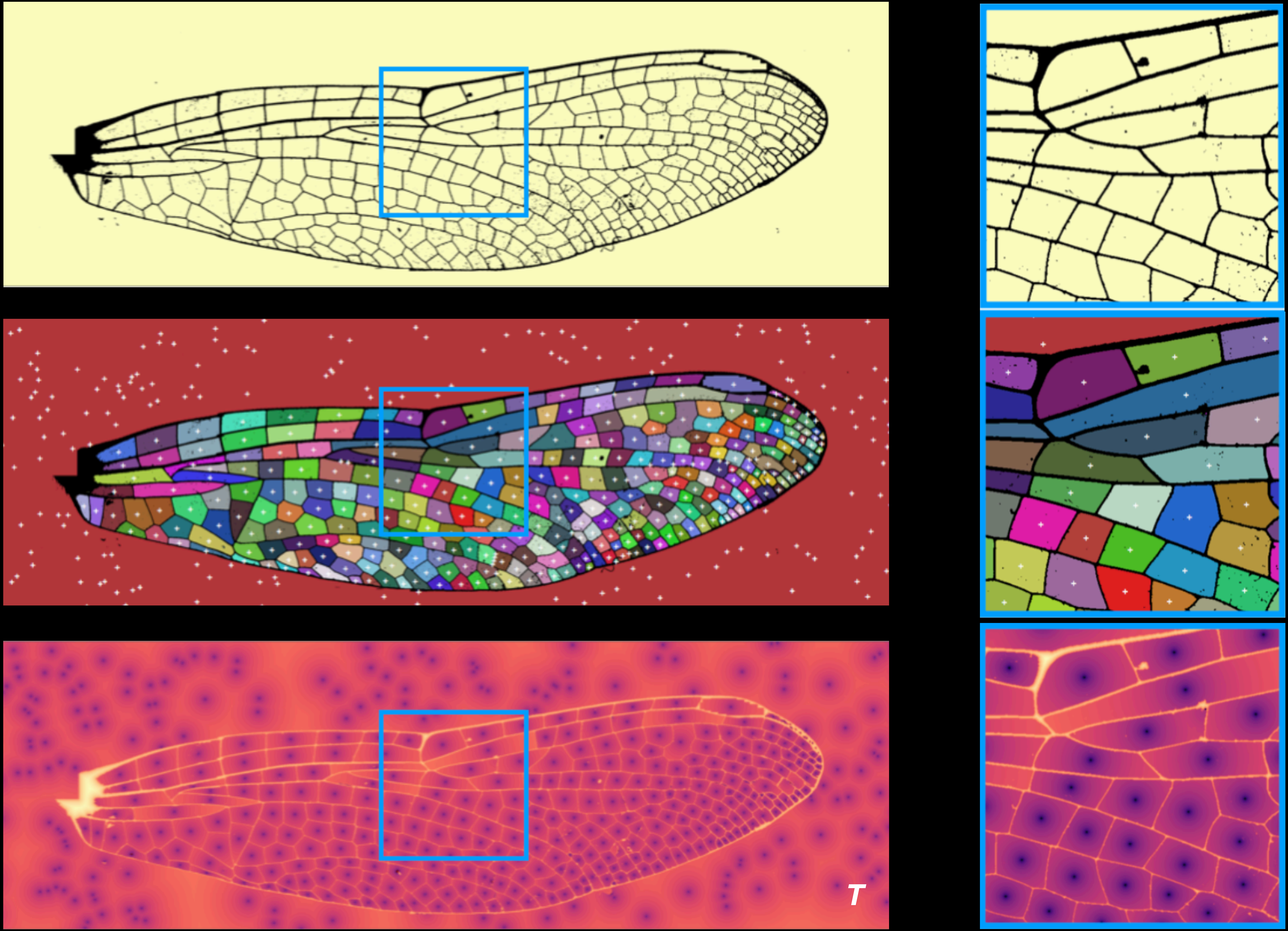

$$F(x)|\nabla T(x)| = 1$$

F: Speed Matrix

T: Travel Time Matrix

Segmented wing image

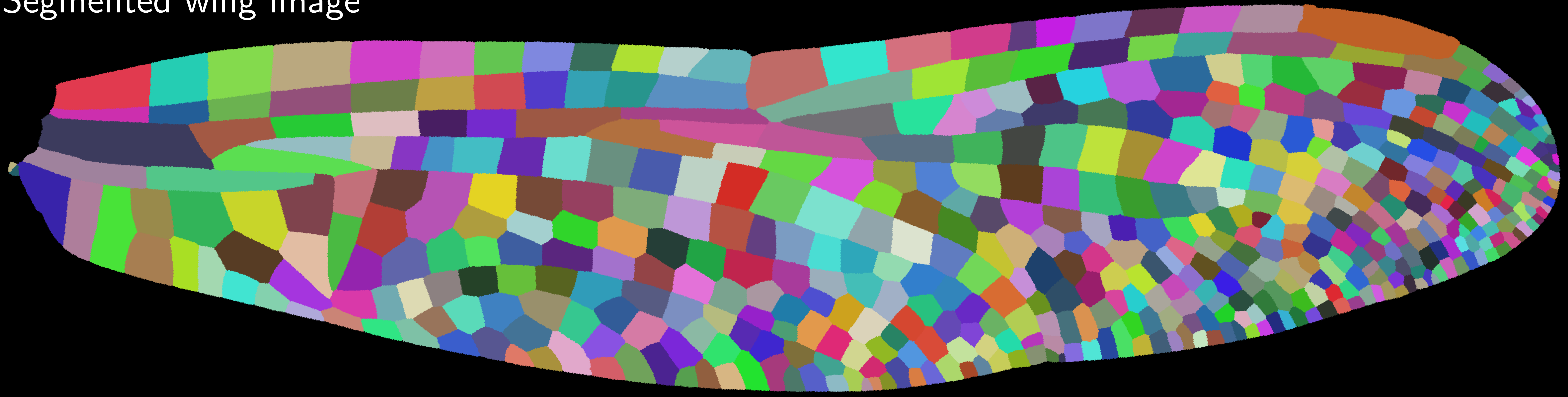

Segmented wing image

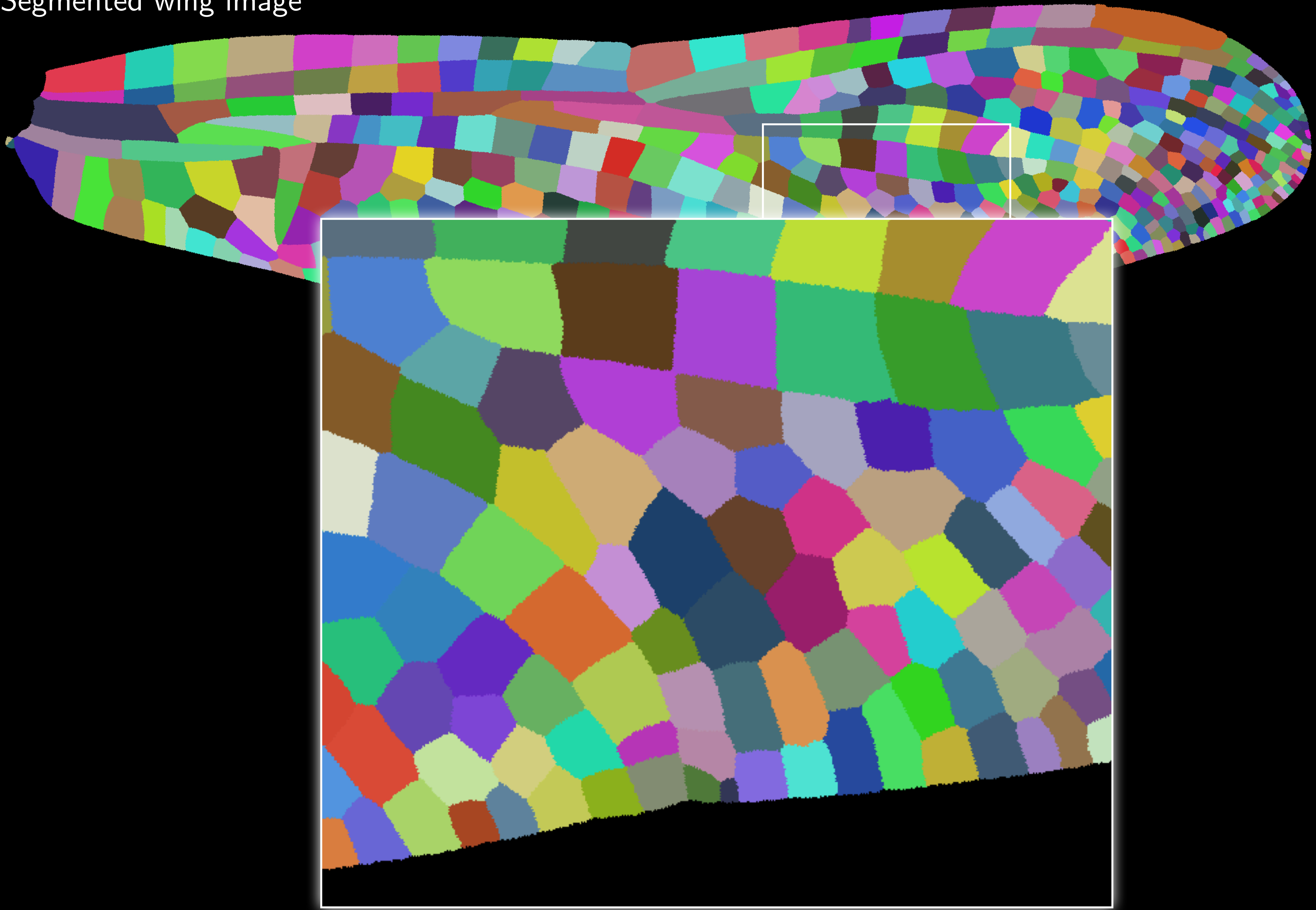

Segmented wing image

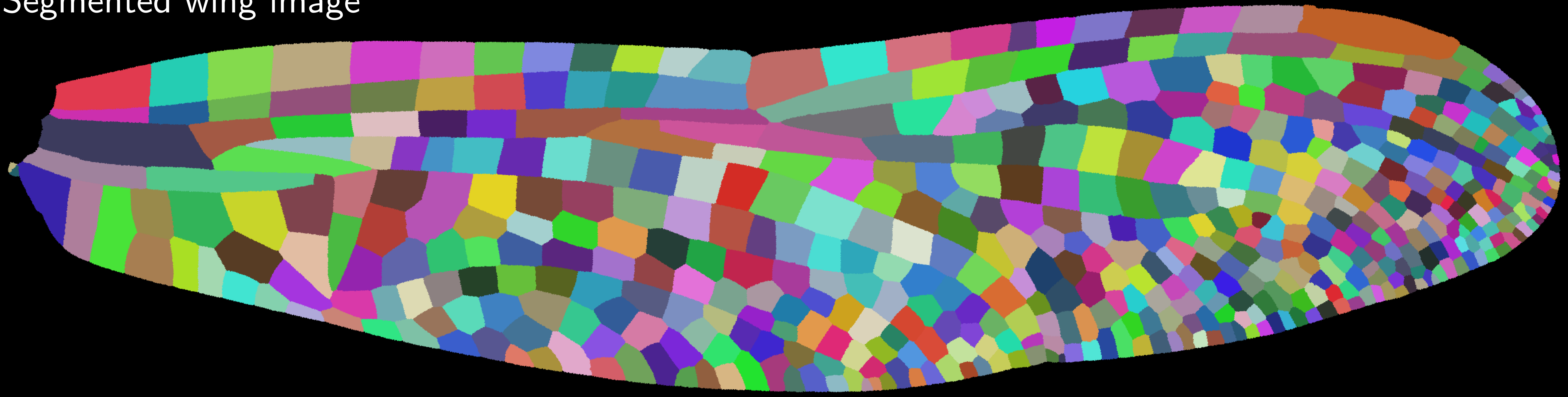

Vectorized wing outline based on color adjacencies

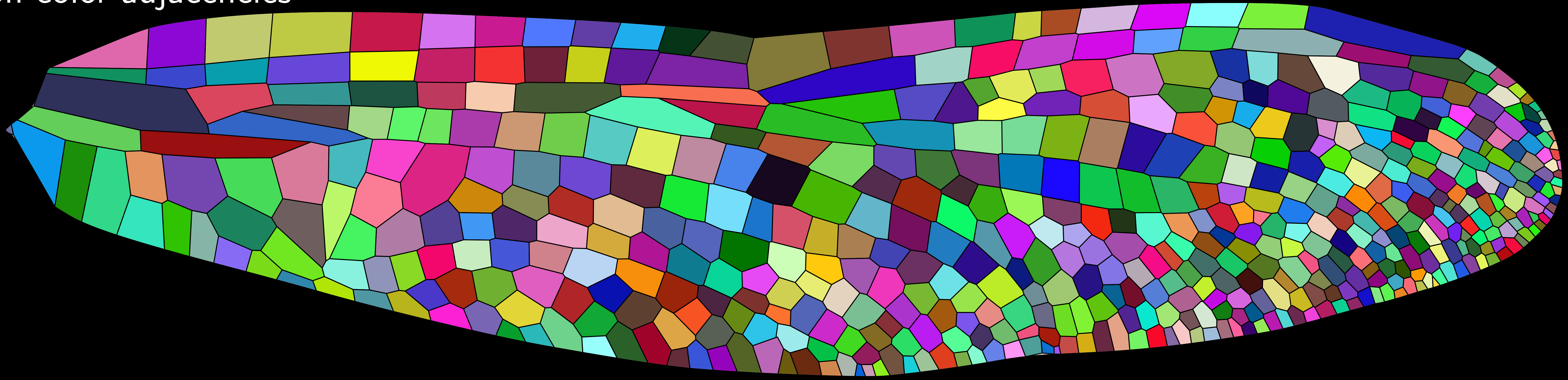

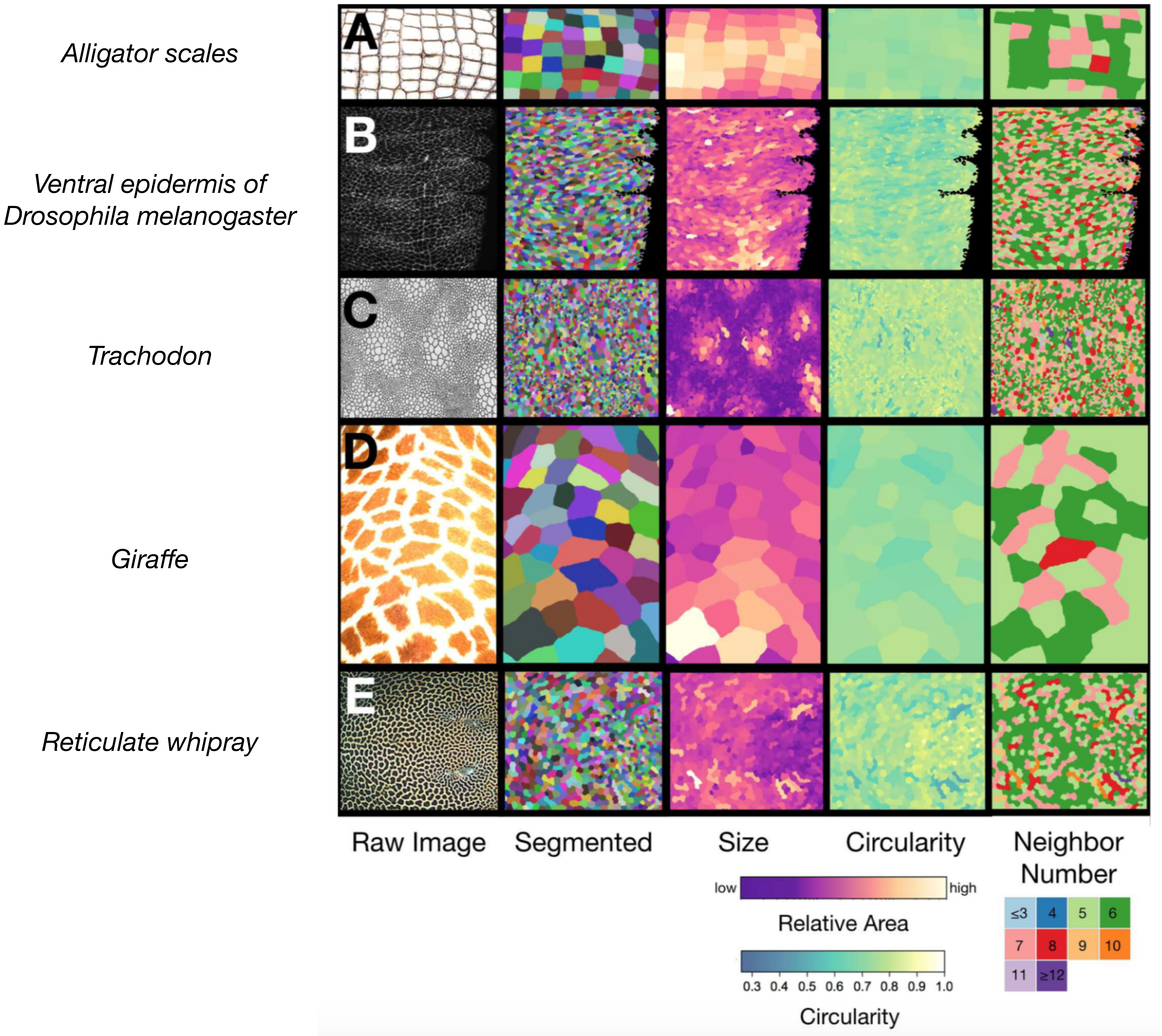
Alligator scales
Ventral epidermis of Drosophila melanogaster
Trachodon
Giraffe
Reticulate whipray
A
B
C
D
E
Raw Image
Segmented
Size
Circularity
Neighbor Number
low
high
Relative Area
0.3 0.4 0.5 0.6 0.7 0.8 0.9 1.0
Circularity
≤3
4
5
6
7
8
9
10
11
≥12

Quantitative measures of wing domains

- For each wing domain with vertices (x_k, y_k), we compute its area

$$A = \frac{1}{2}\left(\begin{vmatrix} x_1 & x_2 \\ y_1 & y_2 \end{vmatrix} + \begin{vmatrix} x_2 & x_3 \\ y_2 & y_3 \end{vmatrix} + \ldots + \begin{vmatrix} x_n & x_1 \\ y_n & y_1 \end{vmatrix} \right)$$

- Areas vary from ~0.01 mm^2 to 10 mm^2

- We also compute circularity

$$C = \frac{4\pi(\text{Area})}{(\text{Perimeter})^2}$$

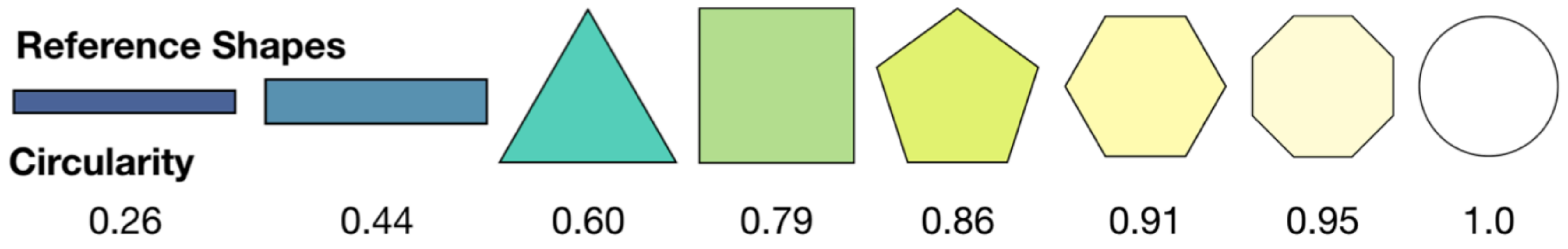

Left–right comparison

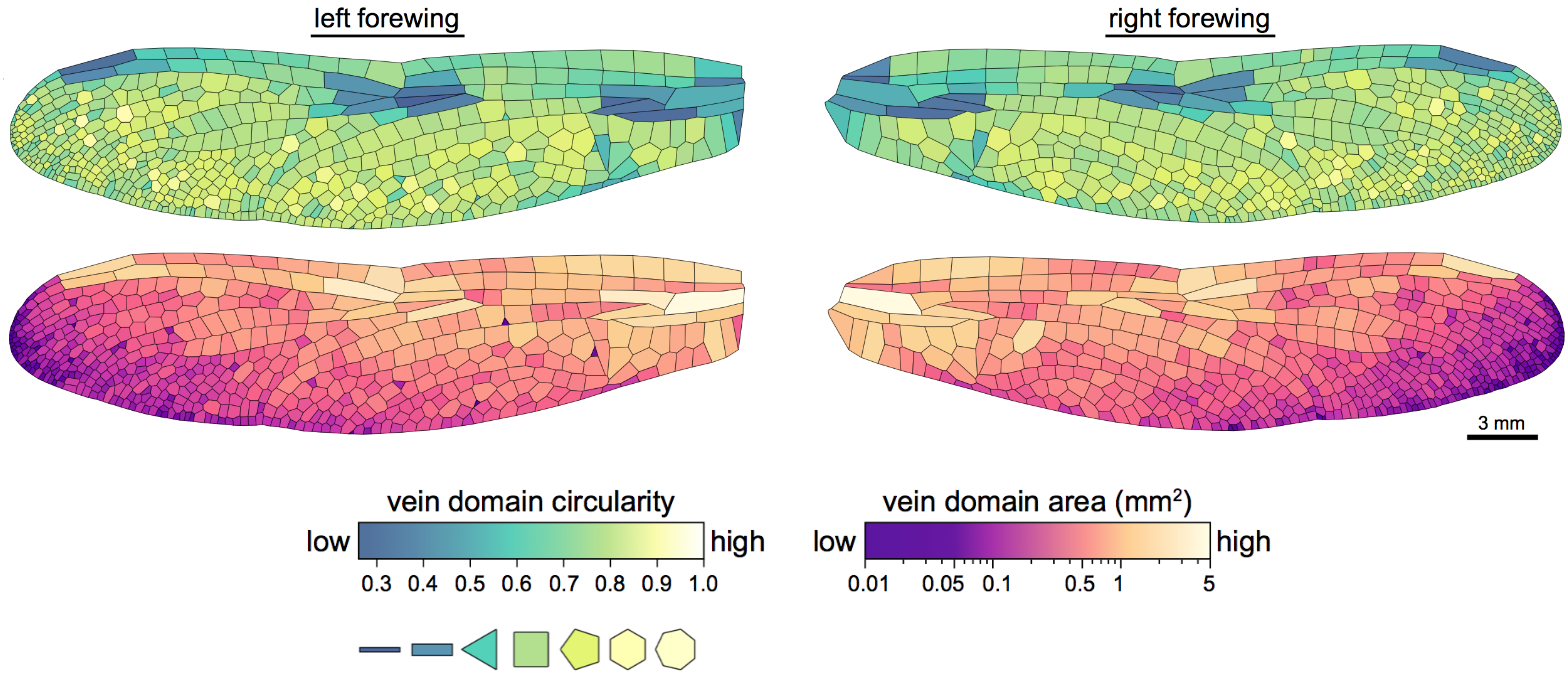

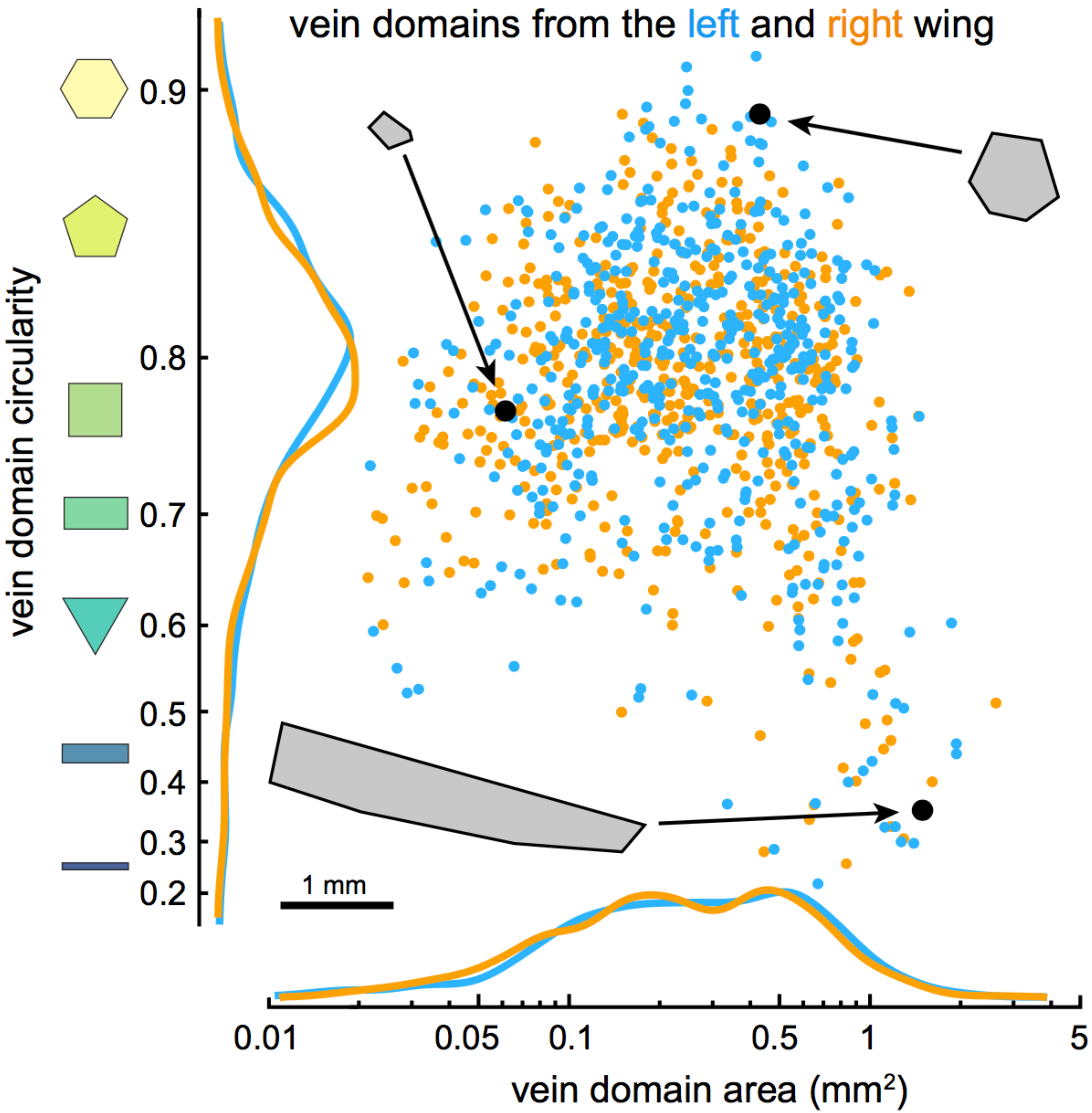

vein domains from the left and right wing
vein domain circularity
0.9
0.8
0.7
0.6
0.5
0.4
0.3
0.2
1 mm
0.01
0.05
0.1
0.5
1
5
vein domain area (mm²)

Validation 1: images to books

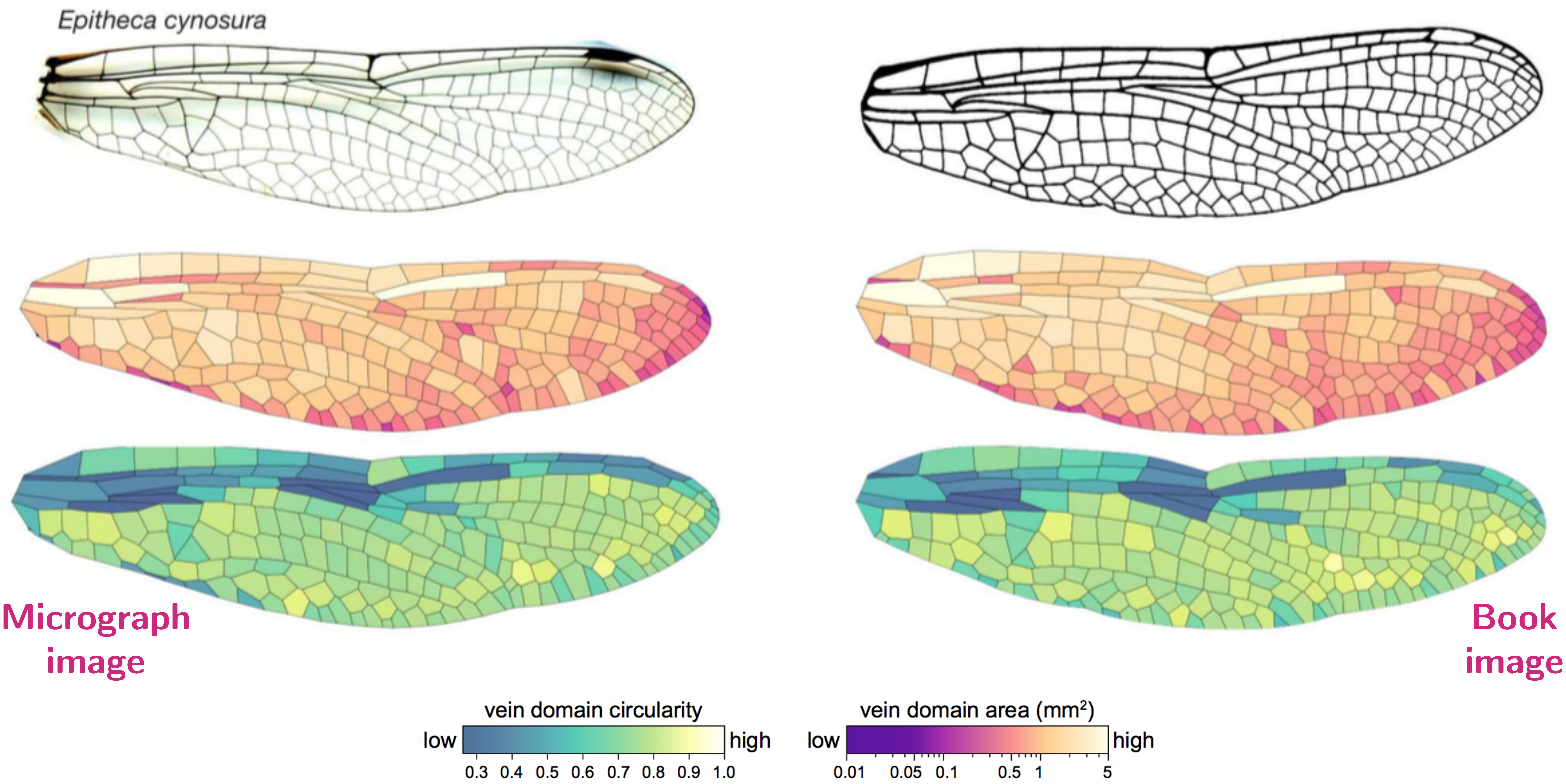

Micrograph image

Book image

Validation 2: book to book

Comparing a selection of species that appear in both books

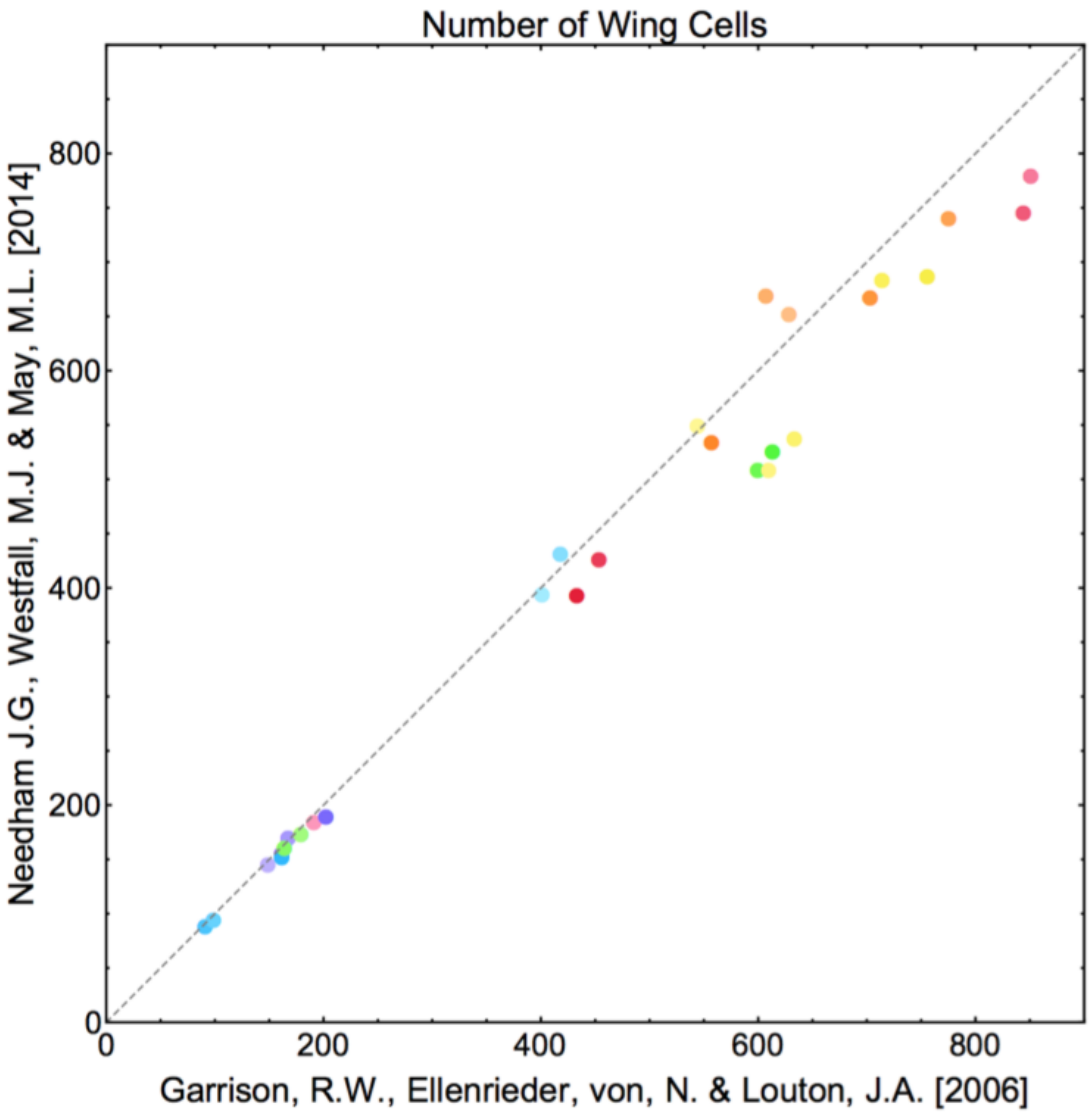

Proximal–distal trace as a signature of a wing

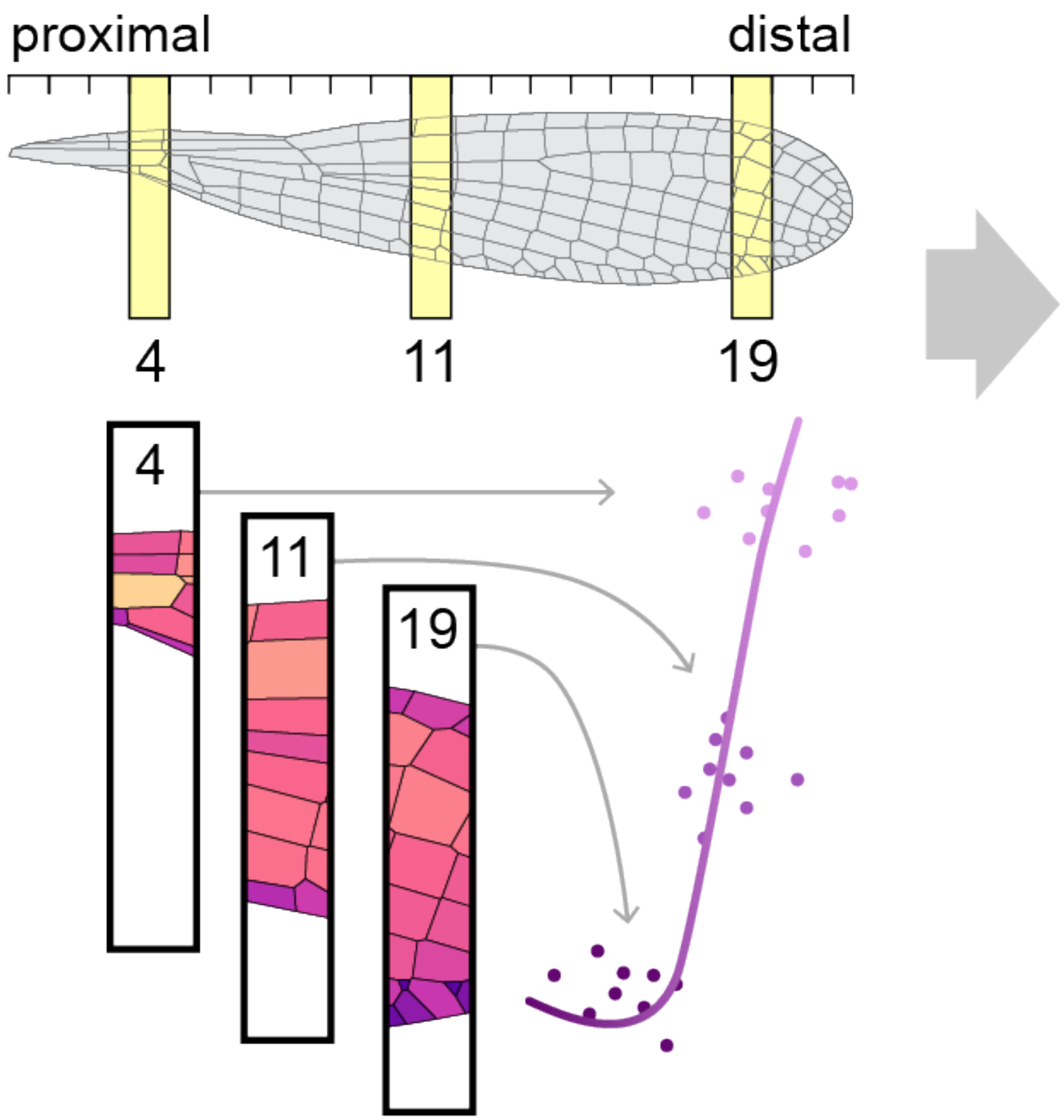

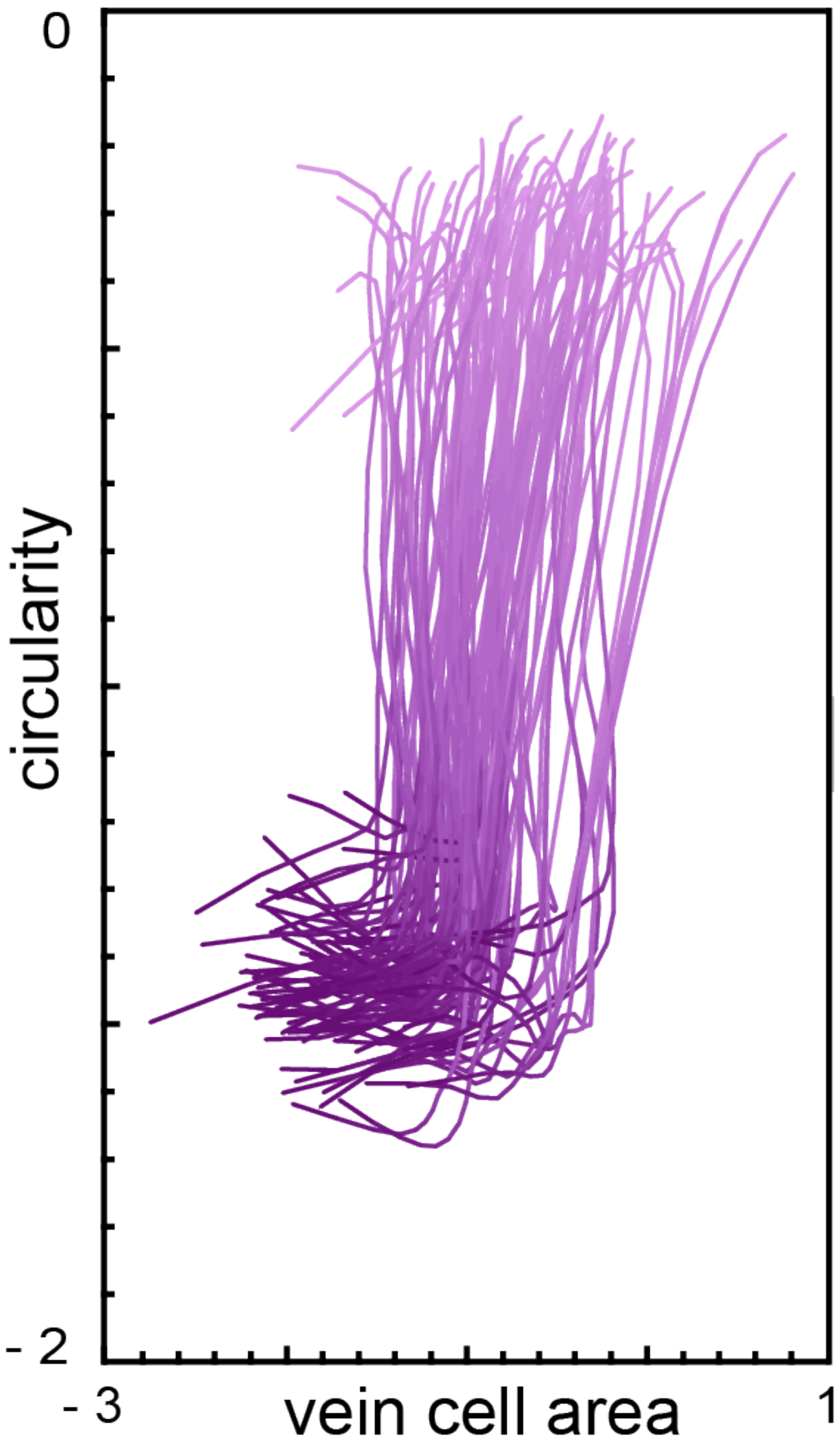

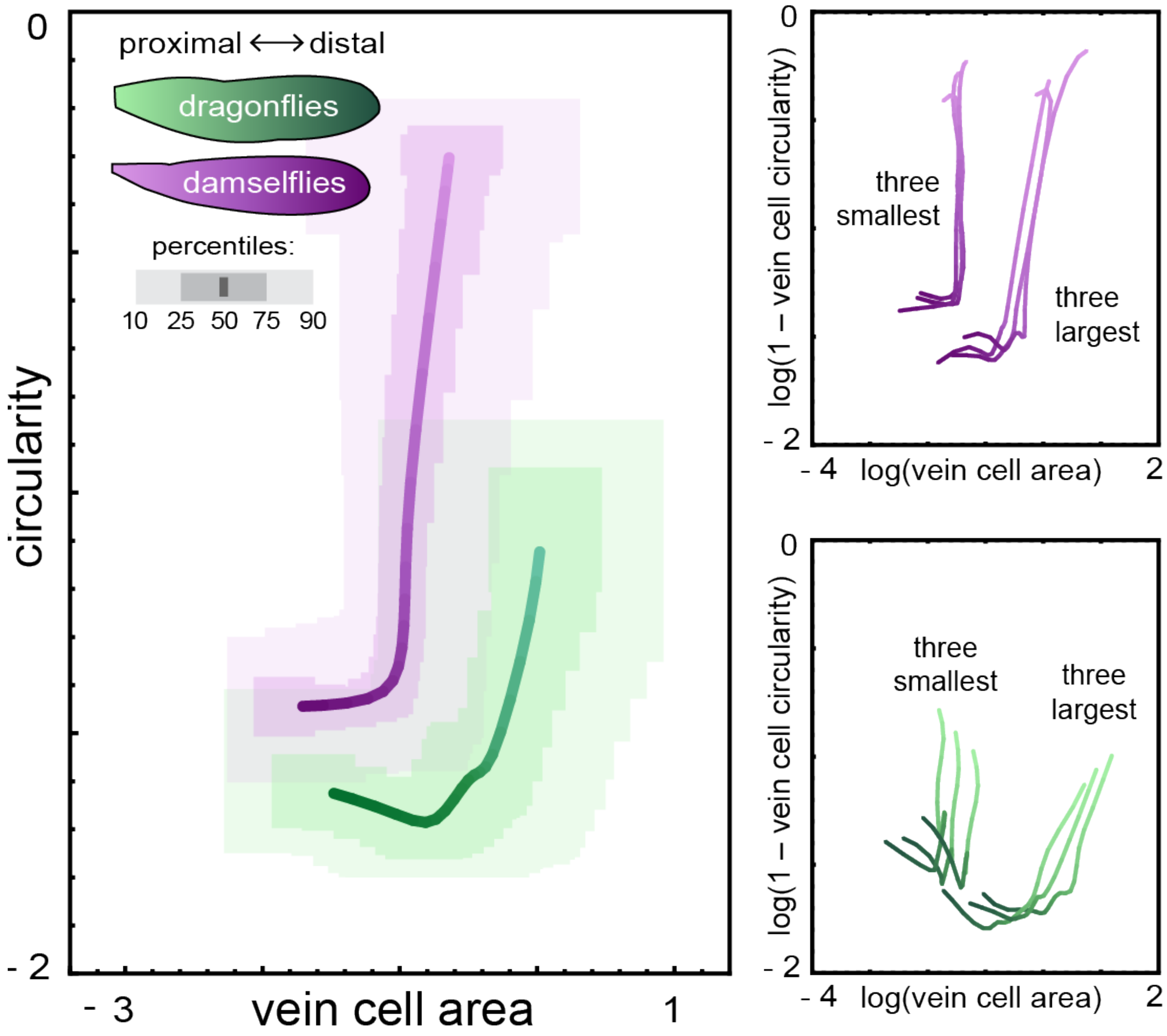

proximal ⟷ distal
dragonflies
damselflies
percentiles:
10 25 50 75 90
0
- 2
circularity
- 3
vein cell area
1
three smallest
three largest
log(1 – vein cell circularity)
0
- 2
- 4
log(vein cell area)
2
three smallest
three largest
log(1 – vein cell circularity)
0
- 2
- 4
log(vein cell area)
2

A model for secondary vein formation

- Experimental studies of wing development suggest that primary veins are laid down early in development
- We hypothesize that a pattern formation mechanism occurs in regions between primary veins

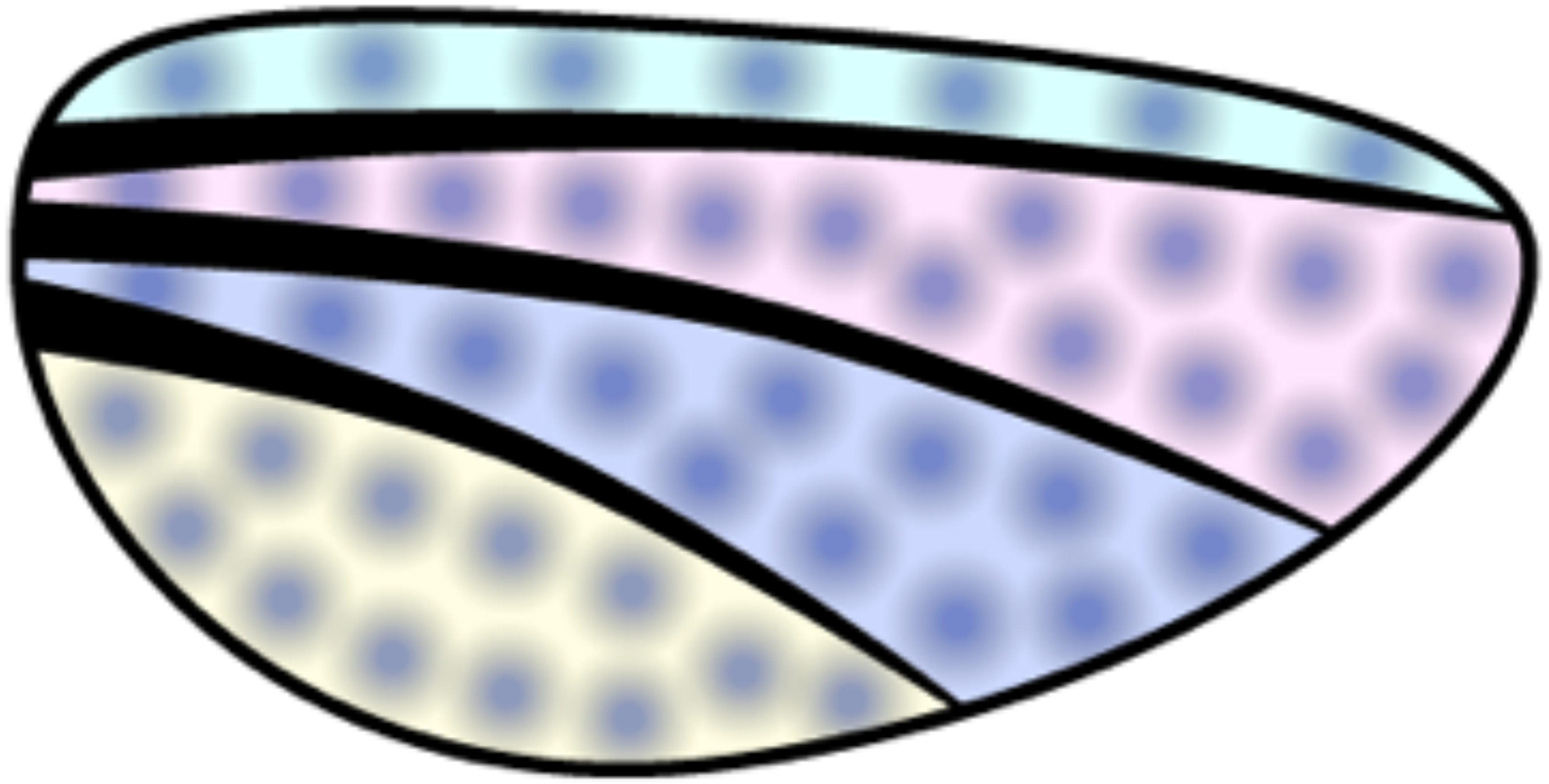

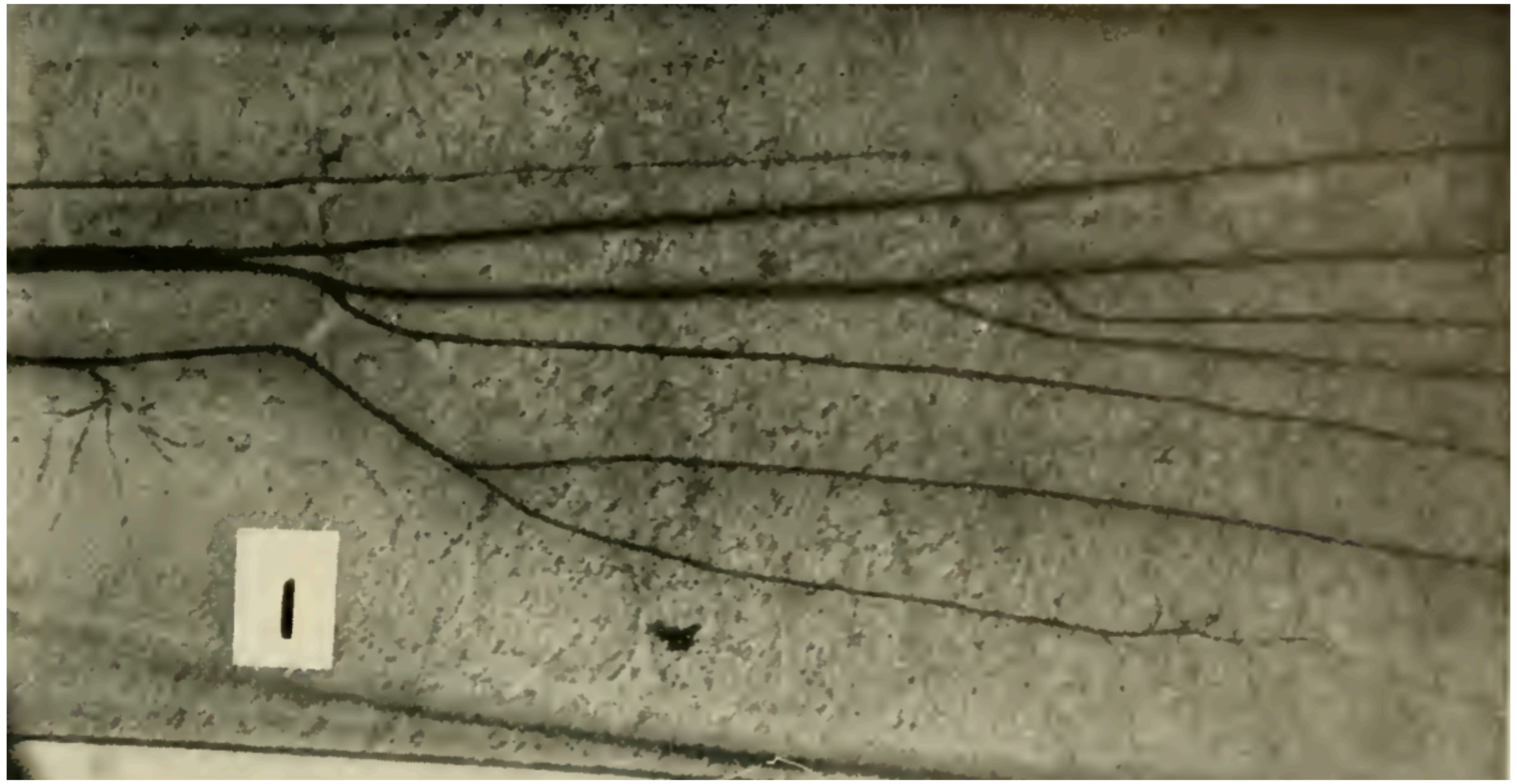

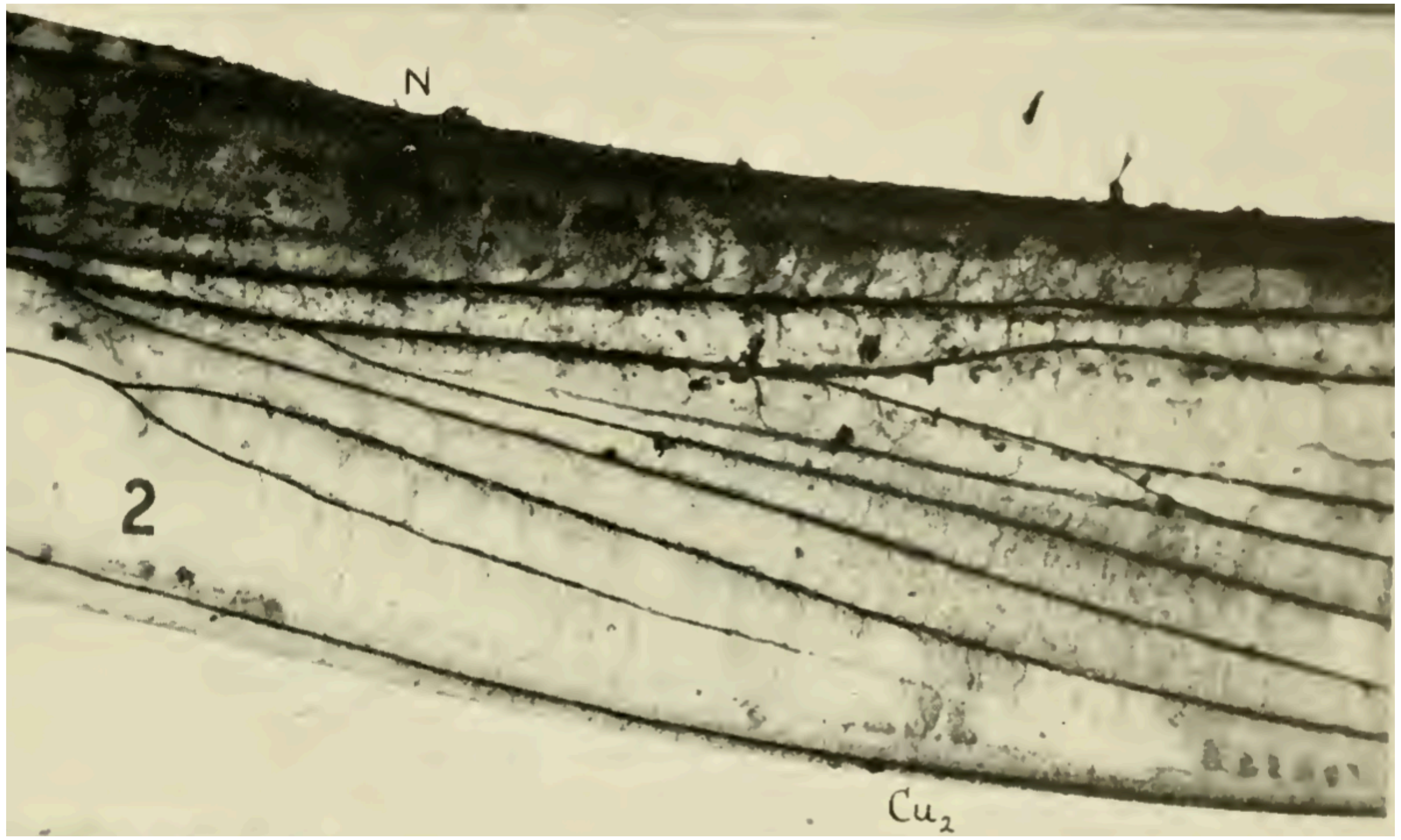

Use Lloyd's algorithm as a proxy for pattern formation

elongate rectangle; density = 10

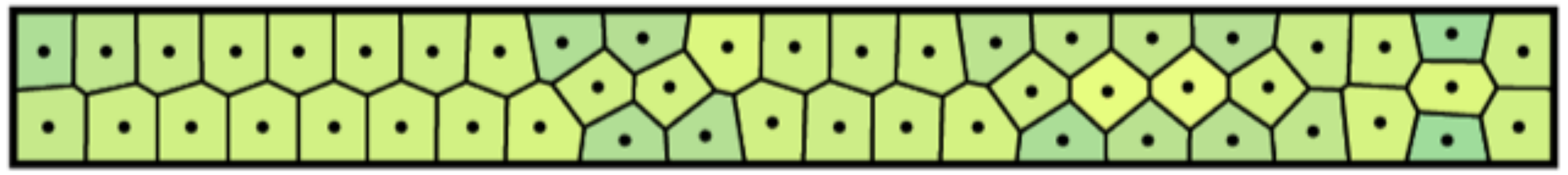

elongate rectangle; density = 50

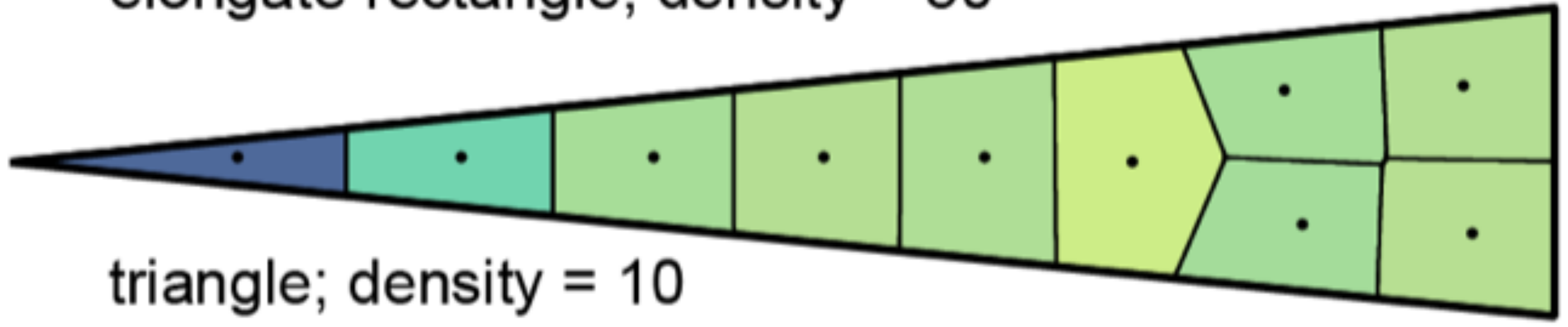

triangle; density = 10

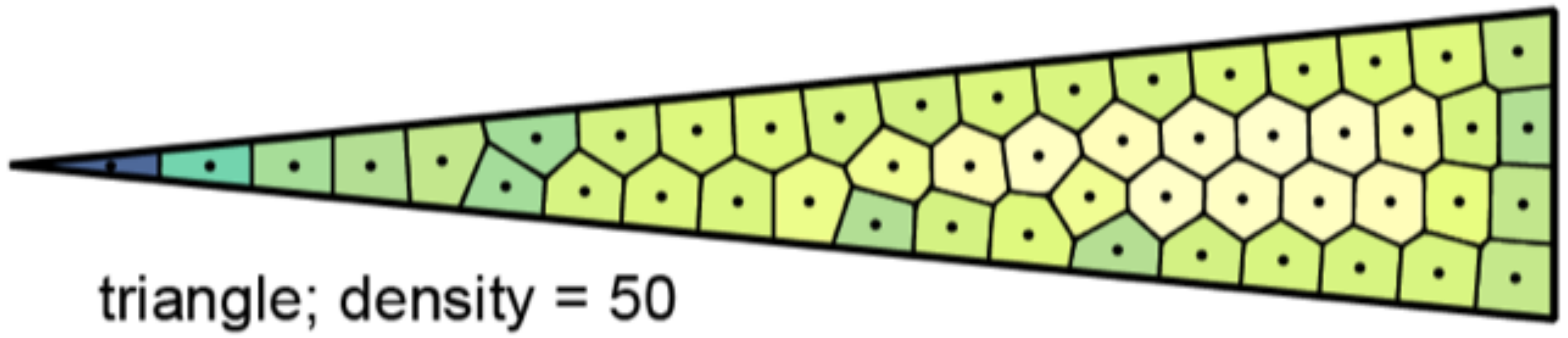

triangle; density = 50

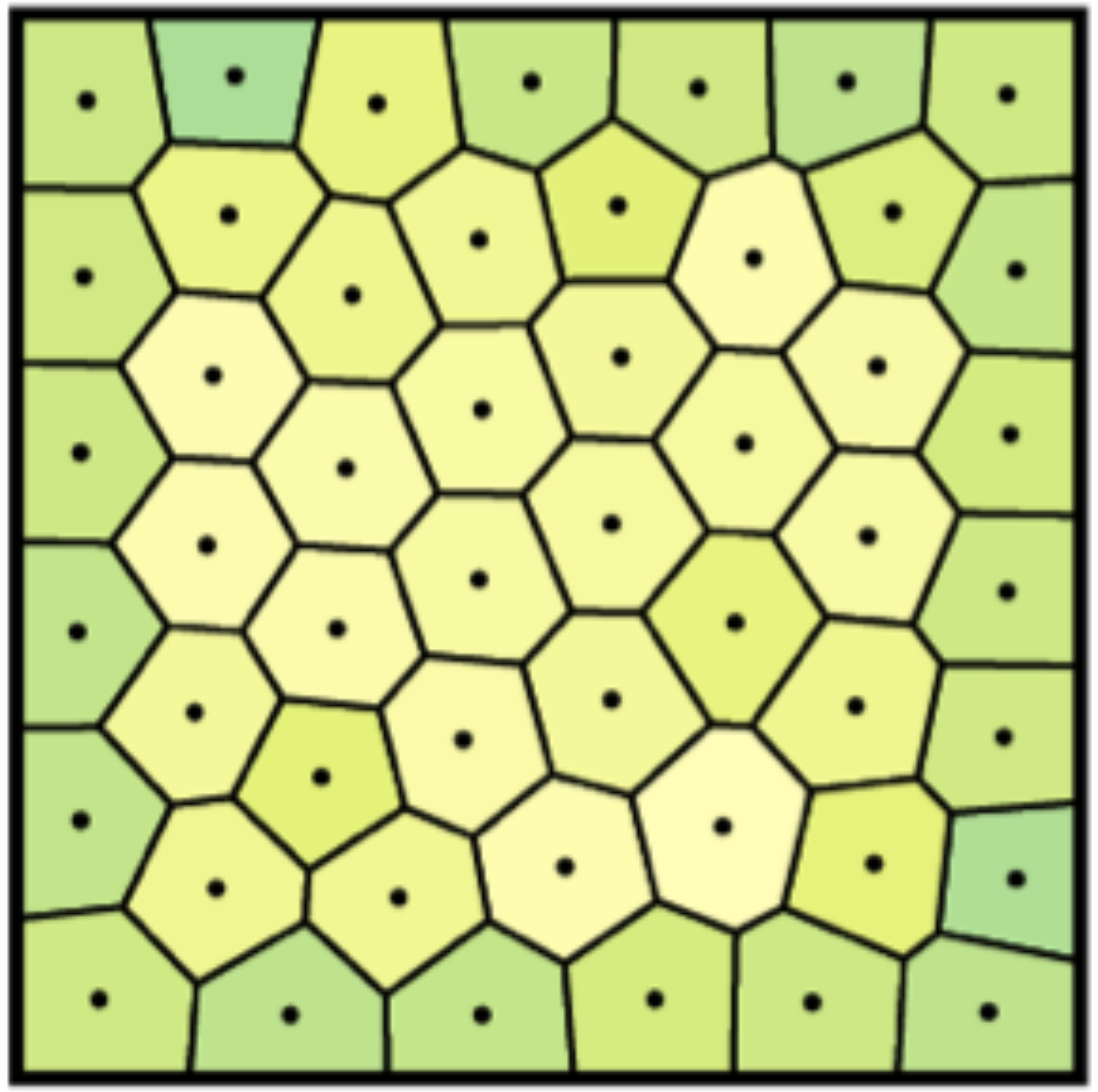

square; density = 50

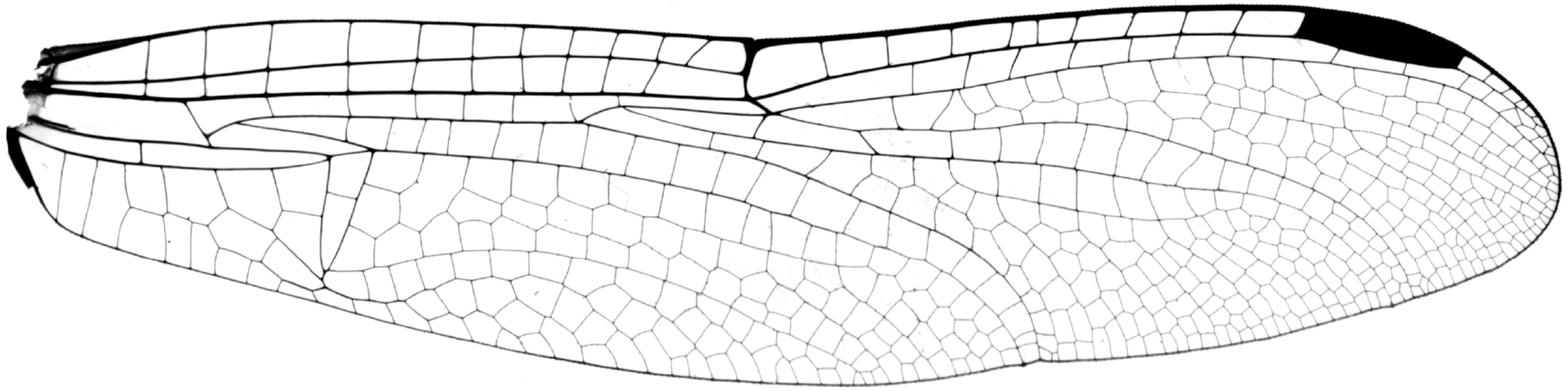

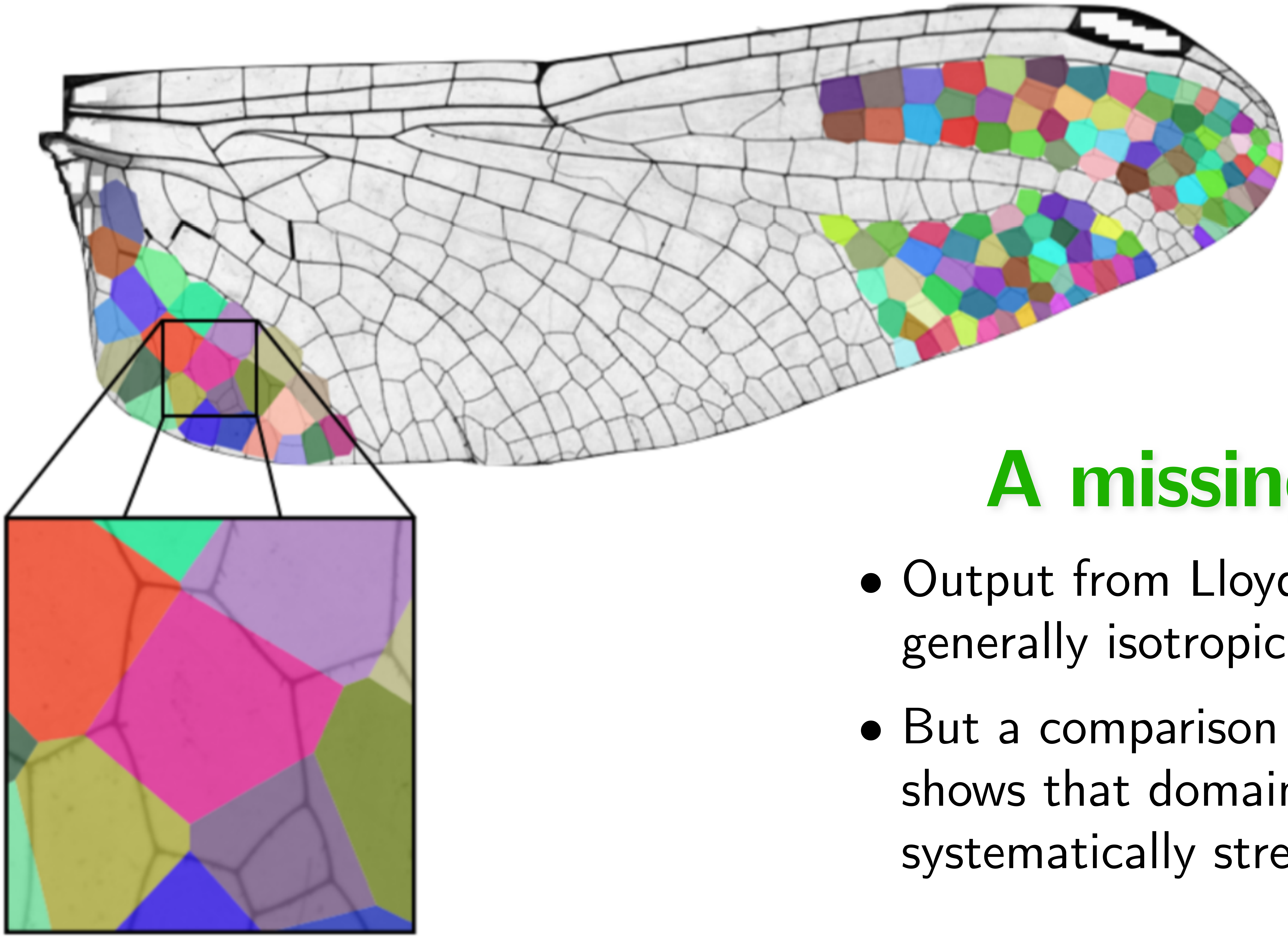

A missing piece

- Output from Lloyd's algorithm is generally isotropic
- But a comparison to wing images shows that domains are systematically stretched

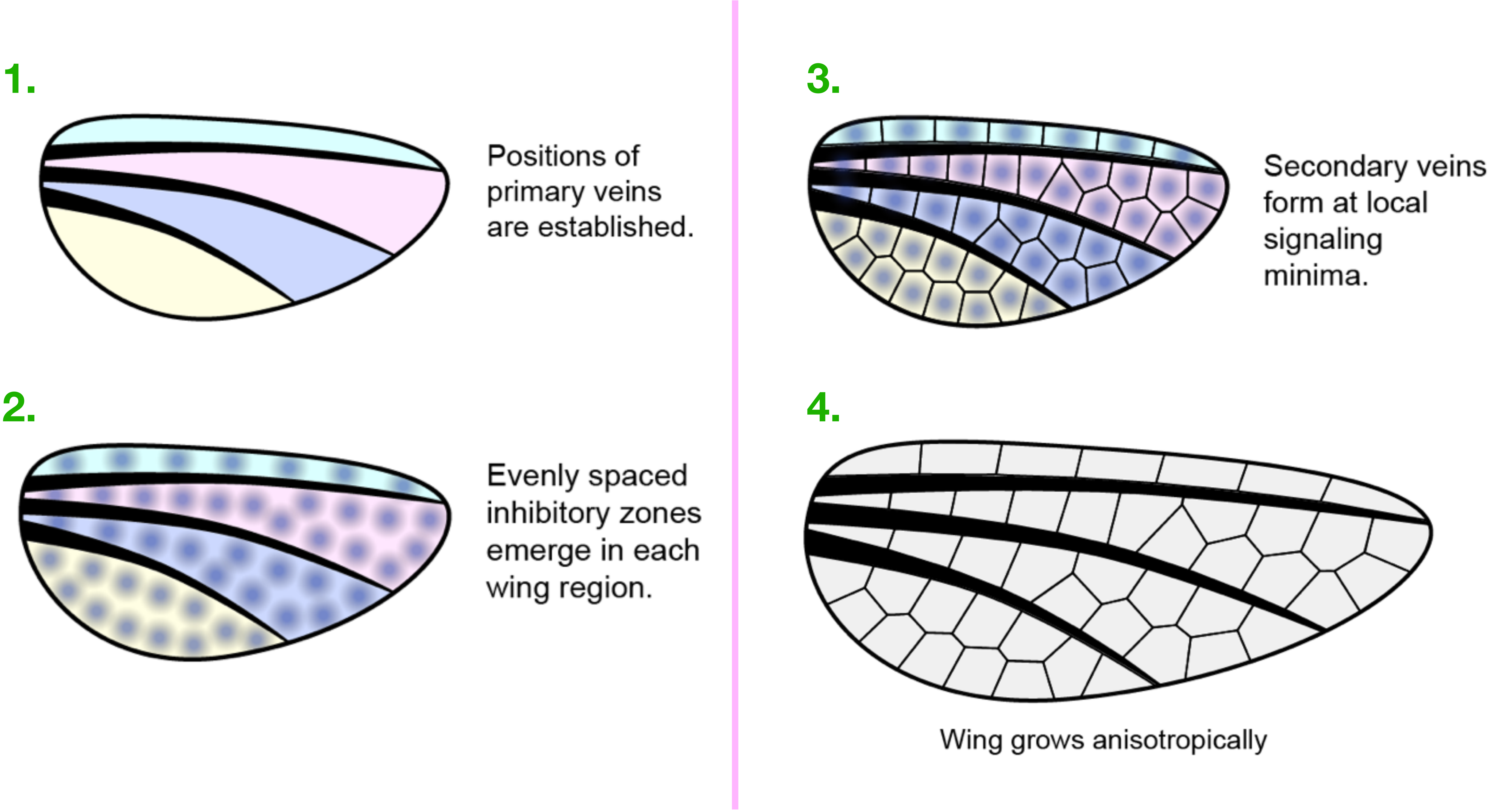
1.
Positions of primary veins are established.
2.
Evenly spaced inhibitory zones emerge in each wing region.
3.
Secondary veins form at local signaling minima.
4.
Wing grows anisotropically

Mapping from the wing pad

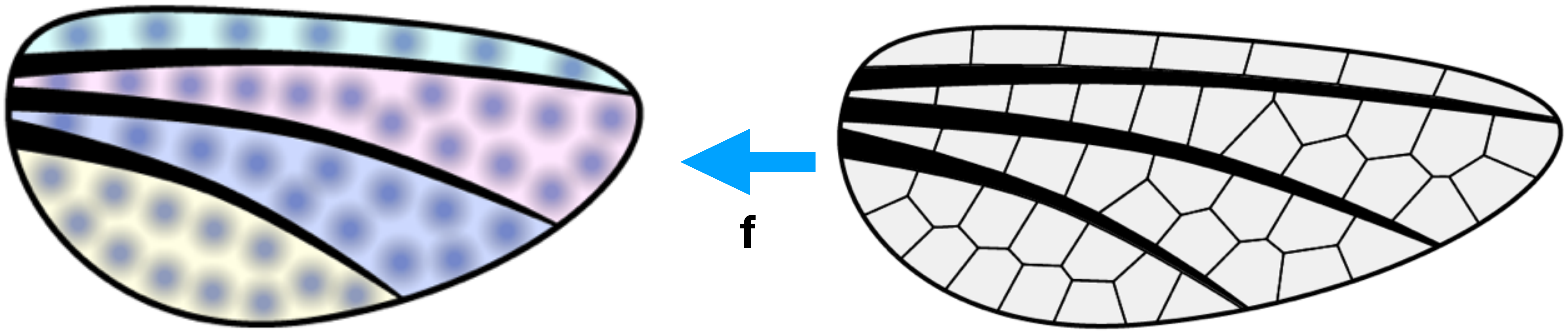

Original wing pad   Fully developed wing

- We search for a mapping from the fully developed wing to the original wing pad of the form

$$\mathbf{f}(\mathbf{x}) = \mathbf{x} + \sum_{i=0}^{N} \sum_{j=0}^{N} \alpha_{i,j} T_i\left(\frac{x}{x_{\max}}\right) T_j\left(\frac{y}{y_{\max}}\right)$$

- Here T_j is the jth Chebyshev polynomial. **Find a map to maximize domain circularity.**

A further constraint

- Initial tests found that the optimization problem was underconstrained
- Added an additional term to penalize non-convexity, defined as the ratio between the shape and the convex hull

$$\gamma = \frac{\sum_i \text{Area}_{\text{transformed}}(\mathcal{P}_i)}{\text{Area(Convex Hull)}}.$$

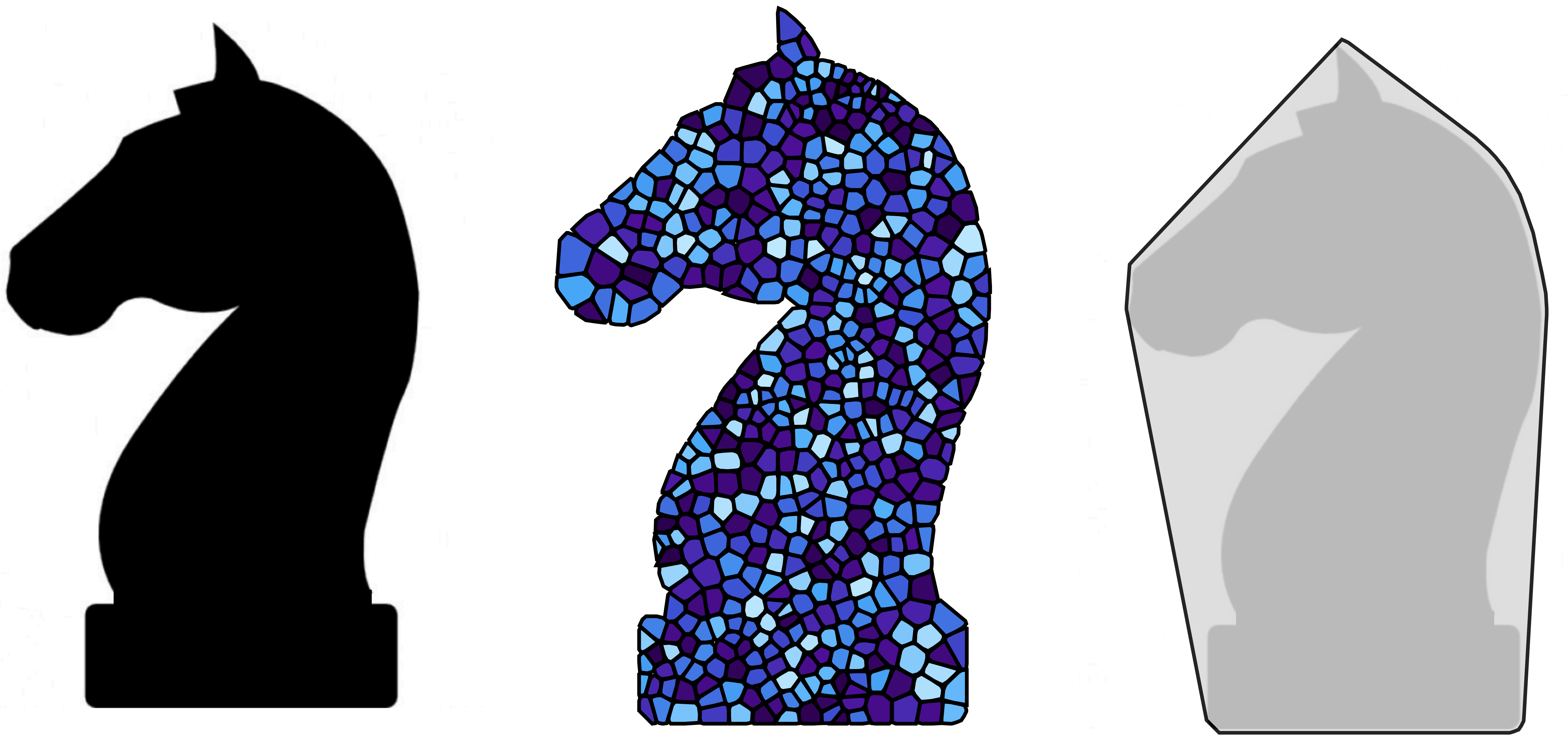

Area: 8298.73

Area: 11088.8

fraction: 0.748

Transform coordinates as

$$\vec{x}' = \vec{x} + \sum_{i=0}^{N} \sum_{j=0}^{N} \vec{\alpha}_{i,j} T_i \left(\frac{x}{x_{\max}} \right) T_j \left(\frac{y}{y_{\max}} \right)$$

where T_i represents the ith Chebyshev Polynomial. Define

$$\gamma = \frac{\sum_i \mathrm{Area}_{\mathrm{transformed}}(\mathcal{P}_i)}{\mathrm{Area}(\mathrm{Convex\ Hull})}$$

where $\mathcal{P}_i$ is the ith polygonal domain. We want to maximise the quantity

$$\max \gamma \sum_i \left(\mathrm{Area}_{\mathrm{orig}}(\mathcal{P}_i) \mathrm{Circ}_{\mathrm{trans}}(\mathcal{P}_i) \right).$$

Use BFGS algorithm to maximize gamma.

Wing pad shape determination

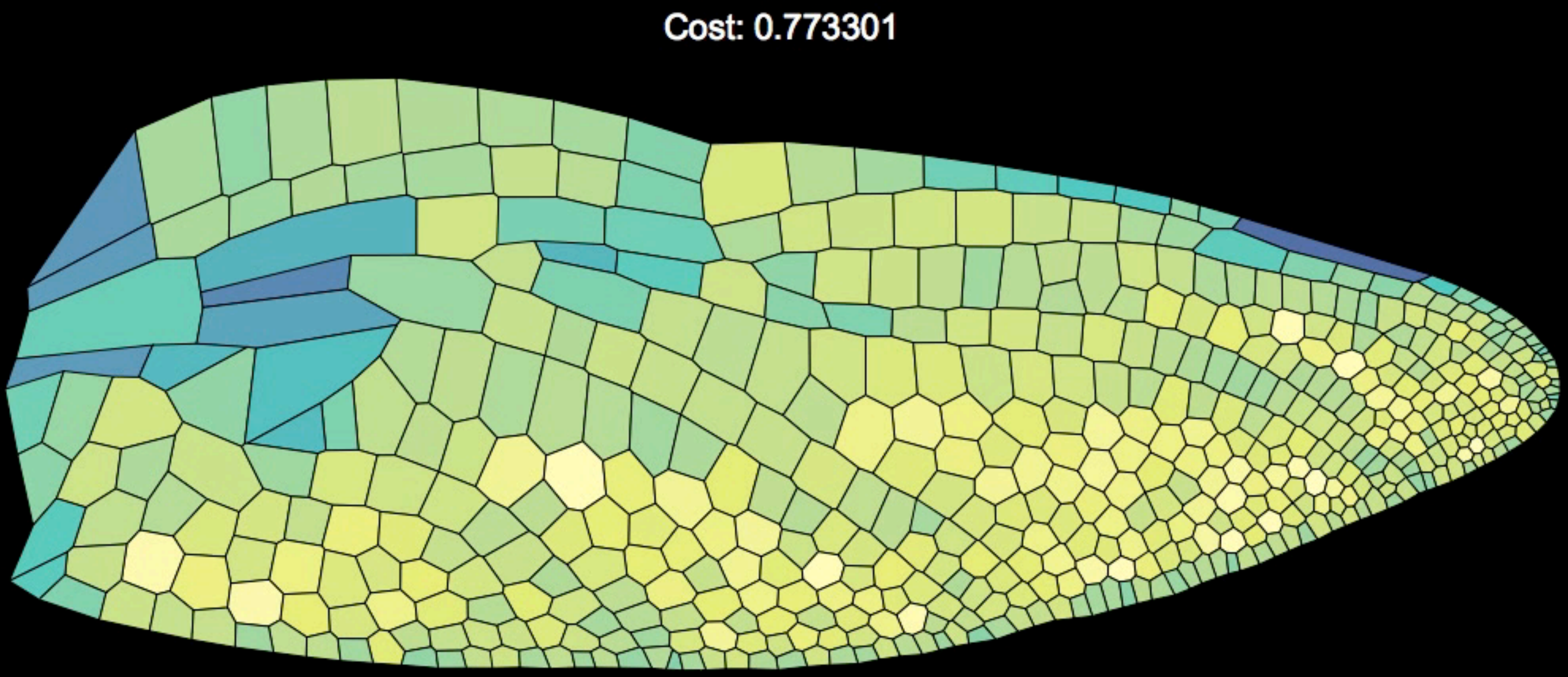

Comparing to manual mapping

Mapping based on wing pad matching

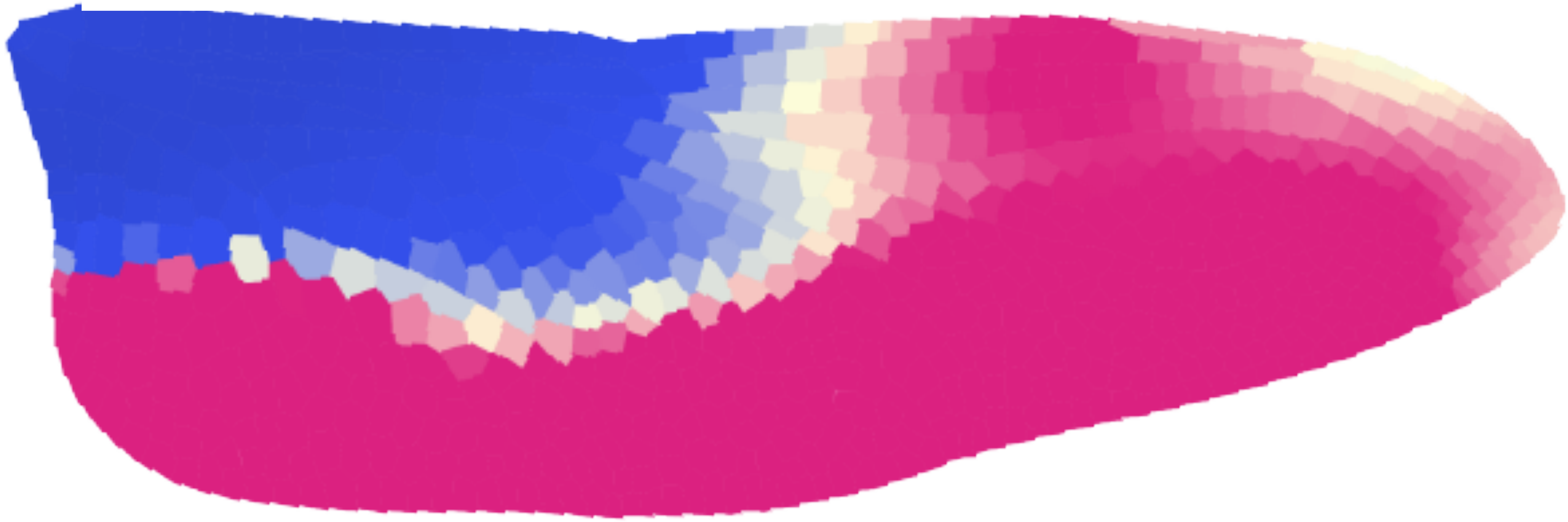

Mapping based on circularity maximization

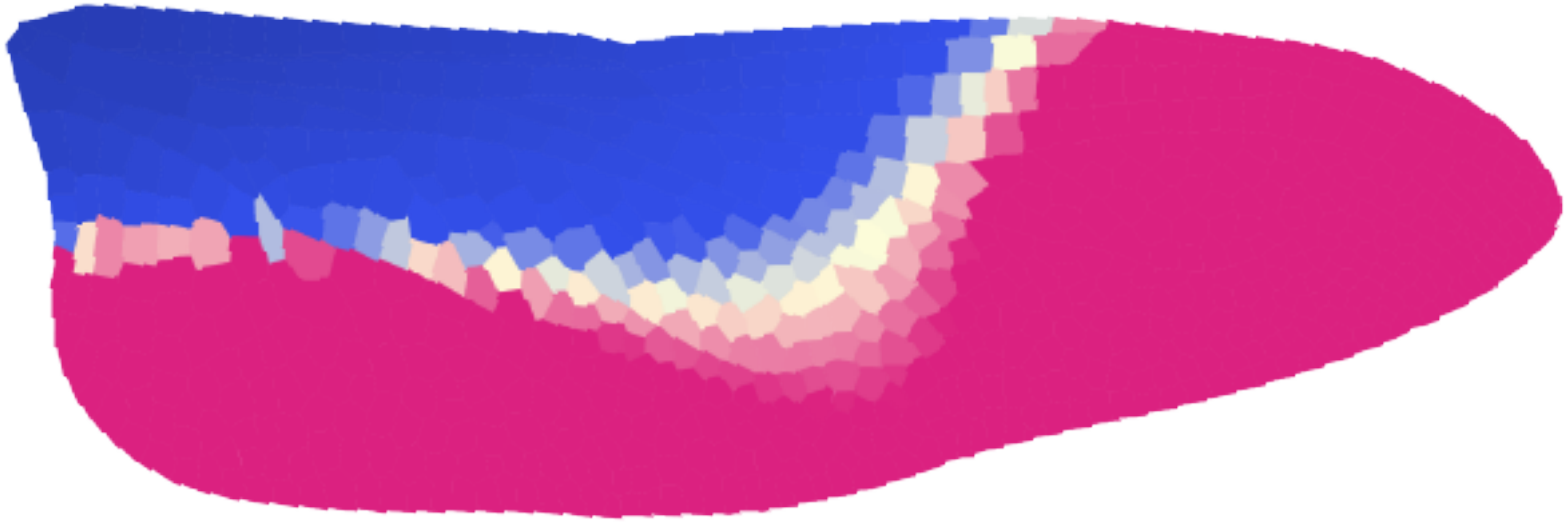

Relative size change

low  high

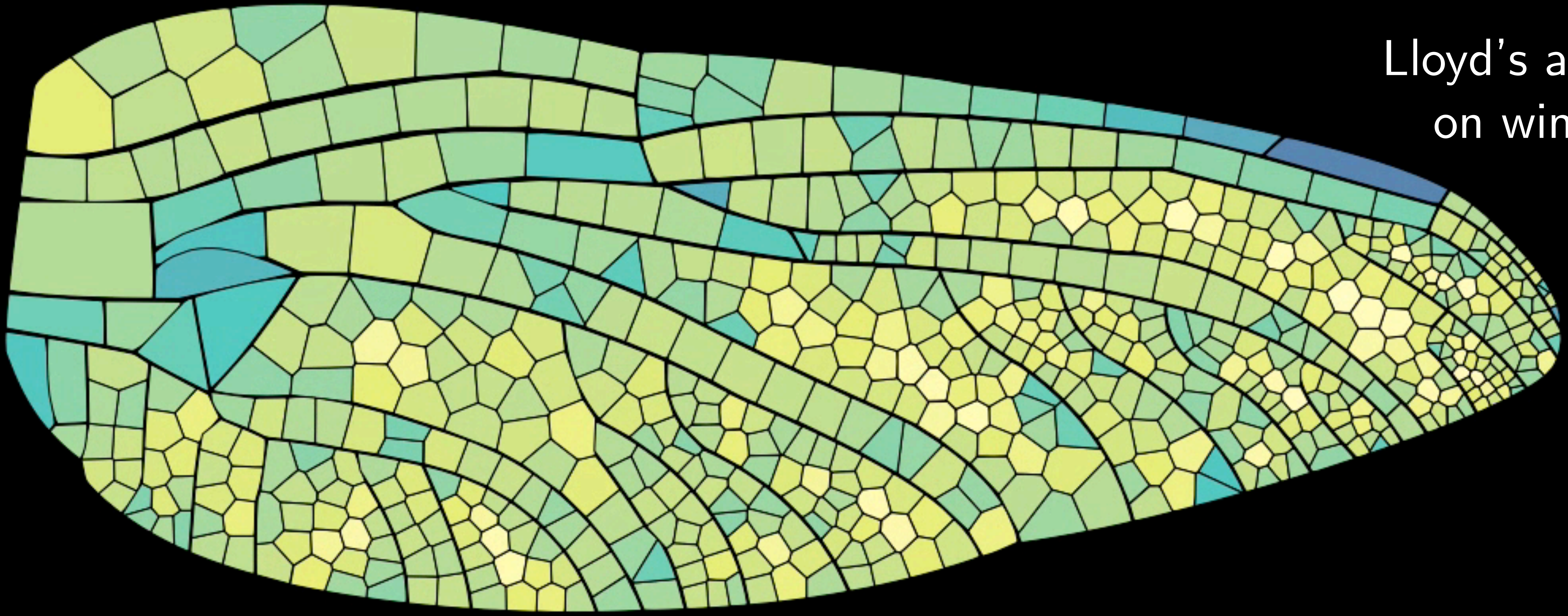

Lloyd's algorithm
on wing pad

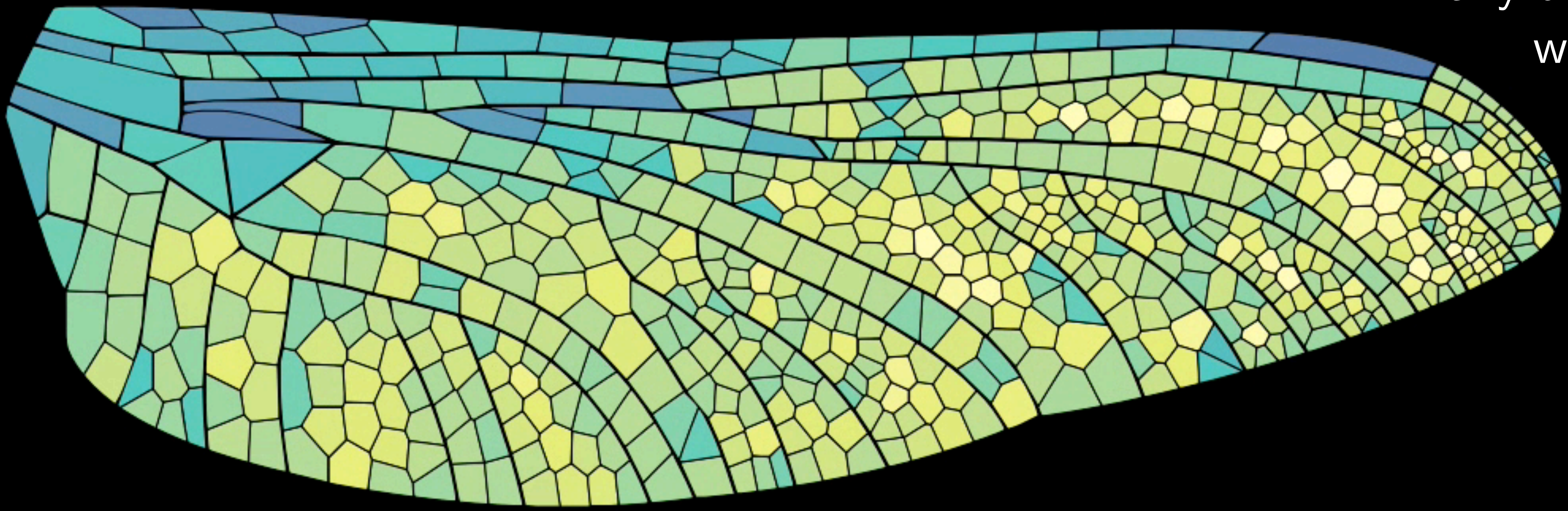

Fully developed
wing

Real vein pattern:

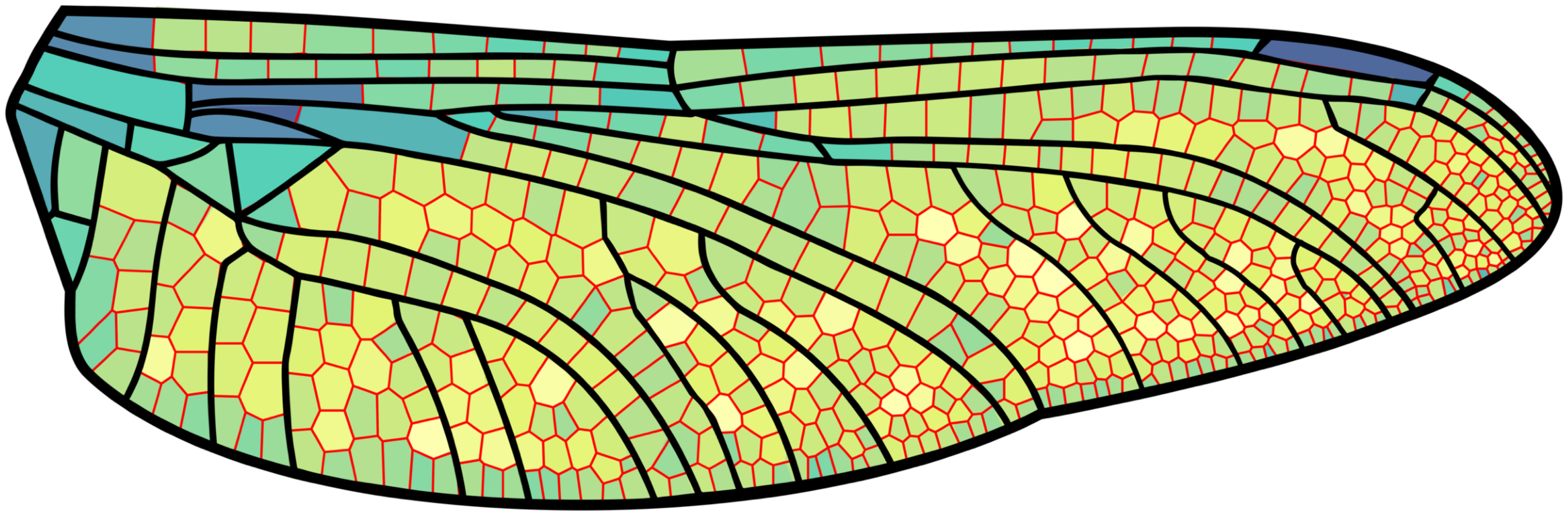

Simulated vein pattern:

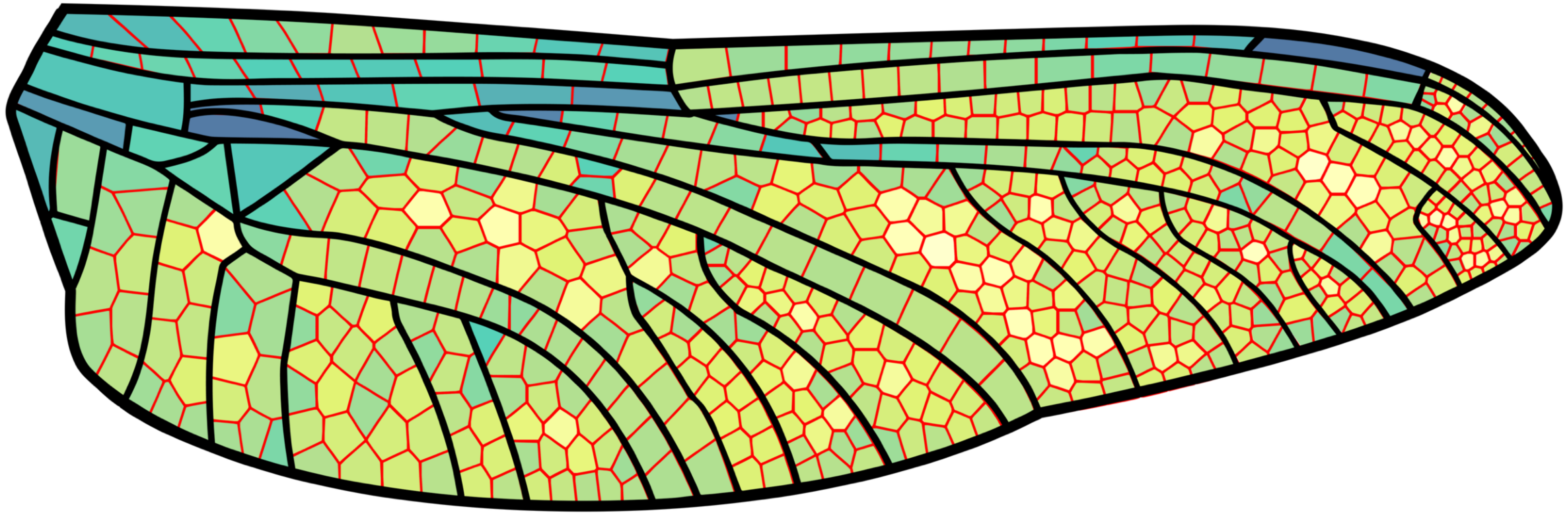

Black veins were fixed in the simulation. Red veins were generated by the model.

Evaluation of simulated wing

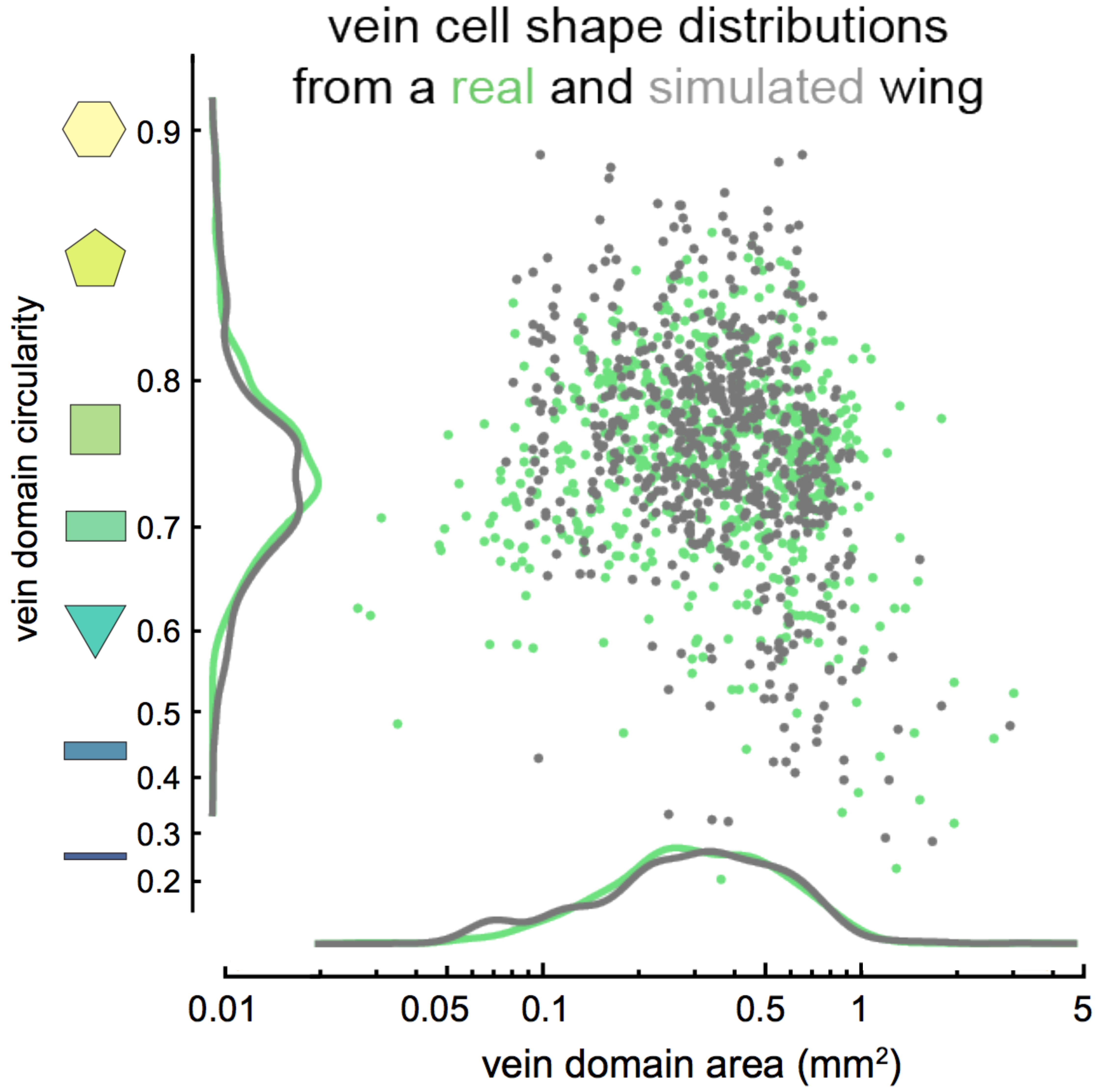

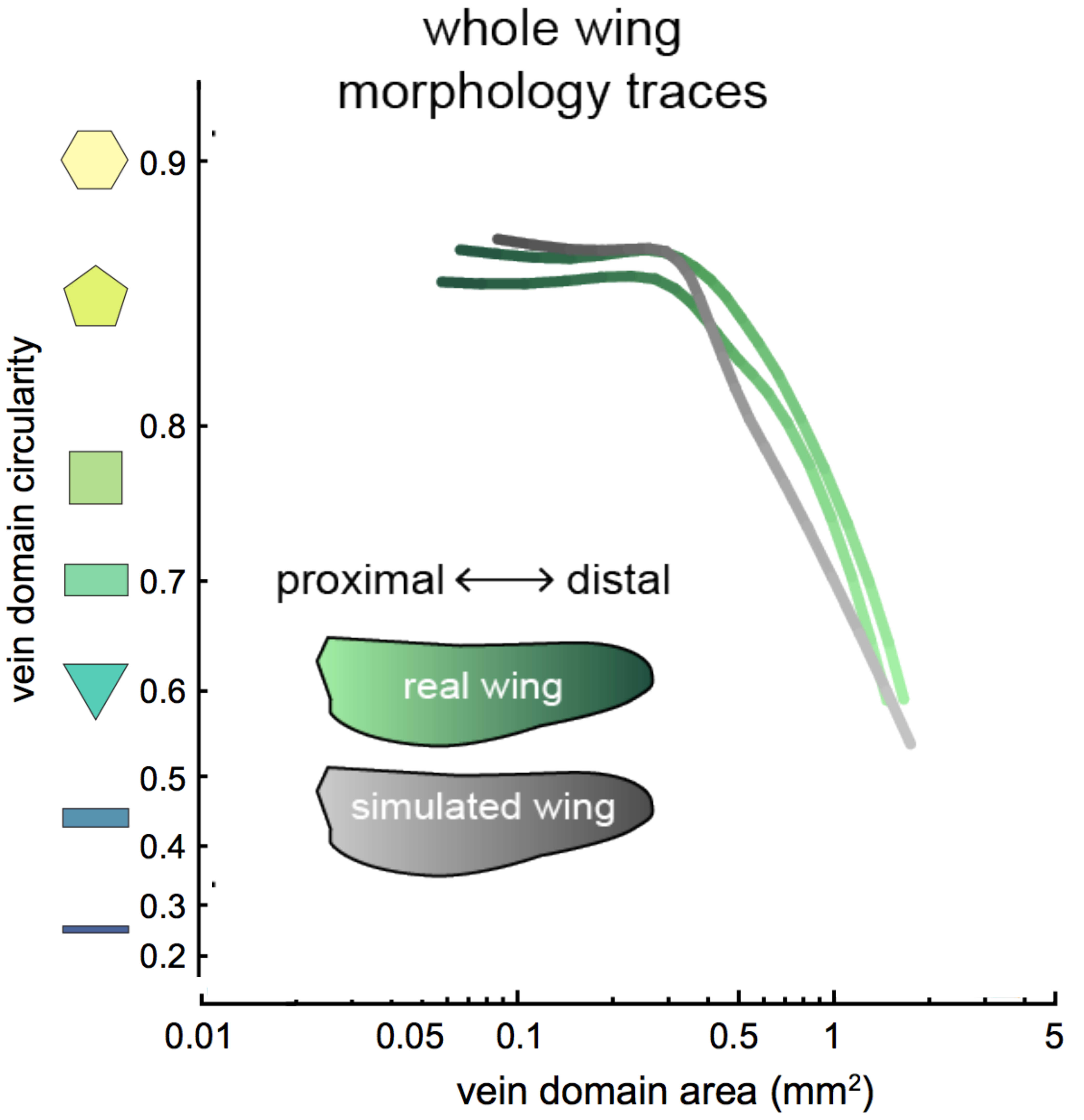

Evaluation of simulated wing

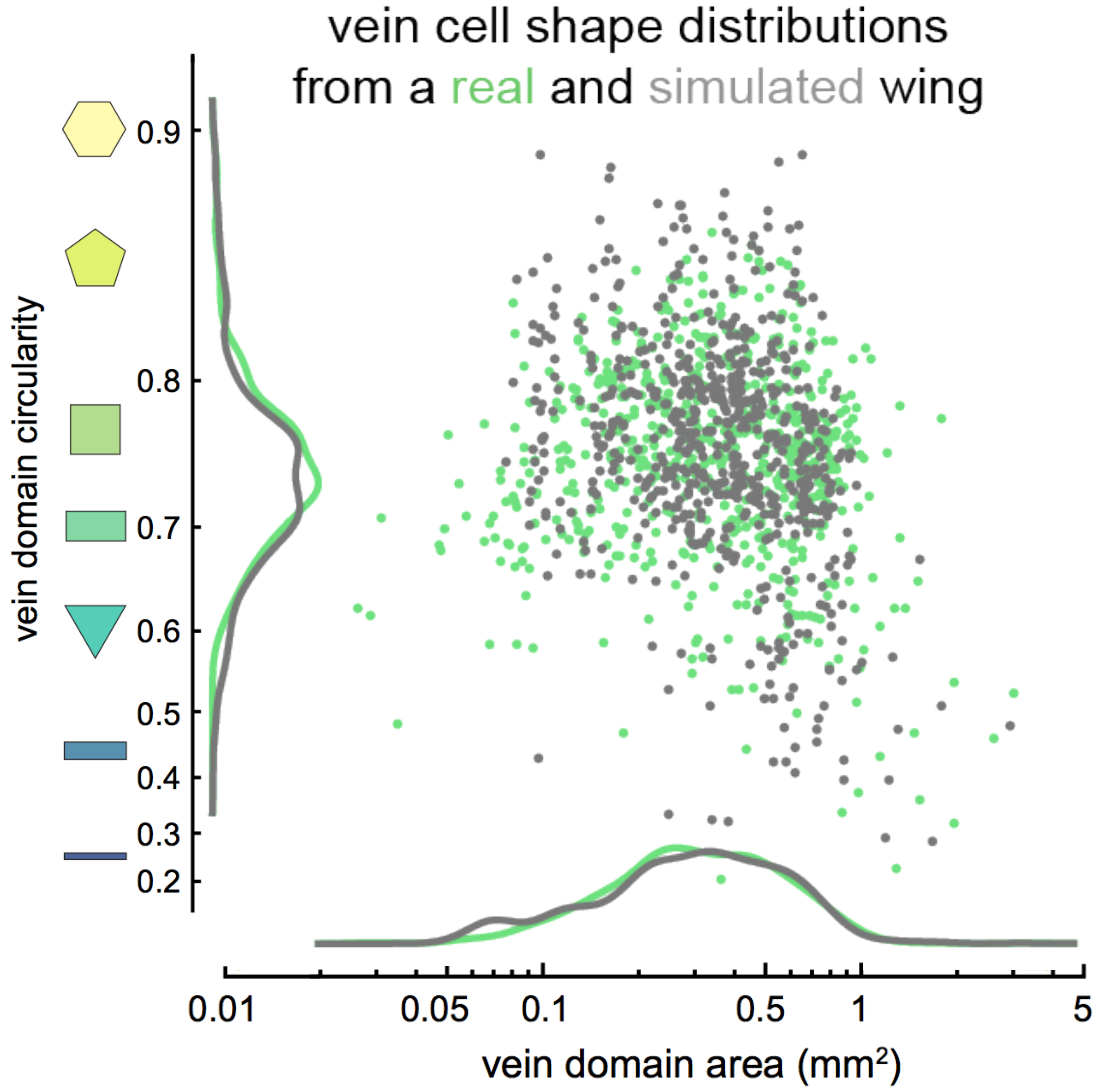

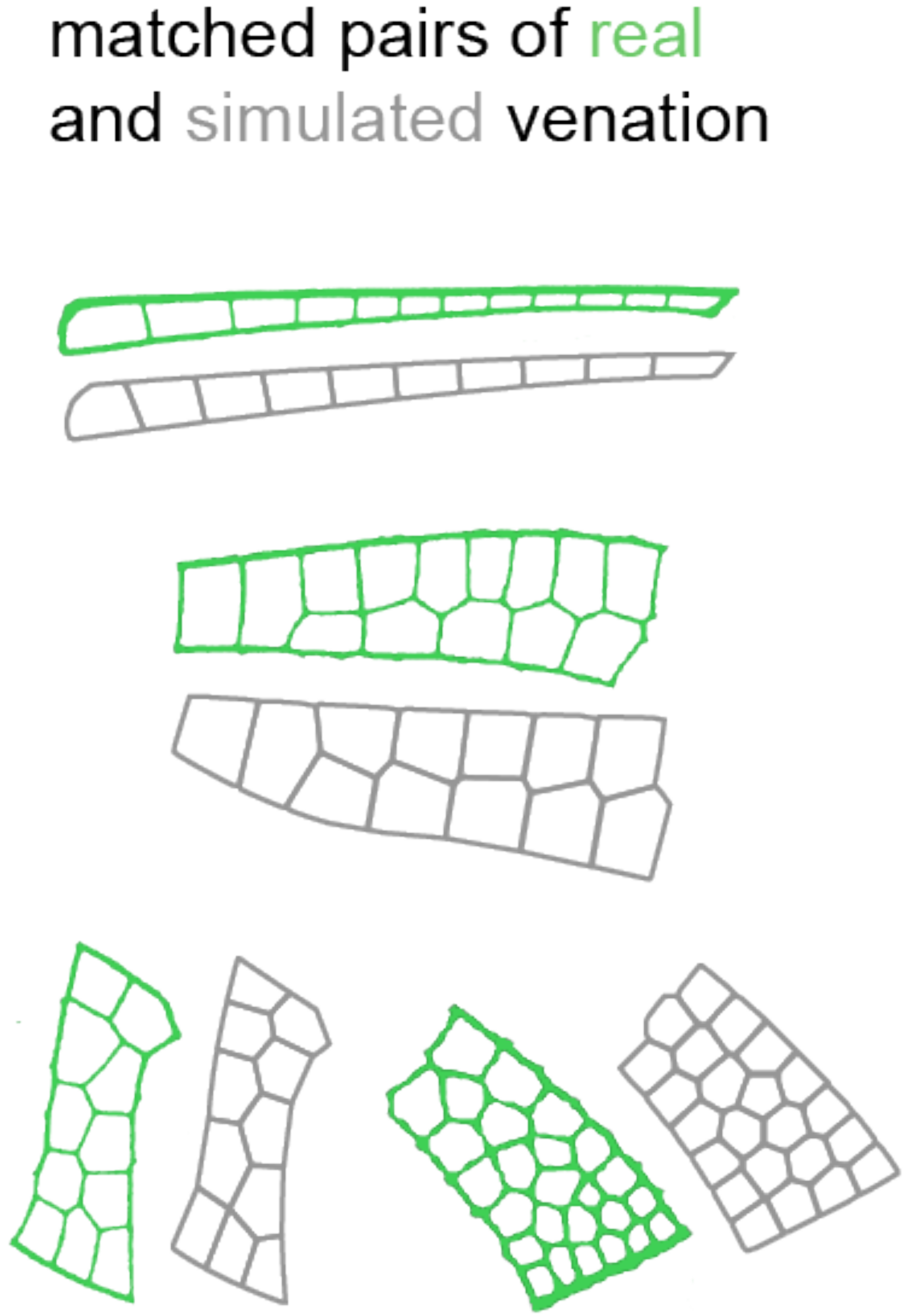

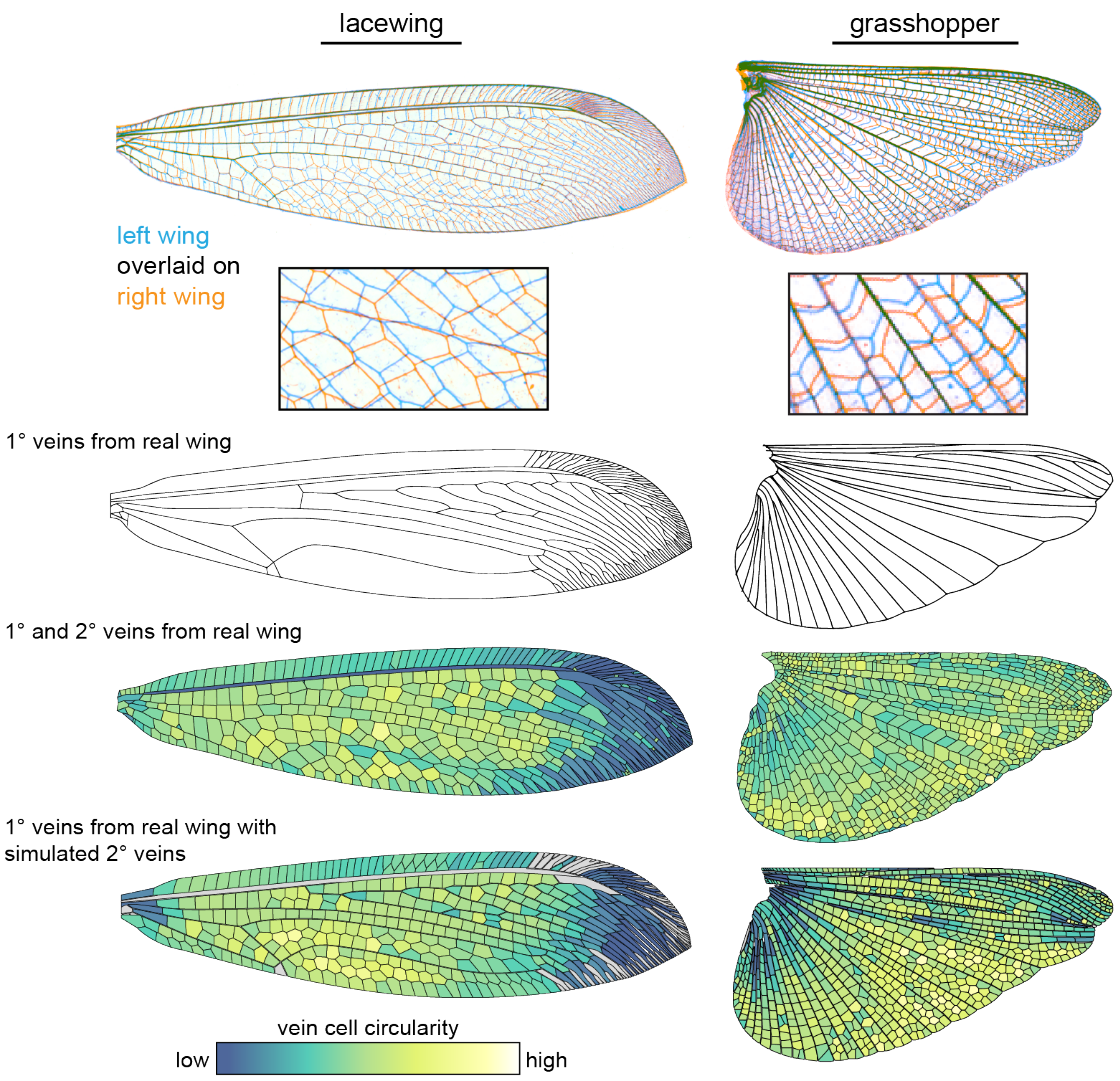
lacewing
grasshopper
left wing
overlaid on
right wing
1° veins from real wing
1° and 2° veins from real wing
1° veins from real wing with
simulated 2° veins
vein cell circularity
low
high